ULTRAVIOLET RADIATION-INDUCED AGGREGATION OF HUMAN LENS PROTEIN γD-CRYSTALLIN: CHARACTERIZATION OF THE PROTECTIVE TRYPTOPHAN CLUSTERS AND KEY SENSITIZING RESIDUES

By
Nathaniel Schafheimer

B.S./M.S. Biochemistry
Brandeis University, 2008

SUBMITTED TO THE DEPARTMENT OF BIOLOGY
IN PARTIAL FULFILLMENT OF THE REQUIREMENTS
FOR THE DEGREE OF

DOCTOR OF PHILOSOPHY
AT THE
MASSACHUSETTS INSTITUTE OF TECHNOLOGY

SEPTEMBER 2013

Signature of Author_____
Department of Biology
September 2013

Certified by_____
Jonathan A. King
Professor of Molecular Biology
Thesis Supervisor

Accepted by_____
Stephen P. Bell
Co-Chair, Department Committee on Graduate Students

ULTRAVIOLET RADIATION-INDUCED AGGREGATION OF HUMAN LENS PROTEIN γD-CRYSTALLIN: CHARACTERIZATION OF THE PROTECTIVE TRYPTOPHAN CLUSTERS AND KEY SENSITIZING RESIDUES

By

Nathaniel Schafheimer

Submitted to the Department of Biology
on August 28th 2013 in Partial Fulfillment of the
Requirements for the Degree of
Doctor of Philosophy in Biology

ABSTRACT

Cataract is the development of opacities in the lens of the eye, producing light scattering and blurring of the visual image. Mature lens cells are enucleated and have degraded their ribosomes, thus proteins in the center of the lens must persist for the duration of a human lifetime. Lens opacities are composed of covalently damaged and aggregated lens proteins. Among the risk factors that promote cataract development is solar ultraviolet radiation. Ultraviolet radiation (UVR) reaches the proteins of the transparent lens, and has been shown to cause protein photo-oxidation, cross-linking, and aggregation in experimental settings.

The crystallins are the primary proteins of the lens, expressed at concentrations up to 400 mg/ml. γD-Crystallin (HγD-Crys) is one of the most abundant proteins in the center of the human lens. HγD-Crys contains a large number of UVR absorbing aromatic amino acids, including four conserved tryptophans and fourteen tyrosines, many arranged into structurally important aromatic pairs. Previous work identified an energy transfer mechanism between the tryptophan pairs of HγD-Crys that sharply shortened their fluorescence excited state lifetimes. This was hypothesized to be photo-protective mechanism for a chronically UVR exposed protein.

To understand how UVR causes aggregation and cataract, we examined the photo-aggregation of HγD-Crys *in vitro*. HγD-Crys aggregates in an oxygen dependent manner when exposed to UVA/UVB radiation, forming light scattering species after a lag period. Covalent higher and lower molecular weight species

also appeared immediately upon irradiation. The absorption spectrum of UVR-exposed HγD-Crys samples did not change as aggregation progressed, suggesting a lack of widespread damage to the UVR absorbing aromatic residues. To examine the potential role of the tryptophan pairs in mediating photo-damage to HγD-Crys, we exposed multiple W:F mutant HγD-Crys proteins to UVR. To our surprise, HγD-Crys photo-aggregated more severely in the absence of tryptophan, the strongest UVR absorber in proteins. HγD-Crys constructs containing single tryptophans appeared to be more photo-aggregation prone than those having four or none. These data suggest tryptophan plays a protective role against photo-aggregation, consistent with the photo-protective energy transfer hypothesis.

To investigate whether other aromatic residues played key roles in photo-aggregation, we examined double Y:A or F:A mutant HγD-Crys constructs replacing the tyrosine/phenylalanine pairs. While most of the aromatic pairs did not appear significant for photo-aggregation, replacement of Y16 and Y28 significantly slowed photo-aggregation, suggesting that the two tyrosines mediated photo-damage. Mass spectrometry of irradiated HγD-Crys also identified C18 as a site of photo-oxidation, and C18S mutant γD-crystallin constructs were slow to photo-aggregate in a similar fashion to Y16A/Y28A mutants. A multiple mutant lacking any cysteines photo-aggregated at a similar rate to C18S, showing that thiol chemistry was not necessary for photo-aggregation.

Using this data, we put forth a model of HγD-Crys *in vitro* photo-aggregation. We suggest that the tryptophans serve as an excited state energy sink, and that Y16 and C18 together act as one site of photo-damage that can initiate oxygen dependent radical polymerization of HγD-Crys when exposed to UVR. Deeper understanding of photo-damage to lens proteins can aid in developing better preventative treatments for cataract.

Thesis Supervisor: Jonathan A. King
Title: Professor of Molecular Biology

ACKNOWLEDGEMENTS

First, I owe a great deal of thanks to my advisor, Professor Jonathan King, for patiently supporting me as I addressed this scientifically interesting but complicated question. Jon originally caught my eye when I heard him speaking passionately about the duty of the scientist as a citizen and that graduate students should make sure their research had application to the greater good. That wider perspective was a great boon to me as I took on different responsibilities around MIT, and looked beyond academia for my next career steps. We have argued candidly about elements of science and politics, but I deeply respect you, Jon, and I am truly grateful for all your frank feedback and support.

Thank you to my thesis committee members, Professors Robert Sauer and Amy Keating. Without your interest and feedback over the years, this project could not have succeeded. Thanks are also due to my qualifying exam member, Prof. Dennis Kim, and to my outside defense member, Dr. Fu Shang.

To the other King Lab members, past and present: none of my scientific curiosity would have been worth a damn without you to teach me the ropes of studying protein purification, folding, and aggregation. In particular, Jiejin, thank you for making the hypothesis and doing the fascinating and extensive work on the tryptophan quenching mechanism that led to my project being conceived. Ligia, I have kept the FPLC's alive and kicking, and I think I've done our bench proud; incidentally, your stockpile of lab supplies are still being raided to this day. Thanks for putting up with my precocious first year antics. Kate, you were something of a scientific role model for me, maintaining a calm, methodical manner in lab while still having a lot of fun; I'm glad we got to work together. Fan, our discussions on the aromatic residues in HγD-Crys were really helpful, and I hope I've added to the story you began about the importance of the aromatic pairs. Takumi, thank you for all your advice about mass spectrometry; your protocol for preparing aggregated samples for digestion opened a new front on my project. Cammie, your technical expertise and steady support growing precarious numbers of mutant proteins has been essential and I couldn't imagine the lab without you. Eugene, I'm so glad you joined my bay; your quiet and thoughtful approach has been an illuminating counterpoint to my often quick-to-the-punch style. I know you're going to do great things. Good luck finishing your Ph.D. research! Thank you to Dessy Raytcheva, Cindy Woolley, Kelly Knee, Dan Goulet, and Jeannie Chew as well.
Oksana gets her own mini-paragraph (she is probably laughing about that). Oksana, you've been the best labmate and friend anyone could ask for throughout this entire sordid ordeal. Whether it was putting my plates away when I dashed out, harried, to a meeting, listening to me rant about my latest scientific or personal challenge, or just accompanying me on the daily lunchtime journey to the food trucks, Oksana has been there for this whole thesis (she read it too, so she might as well be second author). Thank you for all that you've done, and don't stress! You'll be Dr. Sergeeva soon enough.

Thank you to my collaborators, Professor Kevin Schey and Dr. Zhen Wang, for their excellent work at the Mass Spectrometry Research Center at Vanderbilt, some of which can be seen in Chapter 3. Thank you to Ioannis Papayannopoulos of the MIT KI Proteomics Lab and Dr. Carlos Baiz of the Tokmakoff lab, for helpful conversations and initial forays into mass spectrometry and FTIR, respectively. Many thanks to Deborah Pheasant at the BIF for helpful conversations and for babysitting the CD spectrometer when I had to dash out.

To my classmates: thank you all for the fun times that reminded me that research was not all there was in the world. In particular, thanks to the Wine and Cheese Club: Josh, Drew, and MK, we really must have a bottle again in a year or so when we're all big-wig PhDs. Thanks for all the memorable Sunday nights!

When my day in lab ended, my job as GRT on FloorPi (3W) in East Campus began. But it never felt like a chore; being a sort of academic older sibling to the undergrads was refreshing and reminded me that there were people, crazy, nerdy people, outside lab. I've had the privilege of providing candy, waffles, and conversation to ~75 undergrads over the years. Thank you, all of you, for making me part of your community.

Thank you to all my colleagues in the Science Policy Initiative and Graduate Student Council Housing and Community Affairs Committee. In a student culture where time away from the bench can be a guilty secret, together we embraced our passions for policy issues and advocacy for graduate students, and did a lot of good. I'm proud to have served with you all!

Professor Frank Solomon, your advice and empathy helped me get back on track when I was veering off course. Vincent Sutera, you were a wizard of a lab manager when I was an undergrad, and in my time at MIT you've continued to support me as a friend, helpfully reminding me that I'm not the first and won't be the last to struggle at research. Thank you both for being guides to me.

My friends in Boston have been unceasingly patient and supportive throughout my science quest, never holding my many research related absences against me and always offering an ear when the latest experiment or tribulation overflowed into our conversations. I can't wait to hang out with you all as a "real" person!

To my mom and dad, Sherrie and Steven: I'm only here because you both took my education and curiosity seriously from day one. Thank you both for all the love and support, even if you didn't always understand my research. To my little brother, Brian: I am grateful for you every time we talk (and honestly beginning to feel bad about dropping you in that picture when you were a baby). Love you bro.

And to the several people who've been romantically entangled with me at different points during this project: thanks. Really (yes, even you). It isn't always easy dating a nerd, but you made my time in grad school richer, certainly more interesting, and added a level of meaning to my days that all the science, extracurriculars, and geekiness could not have. May the friendship of the seasons be with you all of your days.

This work has been supported by a grant from the National Eye Institute #EY015834. The Biophysical Instrumentation Facility for the Study of Complex Macromolecular Systems (NSF-007031) is gratefully acknowledged.

BIOGRAPHICAL NOTE

Education

Ph.D. Expected 2013	Massachusetts Institute of Technology, Dept. of Biology Cambridge, MA
B.S./M.S. June 2008	Brandeis University, Dept. of Biochemistry, Waltham, MA Major: Biochemistry, *Summa cum laude* Minor: Philosophy

Research and Professional Experience

2009 to 2013	Graduate Research Assistant in the laboratory of Professor Jonathan King, MIT Department of Biology, Cambridge, MA
2009 to 2013	Graduate Resident Tutor in the East Campus MIT Dormitory MIT Residential Life Programming, Cambridge, MA
2006 to 2008	Undergraduate Research Assistant in the laboratory of Professor Susan Lovett, Department of Biology, Brandeis University, Waltham MA, *Thesis: YqgF: A possible novel Holliday Junction Resolvase*
Summer 2005-06	Systems Reliability Intern, Ortho-Clinical Diagnostics, Rochester, NY

Publications

Schafheimer, N. and King, J. (2013) *Tryptophan Cluster Protects Human γD-Crystallin from Ultraviolet Radiation-Induced Photo-Aggregation In vitro*. Photochem. Photobiol. *In Publication*

TABLE OF CONTENTS

LIST OF FIGURES

CHAPTER 1

CHAPTER 2

CHAPTER 3

CHAPTER 6

LIST OF TABLES

LIST OF ABBREVIATIONS

(in alphabetical order)

BCA: bicinchoninic acid assay
BME: β-mercaptoethanol
CD: circular dichroism
DTT: Dithiothreitol
EDTA: ethylenediaminetetraacetic acid
FCM: fluid circulation model
FRET: fourier resonance energy transfer
GuHCl: guanidine hydrochloride
HαA-Crys: human αA-crystallin
HαB-Crys: human αB-crystallin
HγD-Crys: human γD-crystallin
HγS-Crys: human γS-crystallin
HPLC: high-performance liquid chromatography
IPTG: isopropyl-β-thiogalactoside
LC MS/MS: liquid chromatography tandem mass spectrometry
MALDI: matrix assisted laser desorption ionization
MRM: multiple reaction monitoring
NADPH: nicotinamide adenine dinucleotide phosphate, reduced
QM-MM: quantum mechanical-molecular mechanical
ROS: reactive oxygen species
SAXS: short angle X-ray scattering
SDS-PAGE: sodium dodecyl sulfate polyacrylamide gel electrophoresis
SEC: size exclusion chromatography
sHSP: small heat shock protein
TEM: transmission electron microscopy
Tris: Tris(hydroxymethyl)-amino methane
UPP: ubiquitin proteasome pathway
UV: ultraviolet
UVR: ultraviolet radiation
WT: wild-type

CHAPTER 1:

INTRODUCTION

Ultraviolet Radiation

Ultraviolet radiation (UVR) is a ubiquitous environmental hazard for life on Earth. UVR induces mutations and other lesions in DNA, leads to reversible and irreversible damage to proteins, and is a major source of damage to the photosynthetic apparatus. An understanding of UVR's effect on lens proteins may contribute to understanding the eye disease cataract. In these first sections, I will review important characteristics of UVR, and how it damages biological materials.

The sun emits radiation similar to a black-body object with a temperature of approximately 5766 K (Fig. 1.1) (1). The solar constant, a measure of solar energy reaching the Earth, is ~1366 W/m^2 and varies over the course of the Earth's orbit. Of that energy, 10% is in the form of ultraviolet radiation (100-400 nm). This range is subdivided into UVC (100-280 nm), UVB (280-315 nm), and UVA (315-400 nm) sections (2). UVC is the most energetic type of UVR (4.43-12.4 eV/photon), but wavelengths beneath 200 nm are strongly absorbed by the atmosphere and those beneath 290 by the ozone layer, making UVC encounters by present day life on Earth unlikely. UVB is the next most energetic class of UVR (3.94-4.43 eV/photon), followed by UVA (3.1-3.94 eV/photon).

The UV range overlaps the absorption spectra of many biologically significant compounds, including DNA nucleotides, protein peptide bonds, aromatic amino acids, and lipids (3-7). When compounds absorb photons, they enter into excited states and can undergo a variety of photochemical reactions leaving covalent damage in their wake (Fig. 1.2).

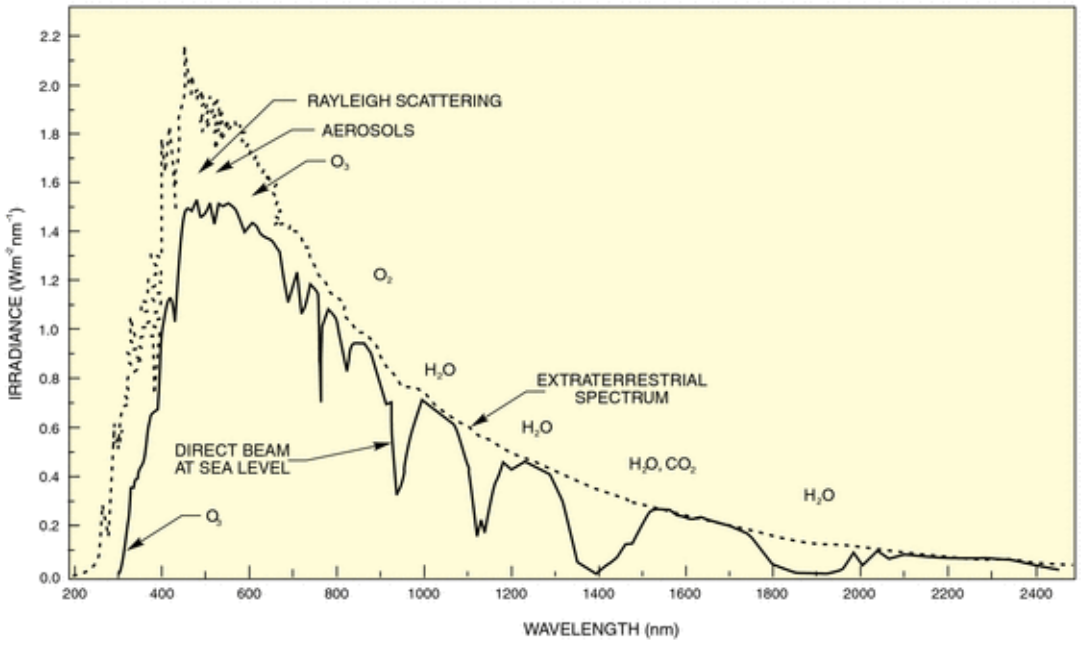

Figure 1.1 The Extraterrestrial and Sea Level Solar Radiation Spectrum. The extraterrestrial solar spectrum (dotted line) compared to the sea level spectrum (solid line), which is attenuated by atmospheric absorption and scattering. Permission to use granted by Newport Corporation. All rights reserved.

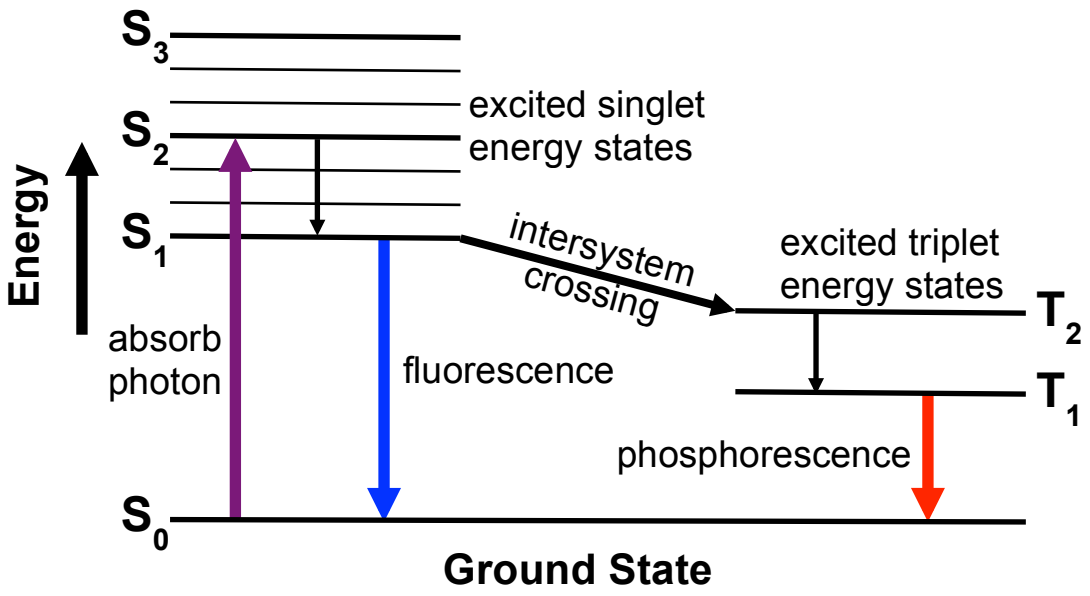

Figure 1.2 Jablonski Diagram of Photo-Excitation States. This basic Jablonski diagram depicts what can happen to an excited state molecule's electrons. The excited electrons will rapidly settle to the lowest singlet excited state available via internal conversion, and from there can either fall back down to the ground state via fluorescence or energy transfer to a compatible nearby chromophore, or undergo intersystem crossing to the triplet excited state which itself can return to the ground state via phosphorescence. In general, singlet states are short lived compared to triplet states. Photochemical reactions compete with fluorescence and phosphorescence.

UVR-Induced Photo-damage and Repair

Prehistoric Earth was exposed to higher intensities of UVR than present day Earth. Prior to the evolution of oxygenic photosynthesis, molecular oxygen was a rarity in the atmosphere (8), and there was no UVR absorbing ozone layer in the stratosphere. A portion of the sun's high energy UVC and a larger amount of UVB reached the surface of the Earth, creating a selective pressure on organisms to form protective behaviors and UVR resistant properties (9). These evolved advantages included phototactic movement away from high light intensity, shielding in the form of pigmentation, and mechanisms to quench excited state species before photochemical damage occurs (10). More elaborate protective mechanisms, particularly efficient repair or replacement of damaged cell components also evolved (11).

The formation of the ozone layer ~2.4 billion years ago may have lessened the weight of UVR's selective pressure, but it is still a threat to terrestrial life. Evolutionary artifacts of Earth's younger days may reasonably be expected to persist in extant organisms. In this section, I will review some of the types of damage UVR causes to DNA and proteins, and the methods available in human cells to mitigate the effects of said damage. Special attention will be paid to the cells and tissues of the lens and eye, on which this research focuses.

DNA Photo-Damage

DNA damage by UVR has been extensively studied because radiation is a potent mutagen and carcinogen (12). Damage can occur directly, through

excitation of the nucleotide, or indirectly, through excitation of a photo-sensitizing species (3). The most common direct photo-products of UV damage to DNA are dimers of adjacent pyrimidine bases. These fall into two classes: cyclobutane pyrimidine dimers and 6-4 photo-products. Pyrimidine dimerization creates a lesion that disrupts the DNA double helix, preventing transcription and replication through the damaged site (13).

Photo-damage occurring indirectly, i.e. via a photo-sensitizer, can occur via type I or type II mechanisms. Type I involves the photo-sensitizer reacting with the nucleotide or solvent to produce a reactive oxygen species (ROS) which then modifies the nucleotide (3), whereas type II mechanisms involve the excited photo-sensitizer directly exciting oxygen into singlet oxygen. The primary indirect photoproduct in DNA is 8-oxoguanine from guanine.

Pyrimidine dimers can be directly reversed by the blue-light activated enzyme photolyase, functioning in most organisms but not placental mammals (9). Mammals rely on the less efficient nucleotide excision repair (NER) pathway to remove pyrimidine dimers (12). The repair pathway involves dozens of proteins, but proceeds through the steps of lesion recognition, recruitment of additional recognition, helicase, and endonuclease proteins to the NER complex, cleavage of the single strand upstream and downstream of the damage site, and re-polymerization of the 27-30 nucleotide gap by a repair polymerase (12). 8-oxoguanine, the next most abundant DNA photo-product, in contrast, is recognized by a different repair pathway, the base excision repair (BER) pathway. It is initiated by a DNA glycosylase, specific to the 8-oxoguanine damage,

recognizing the site and cleaving the damaged base from its ribose-phosphate. This abasic site is recognized by a more non-specific series of proteins, which excises the abasic site and re-polymerizes the proper replacement nucleotide (12). Cellular DNA repair mechanisms to combat UVR-induced damage are thus quite robust.

Protein Photo-Damage

In contrast to DNA damage, few mechanisms for repairing photo-damage to proteins appear in the literature; cells tend to target photo-damaged proteins for degradation. As will be discussed in depth later, many cells in the eye lens are enucleated and maintained at very high protein concentrations such that photo-damage to lens DNA is less significant for disease development than damage to lens proteins. Photo-damage to proteins can occur in a wide variety of ways, and several will be described here.

Photodamage to proteins can be direct or indirect, similar to DNA (14). Direct reactions involve an amino acid or protein-bound chromophore that absorbs a UV photon, enters into an excited state and chemically reacts farther. Indirect photodamage occurs when a non-protein species, a photosensitizer, absorbs UV light, enters into an excited state, and either reacts itself with target proteins (type I) or transfers the excited state energy to molecular oxygen, creating singlet oxygen, a ROS that goes on to mediate oxidative photodamage (type II) (15, 16).

Direct Protein Photo-Damage

The photochemically active amino acids can form an extensive array of products, and the relative importance of an individual reaction path is dependent on the chemical environment of the amino acid, making protein photochemistry challenging to untangle. I will briefly summarize a selection of the photochemistry observed for the UVR absorbing amino acids. Tryptophan, tyrosine, histidine, phenylalanine, cysteine, and cystine can all absorb in the UV range and potentially enter into reactive excited states, undergoing direct photodamage (14). The aromatic amino acids absorb most strongly (phenylalanine < tyrosine < tryptophan) (14). The initial singlet excited states of the aromatic amino acids exist on the timescale of 0.01-0.1 μs (15). Chemical reaction of this state is outpaced by fluorescence, energy transfer, and intersystem crossing (15). Excited aromatics can transfer their excited state energies to other aromatic amino acids within the protein, or to molecular oxygen (15, 17-19), and the relative energetics of aromatic excited states (Phe>Tyr>Trp) can result in a rapid funneling of energy to tryptophan and its consequent dominance of the protein fluorescence spectrum. The aromatics' singlet excited states do not typically react themselves, but undergo intersystem crossing to the triplet excited states, which exist on the μs timescale (15). The chemistry of the triplet excited states will be described briefly here.

Triplet excited tryptophan was observed to photo-ionize and eject an electron in flash photolysis experiments (20), leaving behind a tryptophan radical cation. The ejected electron can react with nearby amino acids, like histidine, or

with oxygen to generate superoxide (15). Triplet tryptophan can also react with nearby cystine, generating tryptophan cation radicals. Tryptophan radical cations can undergo indole ring scission forming kynurenine and variations of kynurenine; the cation can also go on to react with oxygen, generating superoxide. This reaction is believed to be the basis of the photobleaching of proteins, the loss of 280 nm absorbance with continuing UV irradiation.

Triplet excited state tyrosine can react with cystine in a similar fashion to tryptophan (14, 15). Triplet tyrosine can also transfer electrons to nearby histidines and oxygen. The resulting tyrosine radical cations can dimerize with nearby tyrosine into dityrosine, or abstract alkyl hydrogens producing a new radical (21). Low levels of peptide bond cleavage products have also been observed due to direct tyrosine photochemistry (5).

The disulfide anion radical generated by the proximity of a disulfide bond to both triplet excited state tryptophan and tyrosine can break into a thiol anion and thiol radical, both of which can attack nearby amino acids or interact with oxygen to generate superoxide or thiyl peroxyl radical (6, 14, 15). This last species can isomerize and give rise to sulfinic and sulfonic acids, both irreversible cysteine oxidation products (22).

Triplet phenylalanine tends to either undergo radical photo-dissociation from the peptide backbone, or react with oxygen (14, 15). Its photoionizing ejection of an electron, leading to a phenylalanine cation radical, leads to hydroxylation of the aromatic ring (23).

Unfortunately, most of the data on direct amino acid photochemistry comes from experiments with purified monomeric amino acids or short peptide chains. Thus the range of reactions observed and their relative rates when in the context of a folded polypeptide *in vivo* may differ from those experimentally observed.

Indirect Protein Photo-Damage

Indirect photodamage to proteins can originate from a number of endogenous photo-sensitizing agents, including porphyrin, flavins, vitamin B6, NADPH, and melanin (24). Important for the lens setting, fiber cells contain significant levels of ascorbic acid and kynurenine based UV filter compounds (25, 26). Ascorbic acid oxidation products have been shown to covalently attach to lens proteins, forming so-called Advanced Glycation End-products (27). The attached ascorbic acid modification has been shown to absorb UVA, reacting in a type I mechanism with nearby protein sites to produce cross-links and oxidation (28). The kynurenine UV filters of the lens can also act as photosensitizers (29). 3-Hydroxykynureneine was shown to oxidize bovine α-crystallins and attach to a cysteine on the lens protein αB-crystallin in the absence of UVR or oxygen (30), and protein attached kynurenine has been shown to be more photochemically potent than free kynurenine (29, 31).

Reactive Oxygen Species and Photo-Damage

Reactive oxygen species can be generated from a number of the direct

and indirect damage processes mentioned above. Our tissue of interest, the lens, is avascular and maintained at a low oxygen concentration, but what is present has been suggested to be sufficient, over time, to cause oxidative damage (32). Eye injury and surgery have been shown to raise the level of oxygen in the lens significantly. The primary ROS involved in type II indirect photodamage is singlet excited state oxygen (24). Lens photosensitizers and protein amino acid chromophores can generate this species by transferring their excited state energy to nearby molecular oxygen; this energy transfer competes with other chemical methods of energy transfer (14, 15). While singlet oxygen can chemically react with many protein sites, it reacts most readily under physiological conditions (in descending order) with cysteine, histidine, tryptophan, methionine, and tyrosine (15).

Reactions between singlet oxygen and protein amino acids are diverse, but with the common motif of peroxide/endoperoxide addition leading to further radical chemistry, photosensitization and a variety of products. Tryptophan forms a number of kynurenine related products when it reacts with singlet oxygen; it is also the only amino acid that appreciably quenches singlet oxygen's excited state (4, 15, 33). Tyrosine and singlet oxygen form cyclized products that break down into peroxides associated with further radical generation and peptide bond breakage (5, 14, 33). Histidine and singlet oxygen form an endoperoxide on the imidazole ring, and from there undergo a series of reactions involving ring opening leading to histidine-histidine cross-links or other products, including urea (15).

In addition to covalent damage to individual amino acids, protein photo-damage can cause free radical polymerization. Free radical polymerization, involves the covalent cross-linking of individual protein subunits into large, insoluble complexes via radical chemistry. While it can involve unfolding, radical polymerization can occur with a protein's near native conformation (34).

Radical polymerization, or oxidative polymerization, as cases of it are sometimes called, has been observed in a number of proteins over the past decades. Roubal and Tappel in 1966 observed that protein polymerization occurred while they were studying the effects of peroxidation on lipids, and proposed a radical polymerization mechanism (35). ROS have been found to induce polymerization of hemoglobin and RNAse A (34, 36). UVR irradiation of peripheral-type benzodiazepine receptor generated ROS and caused the receptor to polymerize into isolatable multimers, with ROS concentration correlated with polymerization (37). Hydrogen peroxide was found to increase dityrosine cross-linking in wheat dough proteins, promoting polymerization (and improving the bread) (38). Hydrogen peroxide also promoted cross-linking and polymerization of sperm mitochondrial capsule proteins through reactions of its cysteines (39). The initiation of radical polymerization by UVR and ROS make it a relevant aggregation pathway in the eye lens.

Nearly all the chemical damages described above are irreversible in fully functional cells, and direly so for enucleated lens fiber cells. But two types of damage, photo-oxidative damage to methionine and cysteine residues by ROS,

both of which occur in the pathology of cataract, can be reversed and illustrate systems of redox protection present to some extent in the lens (40, 41).

Reversible Oxidative Damage: Thioredoxin and Glutathione

Methionine can be oxidized by ROS to methionine sulfoxide, which can react further photochemically or continue to be oxidized to the photochemically inert methionine sulfone, with limited radical cation formation from direct UVR absorption (42). Methionine sulfoxide has been shown to accumulate in the proteins of cataractous human lenses (41). Oxidized methionine can be returned to its reduced state by methionine sulfoxide reductases, present in the eye lens as MsrA, which is highly expressed in lens epithelial and young fiber cells (43). MsrA possesses several catalytic cysteines that interact with oxidized methionine (both free and in protein), reversing the damage, their active sites becoming oxidized to sulfenic acid (40). Oxidized MsrA enzymes are regenerated by the thioredoxin system, one of two major redox protective systems shown to be active in the lens (43). Thioredoxin reduces intra- and inter-molecular disulfide bonds, as well as sulfenic acid oxidation, but becomes oxidized itself (44). Another enzyme, thioredoxin reductase, uses NADPH, also shown to be present in the lens despite the tissue's relative metabolic inactivity (45), to reduce and reactivate thioredoxin. The relative ease at which methionine and cysteine oxidation occurs and can be reversed have led to suggestions that methionines on protein surfaces play a ROS scavenging role (46).

Certain types of cysteine photo-oxidation can be reversed by repair mechanisms. Cysteine thiols in close proximity can be photo-oxidized into disulfide bonds, while individual cysteines can be oxidized to sulfenic acid or, more severely, to sulfinic or sulfonic acids (Fig. 1.3) (22). Disulfides and sulfenic acids can be acted upon by the thioredoxin system outlined above, but they are also managed by glutathione (44, 47). Glutathione is a tripeptide redox regulator with a variety of functions: it can scavenge ROS, protect protein thiol groups, be added to proteins as a regulatory post-translational modification, and reverse oxidative damage to thiols (47). In the lens, where high levels of glutathione are maintained, elevated levels of glutathiolated cysteine residues have also been observed in oxidative stress models of cataract (48). Glutathione can reduce oxidized cysteine in proteins, glutathiolating the site. To remove glutathione and repair the oxidized protein, the enzyme glutaredoxin attacks the glutathiolated protein, producing a repaired protein and a glutathiolated glutaredoxin. Another molecule of glutathione is used to regenerate glutaredoxin, generating a disulfide-linked glutathione dimer that is separated into monomeric glutathione using NADPH (47).

Sulfinic acid was, until recently, thought to be an irreversible oxidation product of cysteine, but the enzyme sulfiredoxin has been shown to reverse the damage in an ATP-dependent reaction (49). Sulfiredoxins were found to regenerate inactive peroxiredoxins (enzymes that use thioredoxin to destroy hydrogen peroxide) that had been oxidized to sulfinic acid. No data exists on sulfiredoxin's presence or absence in the lens, but since its activity depends

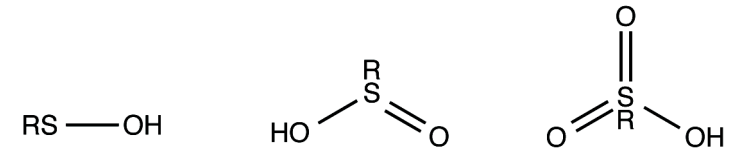

sulfenic acid sulfinic acid sulfonic acid

Figure 1.3 Cysteine Oxidation Products. Oxidation products of cysteine, in order of increasing oxidation from left to right. ‘R’ represents the rest of the protein.

upon ATP, it would likely be of limited effectiveness in fully differentiated fiber cells. A mitochondrially targeted peroxiredoxin has been identified in the lens epithelium and fiber cells, and is upregulated in the epithelium by oxidative stress (50). Sulfonic acid is still assumed to be irreversibly oxidized.

Degradation of Damaged Proteins

For photo-damage other than reversible methionine or cysteine oxidation described above, the only path for dealing with the damaged protein is degradation. Damaged proteins in active eukaryotic cells are degraded primarily by two systems: the ubiquitin proteasome pathway, and the lysosomal system . The lysosomal pathway is not an option in fully differentiated lens fiber cells that have degraded their organelles. In other cell types, autophagy leading to the lysosome can take three forms: macroautophagy, the engulfment of whole organelles and large sections of cytosol into an autophagosome and subsequent fusion with a lysosome; microautophagy, invagination of the lysosomal membrane to engulf and degrade complexes and individual species; and chaperone mediated autophagy (CMA), delivery of unfolded protein substrates to a pore on the lysosome by a chaperone and subsequent extrusion of an individual polypeptide into the lysosome (51, 52). Autophagy, in general, is able to process heavily oxidized proteins that the proteasome is unable to unfold and act upon (51). It has been shown that αB-crystallin damaged by 4-hydroxynonenal, a common lipid peroxidation product, is degraded by the lysosome in lens epithelial cells (53).

The ubiquitin proteasome pathway (UPP) begins with recognition of damaged or misfolded substrates, proceeds by tagging substrate lysines or N-termini with a chain of ubiquitin, a 76 amino acid protein, and ends with binding and degradation of tagged substrate by the 26S proteasome (54). Ubiquitin, a multipurpose protein tag added to proteins in branched or straight chains, acts as a degradation tag recognized by the proteasome. The 26S proteasome is a 2.4-MDa, multisubunit, symmetrical barrel organized into 6 ring-like layers (54). The end layers form the pores of the double-ended barrel and are composed of the 19S regulatory complexes. The 19S is a hexamer of AAA+ ATP-ases whose functions include recognition and unfolding of ubiquitin tagged substrates and ATP-dependent pore opening/closure. The inner 4 rings of the barrel make up the 20S catalytic unit, each layer a heptameric ring of different α or β subunits (rings arrayed $\alpha\beta\beta\alpha$). The β-rings inner surface contains the catalytic protease sites, while the α-rings act as gatekeepers, preventing access to the catalytic site even in the absence of the 19S. Ubiquitin is added to proteins by three classes of enzymes: E1 enzymes (ubiquitin activating proteins), E2 enyzmes (ubiquitin conjugating proteins that transfer ubiquitin from E1, via an E2-ubiquitin intermediate, to substrates), and E3 (ubiquitin ligases that bind specific substrates and contain ubiquitin transferring activity) (54).

Previous work by Taylor and coworkers found that the inner cortex and nucleus of the eye lens, sites where cataract occurs, had greatly reduced apparent UPP activity due to a decrease in ubiquitin conjugation and ligation (55). However, they also showed that all the components of the UPP were present in

the lens, both in the active lens epithelial cells and the enucleated fiber cells of the lens nucleus. Dudek et al. showed that lens proteins simulating deamidation with point mutations, like Q43E βB2-crystallin, were recognized by the UPP from lens epithelial cell lysates *in vitro* and degraded (56). Others, like γD-crystallin and a cataract disposed point mutant of γD-crystallin, V76D, were not ubiquitinated or degraded, showing that different lens proteins had different processing efficiencies by the lens UPP. Further work found that supplementation of UPP model systems with E2 conjugating enzymes and E3 ligases specific for tagging damaged proteins caused the successful tagging and degradation of V76D γD-crystallin (57). This body of work makes clear that the UPP, while active in parts of the lens, is significantly attenuated in the oldest parts of the lens where cataract can develop.

The Lens and Cataract

Much of this work will focus on cataract, a protein aggregation disease of the eye lens. One of the most ubiquitous and chronic risk factors for cataract is UVR exposure, thus UVR-induced protein aggregation serves as a model for cataract. To understand this disorder properly, we must consider the lens, where cataract occurs, the eye in which it functions, and the proteins contained within the lens cells where cataract begins.

The Human Eye

The human eye is a remarkable, elegant organ, detecting light in the visible range (400-700 nm) and forming a focused image using a series of tissues and organelles to provide the optics (58). Students of human anatomy have dissected and studied the eye for centuries. It consists of three layers: outer, middle, and inner (Fig. 1.4).

The Cornea, Sclera, and Limbus

From anterior to posterior, the outer layer contains the cornea, sclera, and limbus. The cornea is composed of a thin epithelial layer of cells on top of laminar layers of corneal stroma (58). The corneal stroma is made up of primarily collagen, enmeshed with glycosaminoglycans, that is bundled to run parallel to the corneal surface. Existing at a gas/liquid interface, the cornea contributes a significant amount of refractive power to the human eye. (58).

The sclera, commonly known as the “white” of the eye, is behind and around the cornea. It is composed mainly of the same collagen and glycosaminoglycan mixture as the cornea, but the organization is not parallel to the surface of the eye (58). This disordered web is opaque to light, but provides the eye a durable outer structure. The limbus is the transition zone between the cornea and sclera, and plays a role in the drainage of aqueous fluid from the anterior and posterior chambers behind the cornea and iris, respectively (58).

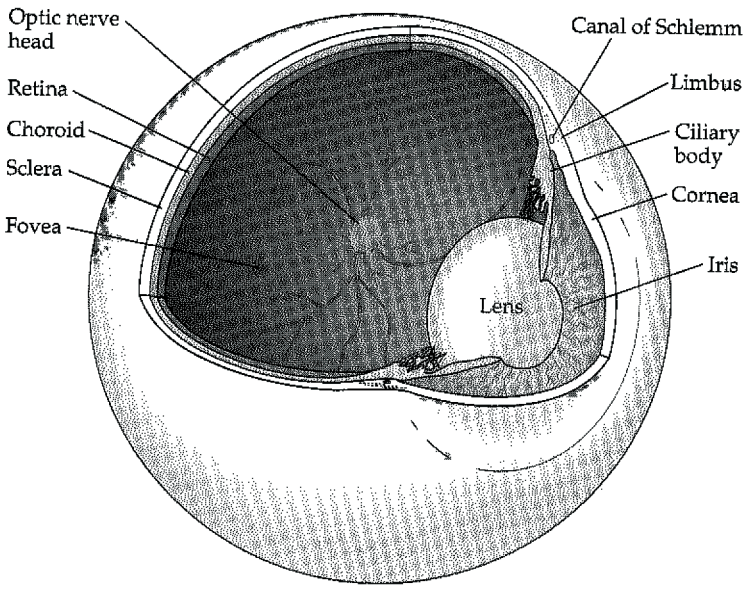

Figure 1.4 The Major Structures of the Human Eye A drawing of the major structures of the human eye.
Oyster, C. W. (1999) *The Human Eye: Structure and Function.* Sinauer Associates, Inc., Sunderland, MA, 78.

The Iris, Ciliary Body, and Choroid

The middle layer of the eye, also called the uveal tract, includes the iris, ciliary body, and choroid. Separated from the cornea by the aqueous filled anterior chamber, the pigmented iris controls the aperture of the eye, with two muscles, the sphincter and dilator, widening or shrinking the pupil (58). By changing the aperture, the iris changes the amount of light admitted into the eye interior while also controlling the diffraction and aberration affecting the image the eye perceives. The iris stroma is composed of disordered layers of fibroblasts, melanocytes, blood vessels, and spaces, giving it a sponge-like structure and supporting its role as a tissue constantly contracting and dilating (58).

Behind and continuous with the iris is the ciliary body, a muscular, heavily vascular ring. The ciliary processes, folds of capillaries and epithelium extending toward the lens, transform blood into aqueous humor, the liquid filling the posterior and anterior chambers (58). The aqueous is maintained at a low oxygen partial pressure compared to the blood by the metabolism of the corneal, lens, and ciliary epitheliums (32). It is high in ascorbate (also an oxygen sink), and low in protein; the aqueous bathes the iris and lens, which release their wastes into it and from which they take required metabolites (58). The muscular portion of the ciliary body acts on the lens. Zonules, long fibrils of elastin-like protein, connect the lens capsule to the ciliary body muscle fibers. When the ciliary body muscles flex, the lens bends, resulting in accommodation (58).

The choroid is the layer of the eye immediately beneath the sclera, a network of blood vessels within a connective stroma of collagen and fibroblasts,

strewn throughout with melanin pigment (58). The choroid's blood vessels supply oxygen and nutrients to the retina. The abundant melanin in the choroid absorbs stray rays of light and light that manages to pass through the retina (58). Such light would otherwise reflect back into the eye, causing a drop in image quality.

The Retina and Vitreous

The innermost layer of the eye is the retina. It contains the photo-receptors that transduce light into a rapidly transmittable chemical signal the body can interpret (58). Light is detected by membrane-bound photo-receptors, rhodopsins, made of different opsin proteins binding 11-cis-retinal, a visible range chromophore whose preferential absorption is tuned by the opsin it binds. Light is absorbed by 11-cis-retinal, which rapidly reacts, transforming into all-trans-retinal and causing a conformational change in opsin that allows it to start a G-protein-coupled signaling cascade (59). The rhodopsin activation cycle, which leads to rapid depolarization of the photo-receptor cell and nerve signaling, and the subsequent retinal regeneration cycle have been extensively studied (59-61). Photo-receptor cells are exquisitely sensitive, such that a single photon can produce a detectable signal; this also means the retina is very vulnerable to intense light and damaging higher energy ultraviolet radiation (61). Behind the photo-receptor cells and arrays of nerve cells and connecting cells, lies the retinal pigment epithelium (58). The retinal pigment epithelium contains large amounts of melanin, absorbing any light the photo-receptors miss, and the cell layer also helps recycle activated all-trans-retinal back into 11-cis-retinal.

Filling the sphere in front of the retina at the center of the eye is the largest eye component, the vitreous gel. The vitreous gel is a gelatinous mixture of water, collagen, and glycosaminoglycan (primarily hyaluronic acid) fibrils in no particular ordered structure, though fibers make attachments with the surrounding eye structures and are thickest in the vitreous cortex (58). The gel to liquid ratio of the vitreous begins high in infants, but drops over the lifetime of the individual, as liquid pockets appear. Dysfunction of the vitreous can lead to a number of vision-disrupting problems, like a rise in pO_2 in the lens (62).

The Lens

The structure of the mature lens is an ellipsoidal ball of cells surrounded by a capsule, with a thin layer of epithelial cells covering the anterior and equatorial surfaces. The majority of the lens' mass consists of layers of long lens fiber cells (Fig. 1.5) (58). Lens epithelial cells divide at the lens anterior, and migrate to the equatorial zone where they begin terminally differentiating into mature lens fiber cells. Each lens fiber cell wraps onto the existing ball of lens fiber cells (58). Fiber cell termini orient to end at sutures, lines along which fiber cells of a layer meet. In this way, lens fiber cells are continuously added in successive layers over an individual's lifetime. The outer layers of the lens, the lens cortex, contain differentiating fiber cells at varying stages of enucleation and levels of metabolic activity (63). The center of the lens, the lens nucleus, contains only mature enucleated fiber cells with the cells closer to the center being the oldest (64).

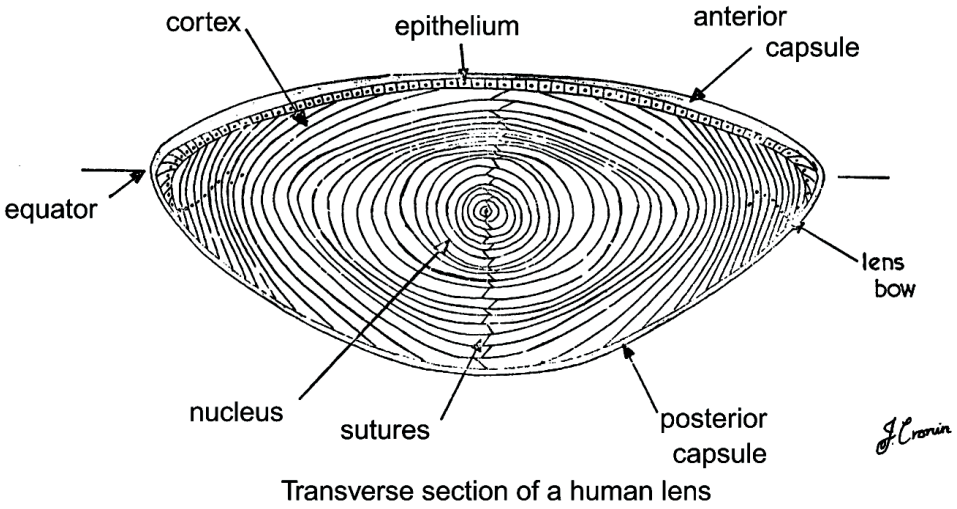

Figure 1.5 The Human Eye Lens A cross-sectional diagram of a mature human eye lens.
Reprinted from Ageing Research Reviews, 1(3), Harding, J., Viewing Molecular Mechanisms of Ageing Through a Lens, 465-479, 2002, with permission from Elsevier.

Lens Fiber Cell Differentiation

Lens epithelial cells reaching the lens equator begin to terminally differentiate into elongated enucleated lens fiber cells, expressing large amounts of the crystallin proteins (to final concentrations of ~320 mg/ml). Lens fiber cells contain significant concentrations of ascorbic acid, which is thought to act as an anti-oxidant, glutathione, a redox regulator, and kynurenine derivatives, which act as UVR filters (25, 26, 65). Fiber cells degrade their nuclei and organelles as part of differentiation (66).

Fiber cell organelle degradation is thought to take the form of an attenuated apoptosis, and inhibition of organelle degradation using exogenous Bcl2, an inhibitor of apoptosis, supports this view (63). αB-crystallin, the small heat-shock protein (sHSP) found at high concentrations throughout the lens and a known inhibitor of apoptosis, has been hypothesized to play a role in preventing complete cell death in differentiating fiber cells. However, several normally essential participants in apoptosis, including caspases 3, 6, and 7, are not required for organelle degradation in lens fiber cells, suggesting alternative mechanisms may be at work (63). Autophagy has also been suggested to play a role in lens fiber cell differentiation due to the appearance of autophagic vacuoles *in vitro* and signs of constitutive autophagic activity in differentiating fiber cells (67). However, in mutants lacking key autophagy-essential genes, organelle degradation was not prevented. Lens fiber cell differentiation appears to involve both known elements of controlled cell degradation and as yet uncharacterized elements.

Lens Development

The lens is one of the earliest recognizably differentiated components of the human eye (58). As the neural tube of a human embryo closes (~1 month after embryonic implantation), bilaterally positioned optic pits form, invaginations of the ectoderm that will grow into the optic vesicle. The optic vesicle is part of the neural ectoderm, from which the retina and the optic nerve will form. The surface ectoderm above the optic vesicle thickens, becoming the lens placode (58). The lens placode invaginates, and the hyaloid artery, a branch of the ophthalmic artery, connects to the growing lens as it buds off from the surface ectoderm to form a separate spherical balloon of epithelial cells, the lens vesicle, within the optical vesicle. By approximately week 53 of development, the posterior lens vesicle cells elongate toward the anterior cells and become the first of many lens cells to fully differentiate into enucleated lens fiber cells (68). The remaining anterior lens epithelial cells will form all of the lens fibers an individual will ever have, while also growing the lens capsule, an encasing layer of collagen and glycosaminoglycans. By the end of fetal development, the hyaloid artery will have regressed, and the lens will be alone, having grown to be ~3.2 mm thick (half the thickness of an adult lens), and containing over a thousand layers of fiber cells (58, 68).

Several genes stand out in their central roles in lens fiber cell differentiation, including *Pax6* and *Sox2,* which act independently and together as transcription factors in the presumptive lens epithelium (69). They upregulate basic-leucine zipper transcription factors of the Maf family, including *L-Maf*, *MafB*

and *c-Maf* which govern the broad expression of the crystallin proteins, the primary proteins of mature lens fiber cells (69, 70). These signaling cascades are themselves induced by signals from outside the lens vesicle, including BMP4/7, FGF, and Wnt/β-catenin signaling (71). Proximity to the optic vesicle and its associated morphogenic signaling are key to proper lens development (58).

Fluid Circulation

The mature lens is an avascular tissue, but a mechanism of fluid circulation was proposed by Mathias et al. (72). They suggested Na^+K^+ pumps in the anterior lens epithelium and posterior differentiating fiber cells create osmotic pressure that powers a paracellular flow of water, and with it required nutrients, from the aqueous (at the anterior pole) and the vitreous (at the posterior pole) toward the lens nucleus. A corresponding transcellular efflux exits the equatorial lens surface. This lens fluid circulation model (FCM), which has been updated and revised by others (73), is also based on a more active view of the mature lens fiber cells in which metabolic needs necessitate active transport. This has been controversial, with opponents arguing that diffusion alone will suffice to cover the meager needs of the relatively inert lens nucleus (74-77). But recent work monitoring fluid flow into and out of bovine lenses has demonstrated that Na^+-influenced circulation occurs (78), and as such the FCM remains a strong explanation of the transport of metabolites in the lens.

Isolation and Longevity

From the above morphological and physiological data, the lens appears to be an island in an already relatively isolated organ. It is a ball of cells encased in a capsule, sitting between the aqueous liquid of the posterior chamber in front and the vitreous gel behind, and held and bent by the zonule strands connecting it to the ciliary body (58). The lens is avascular, lacking any connection to the circulatory system (58). Unlike the cornea, which achieves transparency primarily through ordered layers of extracellular protein and glycoproteins, or the aqueous and vitreous, which are transparent and noncellular, the lens is entirely cellular (63, 79). Cells in the lens nucleus are metabolically inert, with no turnover of proteins over the lifetime of the individual. This long time scale presents unique challenges for a transparent tissue, since post-translational modifications to lens proteins will persist and over time lead to accumulation of damaged proteins.

Lens Transparency and Function

The lens' transparency is essential to its function. Different cellular components have significantly different refractive indices; as light moves through a solution, it is bent and scattered by each medium it passes through based on this property (63, 80). By degrading its organelles and producing large amounts of crystallin proteins, a lens fiber cell becomes as homogenous as possible with regards to refraction (63). This also provides an explanation for the tight wrapping of fiber cells into dense ordered layers, as extracellular space would differ from the intracellular high protein concentration refractive index.

Transparency is only part of the lens' function. The light passing through it must be focused into an image on the retina. The lens makes use of a gradient of refractive indices to greatly increase its optical power and minimize spherical aberration (58, 81). Lower refractive indices correspond to lower protein concentrations and can be found at the periphery of the lens, whereas higher protein concentrations correspond to higher refractive indices and are found in the lens nucleus (68, 82). Transparency and proper focusing depend entirely on lens fiber cells' proteins maintaining solubility and packing.

The lens has a secondary function: blocking the UVR that passes the cornea. The human lens fiber cells contain high concentrations of free UVR filtering compounds in the form of chemical variants of kynurenine, a metabolite of tryptophan (83). The most abundant forms, in human lenses, are 3-hydroxykynurenine-*O*-β-D-gluocoside, 4-(2-amino-3-hydroxy- phenyl)-4-oxobutanoic acid *O*-β-D-glucoside, and kynurenine (65). These filtering compounds absorb UVR across a wide range of UVB and UVA, and are thought to be a protective feature for the retina, which is very sensitive to UVR damage (Fig. 1.6) (84). The UVR filters have been shown to be unstable, with concentrations decreasing with age; lower concentrations were found in the nucleus than in the lens cortex (85).

Lens Proteins: The Crystallins

The primary proteins of the human lens are the lens crystallins, making up more than 90% of the protein content of mature lens fiber cells (66). Lens fiber

cells contain crystallins at concentrations of upwards of 300 mg/ml (66). Bovine lens fiber cells, filled with crystallins, display short-range organized packing, behaving like a very dense liquid, in SAXS experiments (86).

The human lens crystallins are divided into three classes α, β, and γ (Fig. 1.6 and 1.7). α-Crystallins are small heat shock proteins (sHSP's) and the major lens chaperone, making up approximately 35-50% of the lens crystallins content (66, 87, 88). The β/γ-crystallins are highly stable, two domain structural proteins, with each domain almost entirely composed of β-sheets arranged into double Greek Key structures (66). These specialized proteins give the lens its unique refractive properties, and due to the enucleated state of lens fiber cells, must remain stable and folded for the lifetime of an individual. Expression of the various crystallins is developmentally regulated; γ-crystallins, the most stable, are expressed earlier in life and thus more abundant in the lens nucleus, whereas the β-crystallins are more abundant in the cortex, being expressed more strongly later (89). The crystallin proteins will be explored in greater depth below.

α-Crystallin

Humans carry two copies of α-crystallin, αA-crystallin (HαA-Crys) and αB-crystallin (HαB-Crys) (89). They are 173 and 175 amino acids long, respectively, and have ~57% sequence homology between them. HαA-Crys and HαB-Crys together form polydisperse hetero-complexes in lens fiber cells of 26 to 28 units on average (88, 90). HαA-Crys is found only in the lens, whereas HαB-Crys is

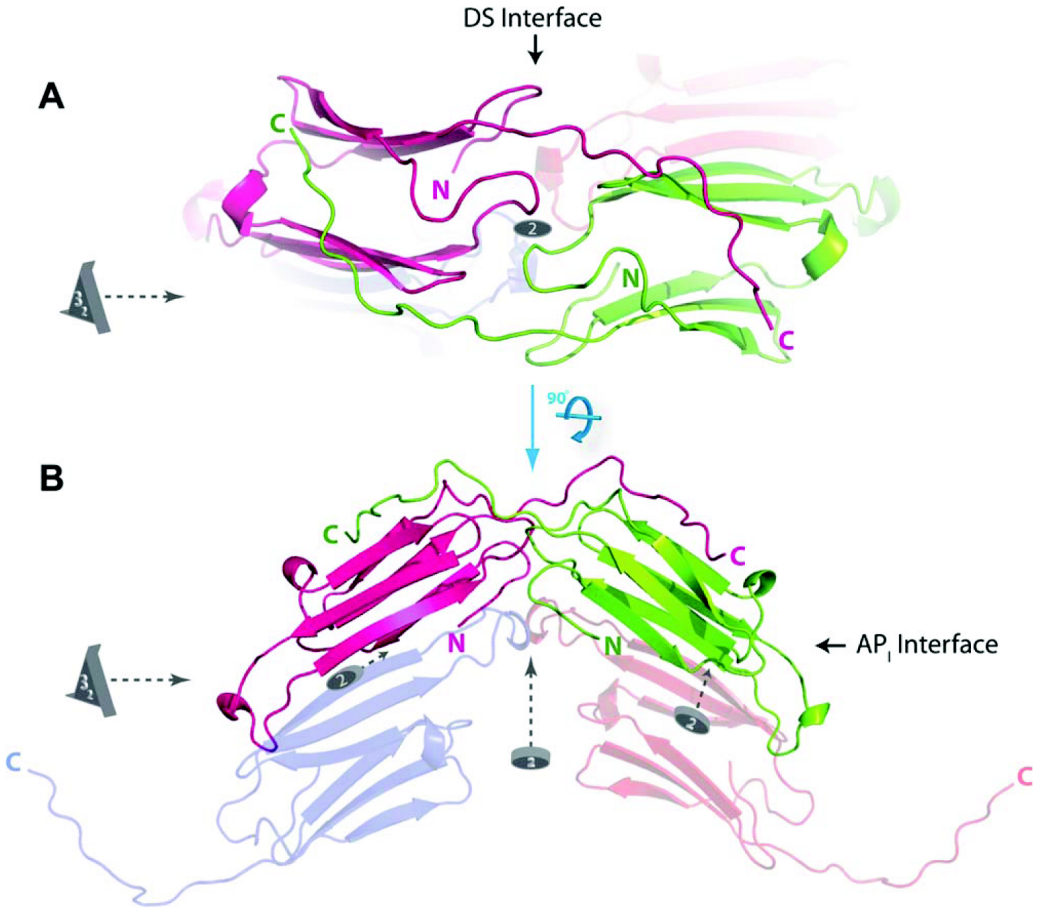

Figure 1.6 Three-dimensional Structure of HαB-Crys. Crystal structure of HαB-Crys residues 68-162, rotated 90° between A and B. The protein is primarily β-sheet, forming a dimer along a β-sheet interface (AP) and a domain swapped interface (DS), and also by swapping its palindromic C-terminal extensions. The multiple possible registers of the AP interface, along with the bidirectionality of the C-terminal extension's swapping suggest a mechanism for HαB-Crys' polydispersity.
Reprinted from Protein Science, 19(5), Laganowsky, A., et al, Crystal Structures of Truncated AlphaA and AlphaB Crystallins Reveal Structural Mechanisms of Polydispersity Important for Eye Lens Function, 1031-1043, 2010, with permission from John Wiley and Sons.
Published by Wiley-Blackwell. © 2010 The Protein Society

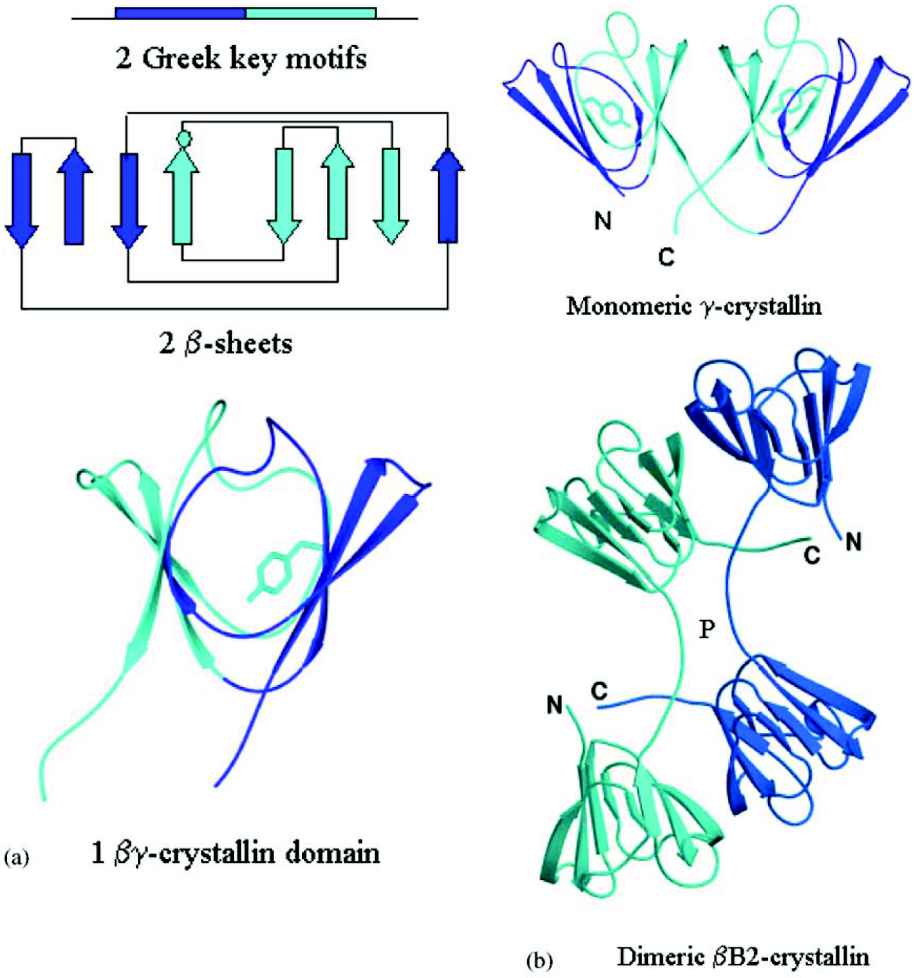

Figure 1.7 Three-dimensional Structure and Layout of the β-/γ-Crystallins. The double Greek Key layout of an individual β-/γ-crystallin domain in schematic form (note the exchange of the 3rd strand of each key and the position of the Greek key tyrosine corner) (top left); a crystal structure of an individual β-/γ-crystallin domain, highlighting the β-sandwich created by the Greek key, along with the structurally important tyrosine of the Greek key tyrosine corner (bottom left); a crystal structure of monomeric γ-crystallin (top right); a crystal structure of dimeric β-crystallin (bottom right).
Reprinted from Progress in Biophysics and Molecular Biology, 86(3), Bloemendal, H., et al, Ageing and Vision: Structure, Stability, and Function of Lens Crystallins, 407-485, 2004, with permission from Elsevier.

found ubiquitously in most human tissues (88). In the bovine lens, their ratio has been estimated to be approximately 3:1 A:B (91).

α-Crystallin is the archetypal member of the sHSP family of chaperones (91, 92), giving its name to the characteristic central domain of the sHSP's (90). sHSP's are a ubiquitous family of ATP-independent molecular chaperones that bind partially folded and aggregation prone species, preventing their aggregation (93). Purified bovine α-crystallin was originally shown by Horwitz to suppress thermal aggregation of bovine β-crystallin *in vitro* (87). Experiments studying knockout mice lacking either α-crystallin gene found that the lens chaperone is important for proper lens formation; mice without αA-crystallin develop cataract shortly after being born (94) while those without αB-crystallin displayed developmental defects and fiber cell differentiation problems (95). Selective removal of α-crystallin from monkey lens protein extracts increased the aggregation vulnerability of the remaining crystallin proteins (92). Increasing temperature has been shown by some studies to enhance α-crystallin's chaperone activity, and it was hypothesized that this was due to hetero-oligomer subunit exchange or increases in hydrophobic surfaces promoting chaperone activity (91, 96, 97). Like other sHSP's, α-crystallin stably binds its substrates without releasing them, maintaining them in a folding competent state but unable to refold them (93). The presence of other chaperones, like HSP70, HSP40, and HSP60, along with ATP brings about the release and refolding of α-crystallin-bound substrates *in vitro*, suggesting that in metabolically active cells, α-crystallin

works with the ATP-dependent chaperone system to prevent aggregation and refold substrates (98).

α-Crystallin's structure has long eluded investigators, but recent work by Horvitz, Eisenberg, Slingsby and coworkers has elucidated much of its structure (90, 99). α-Crystallin's tendency to form large polydisperse hetero-oligomers can confound techniques like X-ray crystallography, but truncated versions of the chaperone containing the central α-crystallin domain have had better luck. HαA-Crys and HαB-Crys structures (residues 59-163 and 68-162, respectively) revealed β-sheet rich structures with several dimerization interfaces: an anti-parallel β-sheet interface, and a C-terminal tail interaction (Fig. 1.6) (90). The anti-parallel β-sheet interface was found to have several possible registers, while the C-terminal tail sequence is palindromic and was found to bidirectionally domain swap with other α-crystallin subunits. These features appear to prevent any long-range ordering of α-crystallin, promoting polydispersity while preventing potential precipitation and crystallization.

β-/γ-Crystallins

The β/γ-crystallins are highly stable structural proteins, each two domains with each domain containing a double Greek Key, and are present in some form in all vertebrates (66, 100). The Greek Key fold is characterized by 4 anti-parallel β-strands paired similar to the repeating "greek key" pattern found on ancient Grecian artwork; in a β/γ-crystallin domain the third strand of each key is swapped with its partner key. The Greek Key fold is also characterized by highly

conserved tyrosine corners, sandwiched between tryptophans; these are present in the second key of each mammalian β/γ-crystallin domains and are important for protein stability (101). Sequence alignment and phylogenetic analysis across species suggests that the present day array of β/γ-crystallin genes arose early in the evolution of vertebrates (100). Single domain crystallin-like proteins have been found in bacteria and archaea, potentially extant copies of precursors to ancestral lens crystallins (102). Present day copies of human β/γ-crystallins are hypothesized to have arisen from multiple rounds of gene duplication (100).

The β-crystallins differ from the γ-crystallins in their stability, their N-terminal extensions, and their assembly into homo- and hetero-oligomers of varying sizes. In mammals, there are 6 β-crystallin genes, each with about 50% sequence identity to the others, and they can be divided into two classes: acidic (βA-crystallins) and basic (βB-crystallins), with βB-crystallins possessing C-terminal extensions (66). The human β-crystallins unfold and aggregate at lower temperatures than human γ-crystallins, indicating lower structural stability (66). Work by Bateman et al. showed that β-crystallins gain stability and undergo significant domain conformational changes when in hetero-dimers as compared to homo-dimers, and that hetero-dimers formed when mixing solutions of homo-dimeric human β-crystallins *in vitro* (103). Lampi and coworkers have researched the effects of deamidation, a common lens post-translational modification, on β-crystallins and found that deamidation destabilized them, promoting aggregation that is only partially prevented by α-crystallins (104).

γ-Crystallins, unlike β-crystallins, are monomeric and lack the N-terminal extensions of β-crystallins. In humans there are 7 γ-crystallin genes, A-F and S. Hγ(A,B,C, D, E, F)-Crys genes are located in tandem on chromosome 2, whereas the HγS-Crys gene, which is more divergent in sequence, is located on chromosome 3 (66, 89). HγA-Crys and HγB-Crys are not expressed in significant amounts compared to the abundant HγC-Crys, HγD-Crys, and HγS-Crys. The γE- and γF-crystallin genes are pseudogenes with stop codons disrupting their reading frames. HγC-Crys and HγD-Crys are expressed early in life, and are thus the primary γ-crystallins in the lens nucleus; HγS-Crys is more strongly expressed later in life, and occupies the lens cortex (66).

Human γD-Crystallin

Human γD-Crystallin (HγD-Crys) makes up 11% of the protein in the young human lens, making it one of the most abundant and oldest proteins in the human lens (105, 106). A number of cataract associated HγD-Crys mutants have been discovered, and these have provided some insights about the protein characteristics that lead to cataract.

The Folding and Stability of HγD-Crys

HγD-Crys has been used as a model for protein folding and stability (107-111) (Fig. 1.8). Slingsby and coworkers obtained a high resolution X-ray crystal structure of HγD-Crys in 2003, enabling detailed structural analyses (112).

a

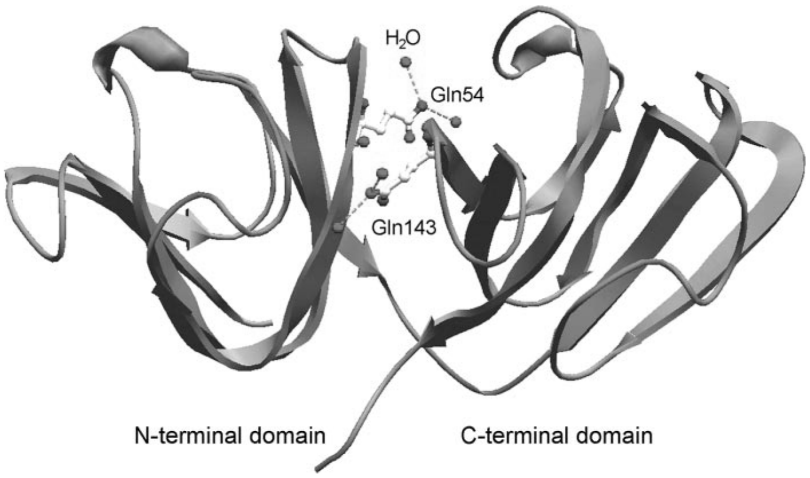
H2O
Gln54
Gln143
N-terminal domain
C-terminal domain

b

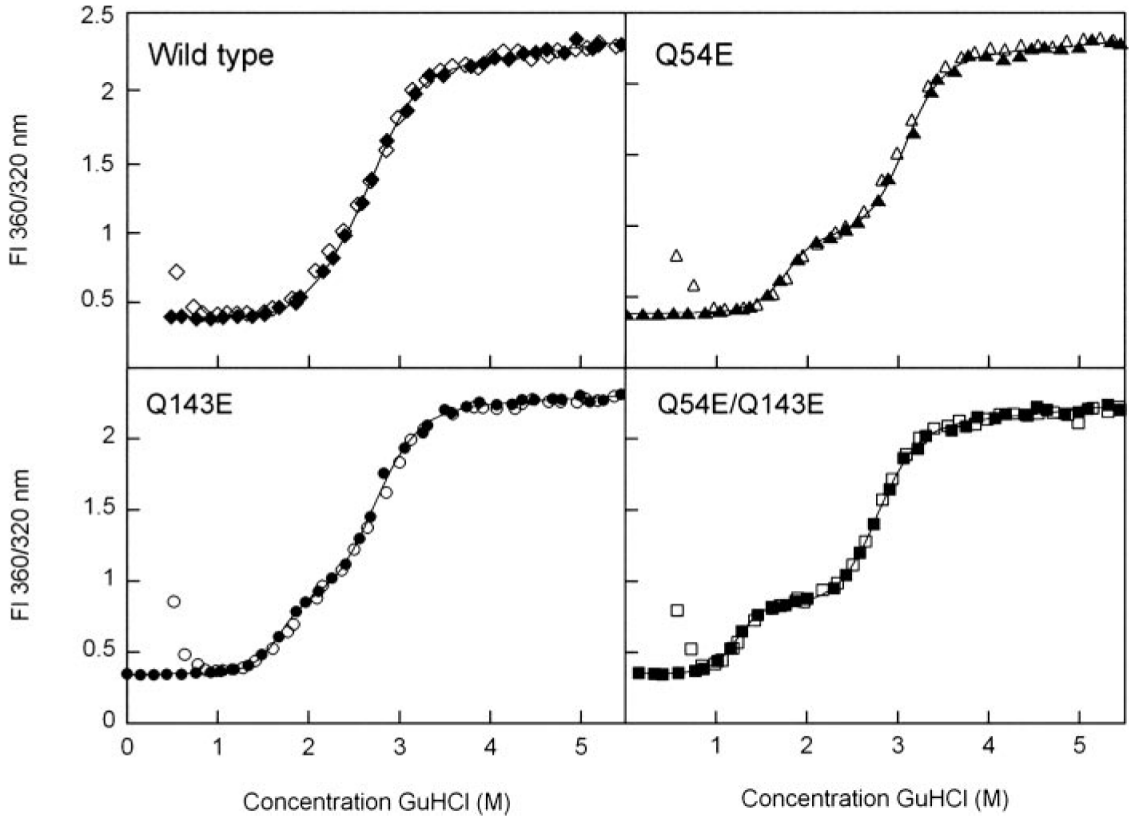
Wild type
Q54E
Q143E
Q54E/Q143E
FI 360/320 nm
FI 360/320 nm
Concentration GuHCl (M)
Concentration GuHCl (M)
0
0.5
1
1.5
2
2.5
0
1
2
3
4
5

c

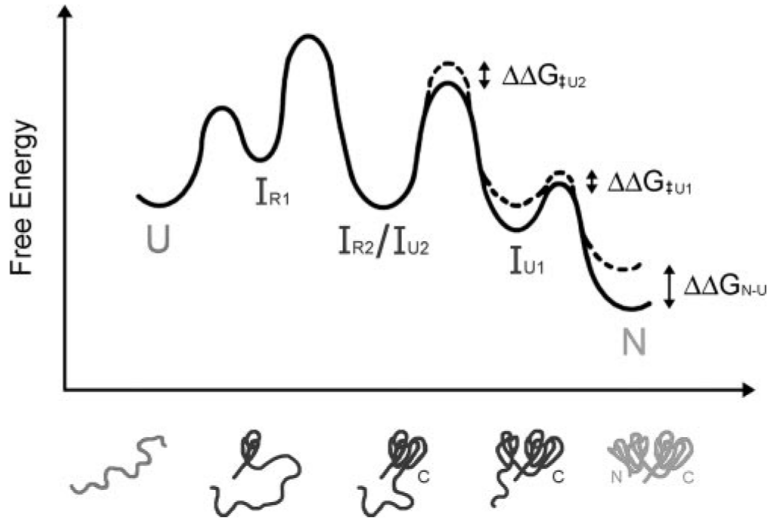

Figure 1.8 The Domain Interface and Folding of HγD-Crys. a) Crystal structure of HγD-Crys highlighting amide residues at the domain interface. b) Equilibrium unfolding (solid)/refolding (open) experiments monitoring HγD-Crys' folded state using tryptophan fluorescence versus GuHCl concentration. Mutating the interface amide residues causes a partially folded conformation to be populated at intermediate concentrations of GuHCl, suggesting one domain (the N-terminal domain, based on other data) is unfolded. c) Folding energy diagram depicting a model of the folding path of HγD-Crys, with dotted lines showing the postulated changes due to mutation of interface residues.
Reprinted from J. Biol. Chem., 281(41), Flaugh, S., et al, Glutamine Deamidation Destabilizes Human γD-Crystallin and Lowers the Kinetic Barrier to Unfolding, 30782-30793, 2006, with permission from the American Society for Biochemistry and Molecular Biology.

Purified recombinant HγD-Crys has been found to be extremely stable, with melting temperatures of ~82°C and requiring high concentrations of guanidine hydrochloride (GuHCl) to unfold (107, 113). Kosinski-Collins and King used equilibrium unfolding/refolding experiments to show that HγD-Crys denatured with guanidine HCl (GuHCl) unfolds in a 3-state manner, with the N-terminal domain unfolding before the C-terminal domain and leaving a partially folded intermediate (107). Work by Flaugh et al. found that the domain interface of HγD-Crys was extremely important for the folding and stability of the N-terminal domain, but not the C-terminal domain (109, 110, 113). Mutating the hydrophobic cluster at the interface or the flanking amide pairs populated a partially folded intermediate with the N-terminal domain unfolded and slowed N-terminal refolding, suggesting that the C-terminal domain folds first and provides a nucleating surface for N-terminal folding. Mills et al. confirmed the stability differential using truncated mutant HγD-Crys containing only single domains; single domains of both HγD-Crys, and also HγS-Crys, folded to native-like conformation and the C-terminal domains were both more stable than the N-terminal domains (111).

Recently, work has investigated the properties of HγD-Crys' aromatic residues. HγD-Crys, a 173 amino acid protein, contains 4 tryptophans, 14 tyrosines, and 6 phenylalanines, significantly more than the average expected occurrence for these residues (114). Aromatic residues play prominent roles in building the tightly ordered hydrophobic cores that are key to folded state stability,

and the selective pressure for stability in a long lived protein such as HγD-Crys could explain such an anomaly.

The Tryptophan Pairs of HγD-Crys

Each domain of HγD-Crys contains a pair of tryptophans, positioned in analogous orientations in each domain. These residues are conserved across nearly all human, rat, and bovine β/γ-crystallin sequences (115). Tryptophan intrinsic fluorescence has long been used to report on protein conformational state (116), and King and coworkers have utilized HγD-Crys' tryptophans to monitor the folded state through equilibrium unfolding/refolding experiments (107-111, 113, 117). Kosinski-Collins et al. observed anomalous native state quenching of HγD-Crys' tryptophans (107, 108). In most proteins studied, tryptophan fluorescence intensity is greater in rigid, hydrophobic environments than loose, hydrophilic ones; HγD-Crys' fluorescence was, unexpectedly, natively quenched, increasing when the protein unfolded (Fig. 1.9). This raised the question: what was causing quenching in HγD-Crys' native state?

Chen et al. studied multiple mutant HγD-Crys proteins with three out of the four tryptophans replaced with phenylalanine, leaving a single tryptophan remaining (118). They found that one member of each tryptophan pair, W68 and W156, was extremely quenched, with a shortened fluorescence lifetime and decreased quantum yield. The other members of each tryptophan pair, W42 and W130, were moderately fluorescent, but the presence of each residue's

a

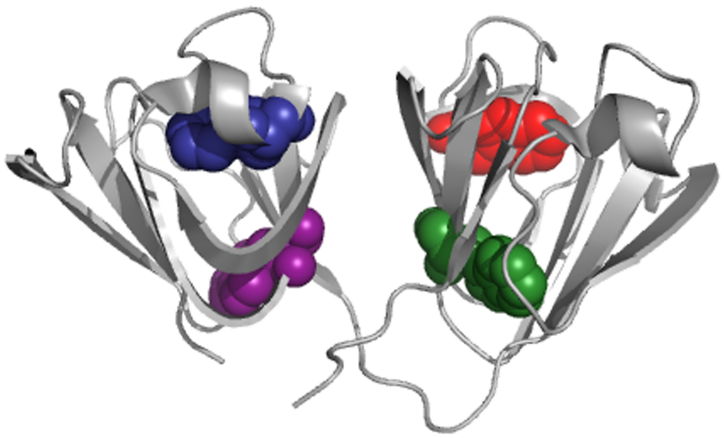

b

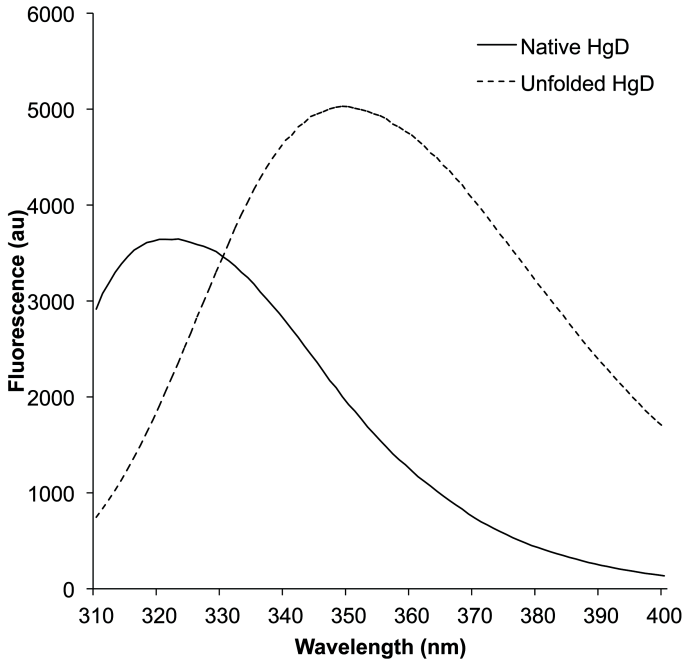

Figure 1.9 The Tryptophan Pairs and Native Quenching of HγD-Crys. a) X-ray crystallography structure of HγD-Crys (112) (PDB ID: 1HK0) displayed in ribbon form, with its 4 conserved Trp residues (W42 purple, W68 blue, W130 green, W156 red) highlighted in space filling form. b) Graph of WT HγD-Crys Trp fluorescence emission spectra upon 295 nm excitation in the native (solid line) and GuHCl unfolded (dashed line) states.
Reprinted from Photochem. Photobiol., Schafheimer, N., King, J., Tryptophan Cluster Protects Human γD-Crystallin from Ultraviolet Radiation-Induced Photoaggregation In Vitro, 2013.

quenched partner, studied with double and single W:F mutant HγD-Crys', shortened the fluorescence lifetime of the active partner (Fig. 1.10) (118, 119). Chen et al. mutated 17 sites surrounding the quenched tryptophans, and also utilized quantum mechanical-molecular mechanical (QM-MM) modeling to investigate the mechanism of quenching (118). They suggested that charged residues arrayed around W68 and W156 stabilized the charge transfer state, allowing electron transfer from the excited indole ring down to the amide backbone (120). Förster resonance energy transfer (FRET) appeared to explain the attenuation of W42 and W130 fluorescence, each ~12 Å from its quenched partner, well within the established range observed in other proteins (121). Further work established that the FRET and super-quenching of conserved tryptophans was at work in HγS-Crys as well, and analysis of available γ-crystallin structures suggested the mechanism could occur in most γ-crystallins (120).

These studies and others laid the foundation for the hypothesis that the shortened fluorescence excited states, energy transfer, and super-quenching of HγD-Crys tryptophans could be an evolved protective mechanism in γ-crystallins (120). HγD-Crys is an extremely long-lived protein, and its stability is essential for lens transparency. The lens is chronically exposed to UVR; photo-damage to HγD-Crys could cause destabilization of its native conformation, unfolding, and aggregation, leading to light scattering and cataract. A mechanism that could mitigate such threats could give a selective advantage.

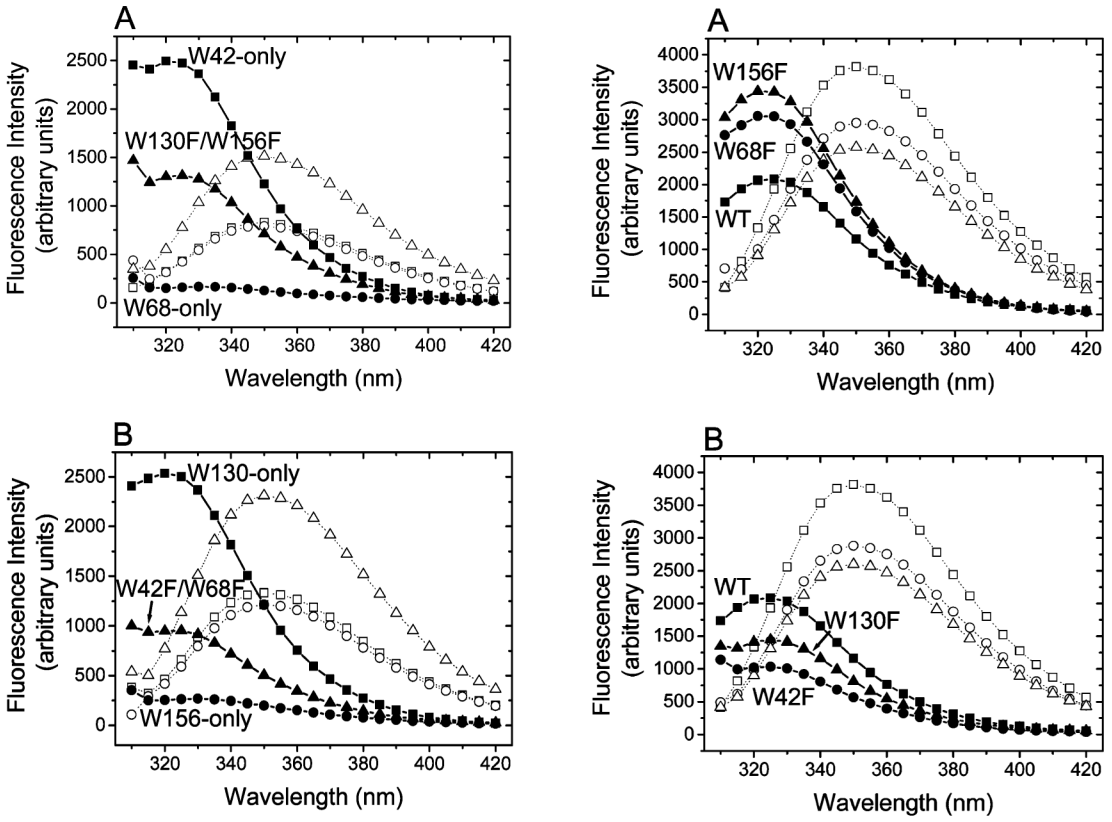

Figure 1.10 Identification of Quenched and Fluorescent Tryptophans. Native (solid) and unfolded (open) fluorescence spectra of mutant HγD-Crys constructs with single or multiple tryptophans replaced by phenylalanine.
Left A. In the native N-terminal domain, with both C-terminal tryptophans replaced with phenylalanine, W42 is quite fluorescent while W68 is extremely quenched, and when present together total fluorescence was attenuated compared to W42. When unfolded in GuHCl, this effect disappears; W42 and W68 appear equally fluorescent and their fluorescence is additive. Left B. A similar phenomenon is at work in the C-terminal domain. In the native C-terminal domain, with both N-terminal tryptophans replaced with phenylalanine, W130 is quite fluorescent while W156 is extremely quenched, and when present together total fluorescence was attenuated compared to W130. When unfolded in GuHCl, this effect disappears; W130 and W156 appear equally fluorescent and their fluorescence is additive.
Right A. When either W68 or W156 is replaced by phenylalanine, total fluorescence of native HγD-Crys rises; the anomalous increase vanishes once the protein is denatured. Right B. Mutation of W42 or W130 to phenylalanine decreases total fluorescence of native and denatured HγD-Crys.

The Tyrosine/Phenylalanine Pairs of HγD-Crys

Kong and King recently explored the roles of the aromatic pairs in stability and folding (115). Each domain of HγD-Crys contains three aromatic residue pairs (Fig. 1.11). Two of these pairs, Y6/F11 and Y45/Y50 in the N-terminal domain and Y92A/Y97A and Y133/Y138 in the C-terminal domain, are conserved between corresponding Greek Keys, positioned in analogous orientations, and designated 'Greek Key pairs.' They are highly conserved among vertebrate β/γ-crystallin sequences (115). The remaining pairs in each domain, Y16/Y28 and F115/F117, are positioned uniquely, and are called the 'Non-Greek Key pairs' and are much more weakly conserved.

Double mutant HγD-Crys constructs with both members of a pair mutated to alanine were significantly destabilized compared to WT, but assumed a native-like conformation (115). Similar to the interface mutants and destabilizing mutants described above, mutants of the N-terminal pairs destabilized just N-terminal domain and caused it to unfold more quickly. Mutating aromatic pairs of the C-terminal domain caused unfolding of HγD-Crys to become faster and more cooperative between domains. Consistent with other data showing that the domain interface of HγD-Crys is a nucleating surface for folding, double mutants affecting the 2nd Greek Key of each domain (which form the interface) slowed refolding compared to WT while those in the 1st Greek Key did not (115). This data suggests important roles for the aromatic pairs in the stability and folding of HγD-Crys.

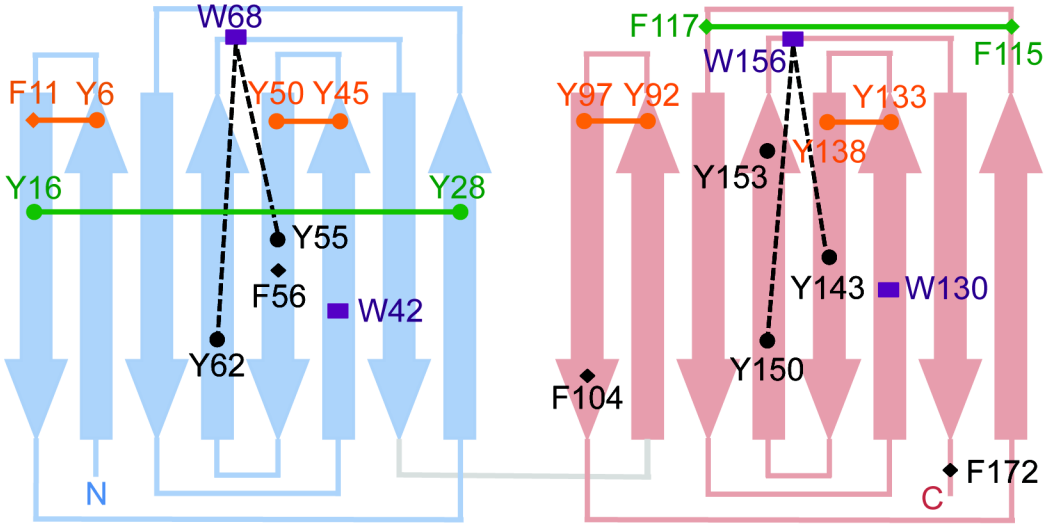

Figure 1.11 Schematic of Aromatic Residues in HγD-Crys. Structure of HγD-Crys in schematic form with the N-terminal domain in blue and the C-terminal domain in red. The positions of the aromatic amino acids are labeled with circles representing tyrosines, diamonds phenylalanine, and purple rectangles tryptophans. Connected orange colored residues are members of the Greek Key aromatic pairs, connected green are members of the non-Greek Key aromatic pairs, and black residues are not members of pairs, with dotted black lines showing participation in a tyrosine, tryptophan, tyrosine cluster.

HγD-Crys Aggregation

Though the aggregated state of the crystallins in cataract is ill-defined, there has been considerable study of the aggregation of the isolated proteins *in vitro*. During equilibrium unfolding/refolding experiments, Kosinski-Collins and King observed that aggregation competed with productive refolding when HγD-Crys was diluted out of high GuHCl to concentrations below 1 M (107). Atomic force microscopy experiments with refolding aggregates revealed that HγD-Crys was aggregating into elongated complexes. Acosta-Sampson and King showed that HαB-Crys recognized partially folded HγD-Crys formed from dilution out of high concentrations of GuHCl and suppressed its aggregation, holding it in a partially folded state (105). However, at least in the adult lens where cataract begins, the crystallins are believed to be native or native-like.

Another form of aggregation that begins with the native state is conversion to amyloid fibrils at low pH. Papanikolopoulou et al. found that at pH 3, HγD-Crys, both full length and isolated domains, forms amyloid fibrils (122). Wang et al. found that HγC-Crys, which has 71% sequence identity with HγD-Crys and is also strongly expressed in the lens nucleus, also formed amyloid fibrils at low pH (123). R120G mutant HαB-Crys is associated with desmin-related myopathy and has been shown to assemble into amyloid fibrils *in vitro* (124). These examples suggest that the crystallins, including HγD-Crys, are capable of forming amyloid aggregates, although it is not clear that age-related cataract involves amyloid.

Thermal unfolding experiments also caused HγD-Crys to aggregate, suggesting that a partially folded, aggregation prone state is populated during the

thermal unfolding process (113). HαB-Crys suppressed thermal aggregation of crystallin proteins (87), suggesting that the thermal aggregation pathway may be similar to those HαB-Crys suppresses *in vivo*. Heat also caused lens crystallins, primarily α-crystallins, to bind lens fiber cell membranes when young human lenses were exposed to mild thermal stress (125). Protein buildup on fiber cell membranes is a characteristic of aged lenses, and Friedrich and Truscott's report suggests a mechanism for the formation of such an obstruction (125). This data suggests that the thermal aggregation path which HγD-Crys can participate in bears some similarities to physiological aggregation processes.

Recent work by Wang and Wen found that HγD-Crys exposed to 254 nm UVC light aggregated covalently, and implicated non-native cysteine disulfide bonds as a mechanism of aggregation (126). The young lens contains high concentrations of glutathione which could suppress disulfide bond formation, but those decrease over a human lifetime (127). Photo-aggregation of bovine γ-crystallin was suppressed by α-crystallin, suggesting, similar to thermal aggregation above, that *in vitro* photo-aggregation resembles *in vivo* processes targeted by the lens chaperone (128).

Cataract

Cataract is a disease of the eye lens involving the development of lens opacities. It affects primarily the elderly, and the disease's progression leads to blurring of the visual image ending with blindness. Cataract is the most common cause of blindness in the world (129). In the United States, there are 22 million

cases of cataract, with over half of Americans affected by age 80 (130). The only treatment for cataract is surgical removal of the lens and replacement with a plastic lens. The surgery, while routine in the U.S., is costly (131). The National Eye Institute estimates that the U.S. spends about $6.8 billion every year on cataract treatment (130). Secondary cataract, a common post-treatment complication, can necessitate a second surgery. Eye surgery requires modern medical facilities, and access and funding for cataract operations are not available to a large segment of the global population (132). Projected population growth in the next decade in developing countries and the increase in the proportion of older individuals in the population will exacerbate the problems of accessing and affording limited eye care resources (133). The estimated economic and social price of cataract associated blindness are steep (131), with billions of dollars in lost productivity and increased morbidity.

Age-Related Cataract: Types and Characterization

Age-related cataract is the most common form of cataract. It can be sub-classified by the region of the lens in which opacities form: nuclear, cortical, and posterior sub-capsular (Fig. 1.12) (79). Its pathology has been viewed in several ways, most commonly, as a protein misfolding and aggregation disorder (66, 134).

The lens nucleus stiffens with age, becoming discolored, and its proteins, which are as old as the human seeing through them, become increasingly covalently modified, membrane associated, and insoluble (68, 135, 136). The

a

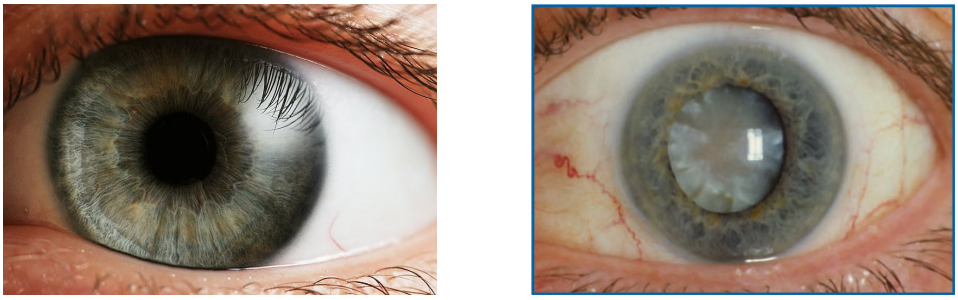

b

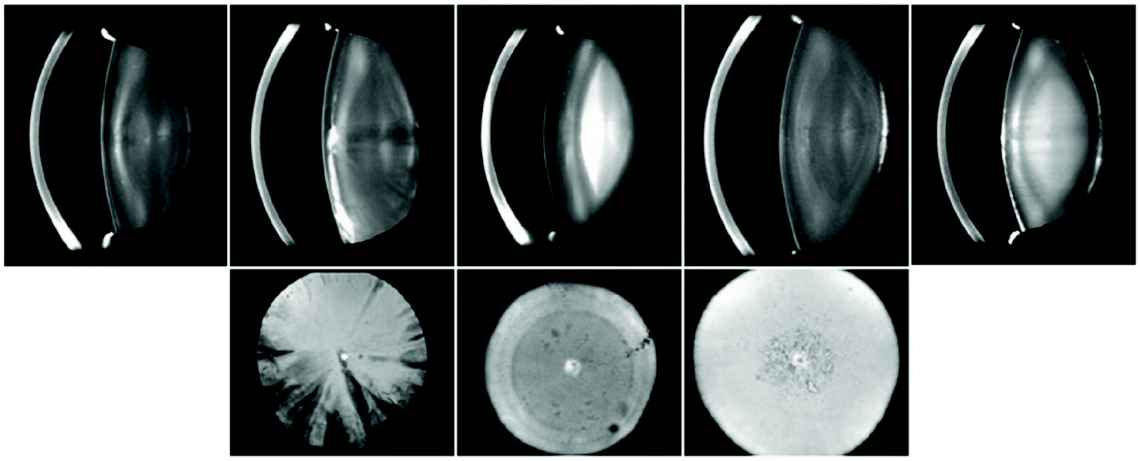

Figure 1.12 Cataract Presentation and Localization. a) A normal human eye (left) and a human eye with advanced nuclear cataract (right). b) Slit lamp Scheimpflug images of eyes with different types of cataract (top), and retroillumination images of those cataract classes (bottom).
(b) Reprinted from Seminars in Cell & Developmental Biology, 19(2), Beebe, D. C., Maintaining Transparency: A Review of the Developmental Physiology and Pathophysiology of Two Avascular Tissues, 125-133, 2008, with permission from Elsevier.

difference between these ‘normal’ aging changes and nuclear cataract is the degree to which proteins become insoluble and aggregate. Aged lenses containing nuclear cataracts had decreased free glutathione and increased lens protein methionine and cysteine oxidation when compared to healthy lenses, suggesting that oxidation may be important for nuclear cataract (127, 137). Patients treated with hyperbaric oxygen were found to have a high risk of nuclear cataract after treatment, supporting this association (137, 138). Covalent modifications to lens proteins will be discussed in depth below.

Cortical cataracts occur in the cortex, the lens periphery. Unlike nuclear cataract, which is often a uniform change to the lens nucleus based in part in normal aging processes, cortical cataracts often involve disruption of fiber cell structure, beginning with small areas of cortical cells near the equator, and these changes are not normally age-associated (139, 140). Cortical cataracts progress in severity as the protein aggregation and cell disruptions spread from the equatorial ‘center’ of the fiber cells toward their tips (140). Only disruptions in the cortical cell tips will block light passing through the lens . Risk for cortical cataract has been consistently associated with increased UVR exposure, although, as will be discussed later, estimating UVR exposure to the eye is problematic (141).

Posterior subcapsular cataract is thought to occur when fiber cells fail to differentiate properly and continue migrating toward the posterior of the lens (140). As these cells accumulate at the back center of the lens, they increasingly

scatter light, making the visual image perceived blurry. Little is known about what causes posterior subcapsular cataract, though it is associated with myopia, diabetes, and steroid treatment (140).

Covalent Damages In Cataract Proteins

A number of covalent protein modifications have been observed in aging and cataractous human lenses. Deamidation, glycation, protein truncation, and oxidation have all been found enriched in older lenses (66, 142). I will briefly highlight evidence for each major modification's contribution to cataract here. Covalent changes to human lens proteins accumulate over the course of a lifetime, and mature-onset cataract only develops late in life. It remains to be determined whether the important, cataractogenic damage is the sum of the damage that occurs throughout life, or only damage that occurs late in life near to the development of cataract symptoms.

Non-enzymatic deamidation of asparagine and glutamine side chains was the most abundant age-dependent modification observed in several studies comparing young and old human lenses (143, 144). Multiple specific deamidation sites in the lens proteins, the α-, β-, and γ-crystallins, were found using HPLC and mass spectrometry. Deamidation was shown to destabilize protein native state structures *in vitro* (104), and in α-crystallin to inhibit chaperone activity (145), suggesting that this modification may contribute to aggregation and cataract.

Advanced glycation end-products, in which lens protein lysines become attached to glucose or auto-oxidized ascorbate, have also been shown to accumulate in aged lens (146). Glycation by ascorbate has been found to photo-sensitize lens proteins to further covalent damage from ultraviolet light (27, 28). It is interesting that even protective compounds like the anti-oxidant ascorbate can apparently modify and photo-sensitize lens proteins (26).

Truncated protein products were shown by Friedrich et al. to accumulate with age in lens fiber cells, and also to bind to fiber cell membranes, potentially blocking lens circulation (136). Other work using MALDI imaging mass spectroscopy to analyze cryo-sections of rabbit and bovine lenses showed that α-crystallin, the lens chaperone, was present in primarily truncated forms in the older, central portions of the lens, and only whole in the periphery (147, 148). These data suggests that aged lenses contain a high amount of truncated protein, which may contribute to aggregate formation.

Oxidation is a major protein modification found to increase with aging in the lens (66, 142). Increases in oxidation of cysteines to disulfide bonded cystine were seen when comparing nuclear cataractous lenses to age-matched normal lenses (41). Oxidation of Trp, Tyr, and His residues of purified bovine lens proteins was seen by Balasubramanian et al. when samples were exposed to singlet oxygen *in vitro* (24), and some oxidation products led to covalent cross-linking of lens proteins. From this, it appears oxidation of lens proteins could lead to cataract by the creation of covalent cross-links, or by oxidation of

aromatic amino acids of the hydrophobic core, disrupting the stable packing of the protein and leading to partial unfolding.

Unfortunately, in humans there is no time course data for the development of cataract with age. Cataractous lenses examined post-mortem represent late time points in the progression of the disease. Lacking earlier data, the covalent damages that have accumulated in cataractous lens proteins may be a cause of cataract or a consequence of some other change in the lens that is actually at the root of the disease. But the age-dependent drop in several lens compounds that protect against covalent damage, like glutathione and kynurenine, supports covalent modification as a cause for cataract (85, 127).

Lens Protein Aggregation

Cataract proteins removed by surgery from the lens were in the form of high molecular weight aggregates consisting of crystallin proteins (149). The aggregates required strong denaturants for solubilization (149). As a result there is very limited direct data on the conformation of the proteins within the aggregate. Electron microscopy of thin sections of cataractous lens did not revealed any distinctive morphologies (150, 151). The stability of the aggregated state and its resistance to proteolysis is reminiscient of amyloid fibrils.

Amyloid Fibrillation

Amyloid fibrils are regular, repeating structures, consisting entirely of β-sheets arranged in a characteristic cross-β structure, with the β-strands oriented

perpendicular to the axis of the elongating fibril (152, 153). Amyloid fibrils begin as small oligomeric protein 'seeds,' assembled from non-native proteins revealing amyloidogenic, often β- sheet rich, segments (153). Oligomers grow into the stable nucleus of a fibril, and from there each end of the fibril elongates by adding on more proteins, templating its extremely stable misfolded state. Amyloid fibrils are distinctive and easily seen via electron microscopy; several dyes, namely thioflavin T and Congo Red, have been found to selectively bind amyloid and display a change in fluorescence or birefringence, respectively (153).

Amyloid formation is at the heart of a number of diseases. Mutant superoxide dismutase 1 can assemble into amyloid fibrils and causes the familial form of the motor neuron disease amyotrophic lateral sclerosis (154). Alzheimer's disease is characterized by amyloid fibril formation of Aβ, a cleaved section of a membrane protein (155). Spongiform encephalopathies (prion diseases), cerebellar ataxias (a polyQ expansion like Huntingtin), systemic amyloidosis, and many more all involve amyloid formation in their pathology, marking this type of protein aggregation as a major unsolved problem for both biology and medicine (153). Despite studies observing HγD-Crys amyloid formation at pH 3 *in vitro* (122, 123), there is no evidence that amyloid fibrils are a major component of mature-onset cataract. However, that does not rule out a role in the initiation of cataract formation.

Non-Amyloid Aggregation

Non-amyloid aggregation examples are diverse in character and context.

In the cell, large associations of insoluble protein, usually in partially folded non-native states, are often bundled as part of inclusion bodies; inclusion body formation can be part of a cell's defense against the spread of aggregation. Huntingtin protein, the aggregating protein whose poly-glutamine expansions are associated with the neurodegenerative disease Huntington, can assemble into non-amyloid and amyloid aggregates (156). Tau, a microtubule stabilizing protein, is associated with Alzheimer's disease and is known to assemble into non-amyloid neurofibrillar tangles with a paired helical filament structure when hyperphosphorylated (157). Mutant versions of Tau that cause tangles to form earlier or more severely carry an increased risk of Alzheimer's (157).

The examples of non-amyloid aggregation described above all involve primarily non-native or partially folded proteins. Native proteins can also aggregate. Perhaps the most well studied example of native aggregation is the sickle cell-associated mutant hemoglobin tetramer. An E6V point mutation in the β-globin subunit creates a surface hydrophobic patch causing the natively folded hemoglobin tetramer to polymerize into long chains when in a deoxygenated state (158).

Propagating domain swapping is a special type of protein aggregation that can involve proteins in the native or partially unfolded state (159, 160). Under mild denaturing conditions, monomeric proteins can exchange some of their secondary or tertiary structural elements with a partner. If this exchange is not closed (i.e. non-reciprocal), the partner can do the same with a third partner, creating an elongating chain of proteins. The elements exchanged can be as

small as individual loops, strands, or helices, or as large as whole domains. E342K mutant alpha$_1$-antitrypsin can polymerize into non-amyloid aggregates by exchanging its cleaved conformation reactive loop with the sheet of a partner alpha$_1$-antitrypsin, and this polymerization is at the root of a genetic variant of the disease emphysema (159). Domain swapping can also produce amyloid type aggregates, as in the case of cystatins, a family of cysteine protease inhibitors (160). Under thermal stress, cystatins can make a closed exchange of their β-sheet segments to form dimers, or a non-reciprocal exchange to form an amyloid type cross-β structure. In the context of the lens, domain swapping was proposed as a possible mechanism for aggregation of partially unfolded domain interface mutants of HγD-Crys by Flaugh et al. (113).

Pathological Significance of Aggregation

Aggregates are detrimental to cells for a number of reasons. Sometimes, like the case of cystic fibrosis, misfolding denies the cell a protein with a vital function. A common variant of cystic fibrosis involves a mutated ion channel expressed in lung cells, which, due to its inability to fold properly, is degraded (161). The absence of its function causes the buildup of mucus in the lungs which leads to the disease phenotype. Aggregates can also physically disrupt the cell. Sickle cell anemia patients' hemoglobin polymers disrupt the normal donut shape of red blood cells, forcing them into rigid sickle shapes that cause the disease phenotype (158). Additionally, aggregation may indirectly disrupt a cell by sequestering functional proteins within aggregate complexes and inclusion

bodies. In the case of cataract, the primary pathology is the aggregated state, which scatters light in a transparent tissue.

HγD-Crys Early-Onset Cataract Mutants

A number of a mutations in HγD-Crys have been identified that cause early-onset cataract, and have helped identify models of cataractogenesis. Pande, Benedek and coworkers examined R14C, a congenital cataract mutation, and found evidence that the aggregates the mutant proteins assembled into were disulfide-based (162). They also explored R58H and R36S, a crystal-cataract mutant and a congenital mutant, respectively, finding that both crystallized much more readily than WT despite native folding. It was found that R58H and R36S HγD-Crys had higher crystal nucleation rates than WT, suggesting changes in protein solubility behavior could promote aggregation (163). The importance of solubility was further expounded when Pande et al. characterized P23T; it was found to have increased hydrophobicity, and expose hydrophobic surface patches on the N-terminal domain that lowered its solubility (164). Pulla Rao Vendra and Balasubramanian investigated E107A, a congenital cataract associated mutation, and found that it, too, lowered the solubility of HγD-Crys without significantly changing stability or conformation (165). These mutations represent a theme that many early-onset cataract associated mutations studied do not act via destabilization, but rather through changing surface charge makeup and solubility.

This is in contrast to some other mutant proteins studied that act on stability and chaperone affinity to cause the development of light scatter. Banerjee et al. found, in apparent conflict with Pulla Rao Vendra 2010, that the E107A mutation did not change solubility but instead altered HγD-Crys' pI and increased its binding to HαB-Crys, contributing to the formation of light scattering phase separation (166).

Moreau and King found that L5S, V75D, and I90F HγD-Crys mutants, all congenital cataract associated mutations in mice, are significantly destabilized compared to WT (117), displaying increased unfolding speed when exposed to denaturant. Additionally, the native state of I90F and V75D exhibited an aggregation pathway not found in WT; the aggregated state was not amyloid in character. I90F HγD-Crys aggregation was not suppressed by HαB-Crys, demonstrating chaperone escape as a method of cataract development (167). Stability and chaperone mis-interactions represent another avenue for mutations to lead to cataract.

A Protein Aggregation Model for Cataract

In the prevailing protein misfolding/aggregation model of age-related nuclear cataract, covalent damages accumulate on lens proteins over the course of an individual's lifetime, causing partial unfolding into aggregation prone conformations (Fig. 1.13) (105). Because mature lens fiber cells lack organelles and most metabolic activities, damaged proteins cannot be degraded (66). Over time, these aggregation prone species accumulate, titrating away free lens

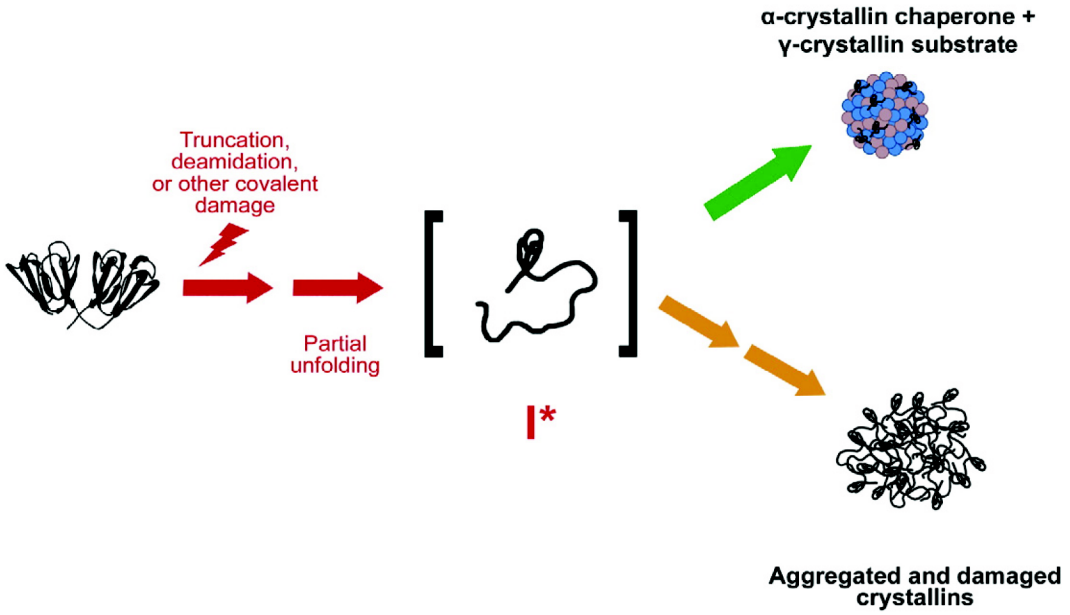

Figure 1.13 A Model for Cataract by Protein Misfolding and Aggregation. A proposed model for age-related cataract.
Reprinted from J. Mol. Biol., 401(1), Acosta-Sampson, L., King, J., Partially Folded Aggregation Intermediates of Human γD-, γC, and γS-Crystallin Are Recognized and Bound by Human αB-Crystallin Chaperone, 134-152, 2010, with permission from Elsevier.

chaperone (105). Once chaperone capacity is reached, lens proteins irreversibly aggregate, assembling into high molecular weight complexes which disrupt the regular protein packing and refractive index of the lens fiber cells, scattering light and blurring the visual image (105).

Risk Factors and Treatment

Besides age, several risk factors have been identified that significantly increase an individual's risk for developing cataract. The influence of latitude, ethnicity, socioeconomics, and the presence of other illnesses like diabetes or glaucoma, with cataract have been examined (133), but these characteristics are less malleable than others studied. Taylor remarked that the direct risk factors can generally be classified under the 5 D's: daylight, diet, dehydration, drugs, and "don't know" (168). Studies have shown that diets deficient in several vitamins, particularly vitamin C, have increased risk of cataract (169). Individuals who have had severe dehydration incidents, like those caused by prolonged diarrhea, are also at increased risk of cataract (170). A number of drugs, both prescribed, like statins, and recreational, like tobacco and alcohol, have been associated with cataract (129, 171). Solar ultraviolet radiation (UVR) exposure has been associated with the development of cortical lens opacities (141, 172), and occupational studies have found linkage of high sunlight exposure to cataract (173). The weakness of the epidemiological linkage of UVR and cataract has been suggested to be due to the difficulty in accurately measuring the lifetime UVR dose of an individual (133, 174), and is discussed further below.

Several alternative experimental treatments for cataract addressing particular risk factors are under investigation, but none have achieved clinically proven success in human patients. Carnosine, a dipeptide of histidine and β-alanine, has been shown, in several chemical derivations, by some studies to have anti-oxidant properties (175). It was also shown to display chaperone-like activity (176), and eye drop solutions of carnosine alone or coupled with other drugs have been shown to be protective against cataract (177). However, this treatment is controversial because other studies have found no protective effect to carnosine treatment (134).

Short peptides of the lens chaperone, αB-crystallin, when injected into rats intraperitoneally, have recently been shown to delay the onset of selenite-induced cataract (178). The treatment suppressed lens protein aggregation, as well as lowering oxidative stress response and inhibiting apoptosis associated caspases in the lens, indicating that the peptides were able to cross the blood-aqueous barrier.

The effects of UVR blocking contact lenses have also been examined. Rabbit and mouse eyes were exposed to UVA/UVB light *in vivo* while covered by no contact lens, a senofilcon UVR blocking contact lens, and a standard non-UVR blocking contact lens. The senofilcon lenses protected rabbit and mouse lenses from lens epithelial swelling, pigmentation, and the development of subcapsular opacities (179-181). Similar protection was seen when human lens epithelial cells and donor lenses were exposed with or without UVR blocking contact lenses (182).

Ultraviolet Radiation, a Possible Cause of Cataract

Solar UVR exposure, despite the absence of unequivocal epidemiological data, is a likely cause of age-related cataract. The lens is under chronic UVR exposure, and as an isolated non-regenerating, transparent, unpigmented tissue it is uniquely vulnerable to the damaging effects of UVR-induced photo-oxidative damage (Fig. 1.14). Studies in which lab animals have been exposed to UVR have shown that exposure leads invariably to cataract development (183, 184). Giblin and coworkers found that rabbit eyes exposed *in vivo* to UVR developed anterior sub-capsular opacification, as well as DNA strand breaks and swelling in lens epithelial cells (179). Vrensen saw the appearance of yellow pigmentation, opacities, and cortical fiber disorder in irradiated mouse lenses *in vivo* (185). Similar results have been observed in guinea pig and rat models (186, 187).

But, although animal models continue to be useful, there are significant concerns with drawing direct comparisons between UVR-exposed animal studies and human cataract pathology. Lens protein content, water content, and filter content vary between organisms (137). Truscott and coworkers have pointed out that mice, rats, and guinea pigs, the model systems frequently used to study cataract, are poor models for human lenses because of their lack of UVR filters (188). Human lenses, along with other diurnal mammals like the gray squirrel, contain high concentrations of UV filter compounds (137, 188). In humans, these take the form of kynurenine (a tryptophan metabolite) or its close chemical variants (83, 85). When gray squirrels were exposed to UVR, disruption of the lens epithelium was observed, along with an increase insoluble protein content

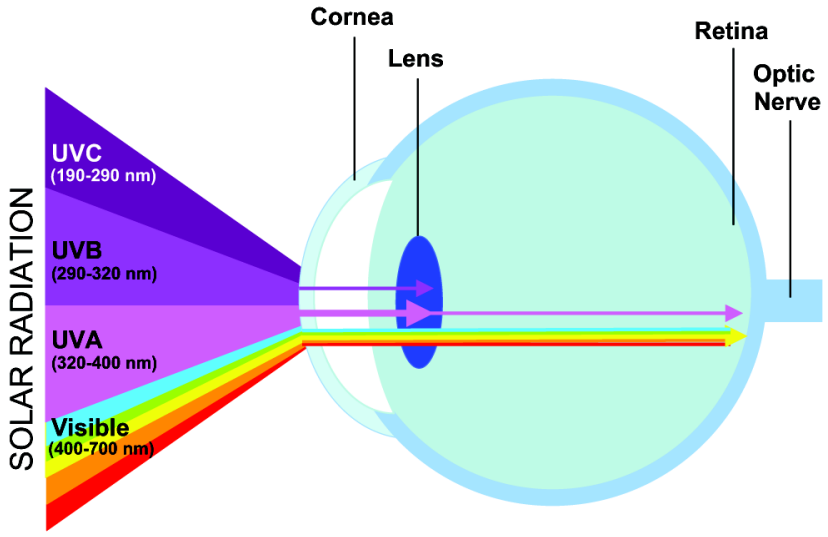

Figure 1.14 UVR Absorption and the Human Eye. A schematic of the human eye and its absorption of UVR. The atmosphere and cornea absorb UVC and a large amount of UVB. The lens absorbs remaining UVB and a significant amount of UVA, such that the retina is exposed to a minimum of UVR.
Reprinted from Experimental Eye Research, 84(1), Estey, T., et al, ALDH3A1: a Corneal Crystallin with Diverse Functions, 3-12, 2007, with permission from Elsevier.

and changes in the sizes observed for proteins in the inner cortex and lens nucleus (189), suggesting that despite the presence of UV filter compounds, UVR causes distinct damage to squirrel lenses.

Ultraviolet Radiation and the Crystallins

Experiments from more than 30 years ago, such as those by Goosey et al., had previously shown that for bovine crystallins, exposure to UVR in the presence of a reactive oxygen species producing photo-sensitizer led to proteincross-linking and the development of non-tryptophan fluorescence (190). Andley and coworkers showed that irradiation of human donor lens homogenates without photo-sensitizer caused a similar reaction, with 300 nm UVR causing covalent cross-linking of mixtures of α- and β-crystallins, respectively, and aggregation of γ-crystallins; these were accompanied by ROS generation and drops in tryptophan fluorescence with concomitant rise in non-tryptophan fluorescence (191, 192). Andley et al. went on to find that the action spectrum for the cross-linking overlapped the crystallins' absorption spectra, but was weaker than expected, suggesting that only a subset of absorption events led to cross-linking (193).

A number of studies have tried to investigate the changes to the crystallin aromatic residues due to UVR. Many have monitored decreases in tryptophan fluorescence (191, 194-196), and a rise in non-tryptophan fluorescence that has been suggested to be due to tryptophan indole ring scission to photo-product N-formylkynurenine. Borkman and Tassin used monochromatic 290nm light to

show that tryptophan fluorescence in human α-, β-, and γ-crystallins was destroyed after extended irradiation (197). Li et al. examined the differences between 308nm laser irradiation of bovine α-crystallin and γ-crystallin (198). They found that while both mixtures of bovine proteins showed a loss of tryptophan fluorescence, the α-crystallin samples showed a rise in N-formylkynurenine associated fluorescence, whereas the γ-crystallin samples showed no new fluorescence but instead formed light scattering aggregates. It appears that the different classes of the lens crystallin proteins respond to UVR in different ways, and that the γ-crystallins are associated with light scattering aggregation and, potentially, tryptophan damage.

Kynurenine and its related species have red-shifted absorption spectra compared to tryptophan. They are more photochemically active than tryptophan under UVA, the more abundant range of UVR reaching the lens (199, 200). Thus, potentially slow initial reactions transforming tryptophans to kynurenines within crystallins could be followed by further reactions by the more potent photo-sensitizer. Recent *in silico* work by Xia et al. used molecular dynamics simulations to replace tryptophans within HγD-Crys with kynurenine, and found that the more polar species disrupted the hydrogen bonds of the Greek Key tyrosine corners and broke open the dry cavity of HγD-Crys' hydrophobic core, significantly destabilizing the protein independent of kynurenine's differing photochemical properties (201).

Investigations have also shown that the free kynurenine filter compounds of the lens are a source of damage and protein post-translational modification to

the crystallins. Reszka et al. showed that UVR exposed kynurenine *in vitro* was able to produce superoxide and oxidize cysteine, participating in other radical chemistry in an oxygen dependent fashion (199). Dillon proposed that the yellowing of the human lens with age is due to the UVR-induced attachment of 3-hydroxykynurenine to lens proteins (135). Sherin et al. more recently found that kynurenine attached to proteins has a seven-fold increased fluorescence quantum yield, suggesting that attachment to crystallins could be the first step in more potent photosensitization (31).

Measuring Ultraviolet Radiation Exposure

Studies of UVR-induced damage to extracted lenses and crystallin must deal with problematic decisions about UVR dosimetry. Terrestrial solar UVR exposure varies based on the sun's angle in the sky, with UVB and UVA scattered with different angle-dependent efficiencies, and thus time of day and latitude are key parameters (202). In addition, eye exposure also depends on personal habits (hats, sunglasses), weather (with overcast days unintuitively leading to more intense eye UVR exposure due to squinting changes), and ground reflectance, and these factors' high degree of variation make estimations very approximate (203, 204). As suggested by Sliney, ideally average daily exposure of a human eye to UVR would be measured using dosimeter contact lenses (203, 204). As mentioned previously, measurement methodology, whether using sensors attached to a mannequin, forehead attached sensors on human subjects, or an estimation based on a flat plane detector, has a significant effect

on the final value (203-205). Laboratory UVR exposures are often orders of magnitude in excess of estimated normal daily exposures, raising questions about whether the excessive UVR doses *in vitro* could lead to effects not observed *in vivo* (206). Nevertheless, many covalent modifications to the crystallins and changes to lens properties observed in cataractous lenses have also been seen upon laboratory irradiation, suggesting that *in vitro* UVR exposure shares important characteristics with *in vivo* UVR-induced crystallin damage.

Thesis Context

This thesis project aims to understand the connection between UVR and the aggregation of HγD-Crys. How does UVR change HγD-Crys' structure? What sites are affected? How do these changes cause aggregation? What characteristics and dependencies does photo-aggregation display? HγD-Crys is uniquely positioned to study these questions. γ-Crystallins are monomers, and easier to handle experimentally and interpret results for as compared to the hetero-multimeric β-crystallins or polydisperse α-crystallins. HγD-Crys is one of the oldest and most abundant proteins in the lens; by virtue of the lens' function, HγD-Crys is exposed to UVR at a low chronic level for a human lifetime, and has been found covalently modified in aged and cataractous lenses. A greater understanding of its *in vitro* photo-aggregation behavior could help us understand the types of photo-damage leading to cataract *in vivo*, leading to breakthroughs in cataract prevention, or new more economically feasible treatments.

CHAPTER 2:

Tryptophan Cluster Protects Human γD-Crystallin from Ultraviolet Radiation-Induced Photo-Aggregation *In Vitro**

*This research was originally published in Photochemistry and Photobiology and has been adapted for presentation here. Nathaniel Schafheimer and Jonathan King. (2013) Tryptophan Cluster Protects Human γD-Crystallin from Ultraviolet Radiation-Induced Photo-Aggregation In vitro. *Photochem. Photobiol.* doi: 10.1111/php.12096 © The American Society for Photobiology.

INTRODUCTION

Protein misfolding and aggregation are hallmarks of the pathology of many human diseases (207). Cataract is the leading cause of blindness in the world, projected to affect 20-30 million people in 2020, primarily the elderly, and is associated with misfolding and aggregation of the lens proteins (129). Despite the widespread prevalence of cataract, the relative contributions of identified risk factors to cataract have not been determined (133). One of the several risk factors identified is exposure to ultraviolet radiation.

Ultraviolet radiation (UVR) is a ubiquitous environmental hazard for life on Earth. Although the development of the ozone layer 2.4 billion years ago limited terrestrial UVR exposure to the UVA (400-315 nm) and UVB (315-280 nm) ranges, UVR still exerts selective pressure on extant creatures (9). DNA photo-damage and its downstream impacts on the cellular level have been well studied (208-212). The accumulation of UVR-induced DNA lesions leads to mutations, the obstruction of DNA replication, and, if unaddressed, cell death. Several DNA repair pathways have been identified and characterized that target UVR-induced DNA lesions.

Unlike DNA photo-damage, most types of protein photo-damage cannot be repaired by cell processes. In cells, damaged proteins can be poly-ubiquitinylated and degraded by the ubiquitin proteasome pathway or assembled into large aggresomes and disposed of through autophagocytosis (54). In some specialized tissues, such as the lens, where cataract occurs, neither option is available (56, 58, 117).

The human lens focuses light onto the retina; to do so, it must remain translucent (58). As the epithelial cells in the lens terminally differentiate and produce large quantities of the crystallin proteins, they degrade their organelles and ribosomes (64). Due to the lack of protein turn over in the lens, the damaged and aggregated crystallins are not cleared from the lens fibers and accumulate as cataracts. Covalently damaged lens proteins have been shown to have decreased stability and solubility, and tend toward aggregation (104).

The three crystallin families, α, β, and γ, comprise 90% of total lens protein and are present at ~400 mg/ml (66). α-crystallins are ATP-independent chaperones of the small heat shock protein (sHSP) family. These bind partially unfolded or damaged proteins, sequestering them, but cannot refold them (90, 213). The β- and γ-crystallins are globular, two domain structural proteins of approximately 20 kDa, related by sequence and structure homology (66, 102). Each domain is composed of two Greek Key motifs and contains a number of highly conserved aromatic residues. The β-crystallins form oligomers through domain swapping; the γ-crystallins are monomeric (214).

Due to the lack of protein synthesis or degradation in the lens fiber cells, a model of cataract has been put forth in which aggregation prone species accumulate over the lifetime of an individual and gradually titrate away free α-crystallin; when no free chaperone remains, aggregation occurs, causing cataract (105). HγD-Crys, the γ-crystallin chosen here for study, is extremely stable and one of the more abundant γ-crystallins in the human lens nucleus (107). Several

mutations in the gene for HγD-Crys are known to be associated with congenital cataract (167, 215).

Earlier studies have investigated how bovine lenses, extracted mixtures of bovine crystallins, and extracted mixtures of human crystallins have responded to photo-sensitizers and UVR, which generate reactive oxygen species (ROS) that can mediate photo-damage to proteins (216-218). One photosensitizer studied, N-formylkynurenine, is similar to the tryptophan-based UV filters abundant in the lens (83). Extracted lenses and lens protein extracts grew cloudy when exposed to photo-sensitizers and UVR, with an increase in the insoluble protein fraction population and disruptions to crystallin structure. A rise in turbidity, cross-linked products, non-Trp fluorescence, and the presence of reactive oxygen species was also reported when mixtures of bovine and human crystallins were irradiated in the absence of photo-sensitizers (197). More recently, Estey et al. showed that UVR causes non-disulfide cross-linking and non-native aggregation in the corneal crystallin ALDH3A1 (219).

Other studies found exposure to UVR caused cataract to develop in laboratory animals (183, 184, 187). When Ayala et al. exposed rats to short bursts of 300 nm UVR, they observed the development of light scattering in exposed lenses in the weeks and months following irradiation (184). Other work has found light scattering develops in guinea pig lens after UVA exposure in vivo in the lab (186). Further *in vivo* work by Giblin et al. found that UVA and UVB blocking contact lenses prevented UVR-induced cataract in rabbits (179, 180).

The availability of high resolution crystallin X-ray structures from Basak et al. enabled the discovery of a distinctive energy transfer mechanism at work in HγD-Crys between the conserved tryptophan pairs within the N- and C- terminal domains (Fig. 1.12A) (112, 118). By examining fluorescence spectra and quantum yields of mutant HγD-Crys constructs, Chen et al. found evidence that one Trp of a pair (W68 or W156) has its fluorescence extremely quenched, while the other (W42 or W130, respectively) is moderately fluorescent and was shown to transfer its excited state energy to its quenched partner, resulting in anomalous native state Trp quenching (Fig. 1.9B and 1.10). It was hypothesized that the mechanism could have evolved as a form of resistance to photo-damage (220).

To investigate the molecular mechanism underlying photo-aggregation of the crystallins, solutions of recombinant purified HγD-Crys were irradiated with a mixture of UVA/UVB, and the resulting photo-aggregation monitored via solution turbidity, absorption spectroscopy, SDS-PAGE, and TEM. Based on the fact that tryptophans absorb UVR the strongest and on the previously characterized energy transfer mechanism, we tested an initial hypothesis that photo-aggregation proceeded through direct or indirect photo-damage to one or more of the four Trp residues. Unexpectedly, we show here that damage to the Trp residues is unlikely to be on the pathway leading to the photo-aggregated high molecular weight state. Rather the results reveal that the Trp residues may play a protective role.

MATERIALS AND METHODS

Mutagenesis, Expression, and Purification of HγD-Crys: N-terminally 6x-His tagged wild-type (WT) HγD-Crys expression constructs were modified via site-directed mutagenesis to introduce quadruple and triple W:F mutants (108). Constructs were confirmed via sequencing (Genewiz).

Recombinant WT HγD-Crys and mutant proteins were expressed and purified as described previously (108) with several modifications. Cells were grown to OD_{600} ~1 in Super broth media at 37 °C with shaking. IPTG was added to 1 mM and cultures were transferred to 18 °C followed by shaking overnight. Cells were pelleted by centrifugation for 20 minutes at 17000 *x g* and resuspended in 30 ml Ni-NTA Lysis Buffer (300 mM NaCl, 50 mM $NaPO_4$, 18 mM imidazole, pH 8) containing 2 tablets of Roche Complete EDTA-free protease inhibitor. After addition of lysozyme to 3 mg/mL and DNAse to 3 µg/mL, pellets were lysed via ultrasonication, and centrifuged at 17000 *x g* for 45 minutes. Supernatants were filtered and applied to a Ni-NTA column (GE Healthcare). Protein was eluted using a linear gradient of increasing imidazole concentration. Fractions containing the protein of interest were pooled and dialyzed three times against storage buffer (10 mM ammonium acetate, pH 7.0).

Protein Concentration Measurement: Stock protein sample concentration was determined using absorbance at 280 nm with the following extinction coefficients (determined using SIB's ProtParam): WT HγD-Crys 42,860 M^{-1} cm^{-1}, triple W:F HγD-Crys 26,360 M^{-1} cm^{-1}, quadruple W:F HγD-Crys 20,860 M^{-1} cm^{-1}.

Photo-aggregation Experiments*:* Samples of HγD-Crys were prepared at 0.25 mg/ml or 1 mg/ml in 1x Reaction Buffer (100 mM Na_2PO_4, 1 mM EDTA, pH 7). Samples were irradiated at room temperature in a quartz cuvette (Starna Group) using a UVP Inc. UVLMS-38 lamp equipped with a 302 nm midrange bulb delivering a range of UVA/UVB light. UVR dose delivery was set to 2 mW/cm^2, varied by adjusting the cuvette's distance to the lamp, and determined before each experiment by a UVX Radiometer with midrange UVX-31 sensor. Turbidity readings at OD_{600} on a Cary UV/Vis Spectrometer were taken at regular time points during irradiation. Samples removed and analyzed via SDS-PAGE were reduced and boiled and electrophoresed through 14% acrylamide gels at 170 V for 1 hour; gels were stained using Krypton Fluorescent Protein Stain (Thermo Fisher Scientific) and imaged on a Typhoon 9400 (Amersham Biosciences). Samples removed and analyzed using the bicinchoninic acid assay for protein concentration were filtered with a 0.2 μm membrane to remove aggregated protein and treated following the kit manufacturer's protocol (Thermo Scientific Pierce). The results were read on a Fluostar Optima plate reader (BMG Technologies). Aggregation rates were measured by calculating the steepest linear slope of the OD_{600} versus exposure time curve.

Oxygen-free irradiation experiments were conducted using a Coy anaerobic chamber under nitrogen. After an overnight incubation, samples were sealed into screw-top quartz cuvettes (Starna Group) with rubber stoppers before removal from the anaerobic chamber, and immediately used in photo-

aggregation experiments. An oxygen sensitive dye solution (7.5 mM methyl viologen, 9 mM dithionite) in an identically sealed cuvette was used to confirm anaerobic conditions.

Action spectrum analysis of photo-aggregation was achieved using small Newport Stabilife UVR cutoff filters to construct a shielding cage around the sample cuvette, and photo-aggregation experiments were conducted as above.

Transmission Electron Microscopy: Five-microliter samples of irradiated and unirradiated 0.1 mg/ml HγD-Crys sample in storage buffer were directly applied onto glow-discharged, carbon-coated, Formvar-filmed 400 mesh copper grids (Ted Pella). They were subsequently negatively stained with 1% uranyl acetate and blotted dry with filter paper. Sample grids were viewed in a transmission electron microscope (1200 XII; JEOL) and images were taken using an Advanced Microscopy Techniques XR41S side-mounted charge-coupled device camera.

Absorbance Spectra Measurements: Samples were collected from photo-aggregation experiments and diluted into reaction buffer and 5 M guanidine hydrochloride (GuHCl) in black-walled tubes to minimize light scatter interference by aggregated protein. Samples were then incubated at 37 °C for 6 hours before scanning absorbance. Absorbance spectra of irradiated and unirradiated HγD-Crys samples were collected using a Cary UV/Vis Spectrometer.

Circular Dichroism Thermal Unfolding Measurements: CD spectra of the WT and mutant proteins were obtained using an AVIV model 202 CD spectrometer (Lakewood, NJ). Protein samples were prepared at a concentration of 0.1 mg/ml in 10 mM sodium phosphate, pH 7.0. Data were collected at 218 nm in a 1 cm quartz cuvette. Sample temperature was increased from 25°C to 95°C in 1°C steps with 1 minute of equilibration time per °C, followed by 5 second reads. Data were buffer-corrected, and mean residue ellipticity was calculated. The mean residue ellipticity versus temperature data were fit to a sigmoidal curve using Kaleidagraph (Synergy Software), and the unfolding midpoints were calculated. The unfolding temperatures reported are averages of 3 thermal unfolding experiments.

RESULTS

HγD-Crys photo-aggregation under UVR

We exposed purified HγD-Crys to UVR to investigate the underlying mechanism of photo-damage in this highly stable lens protein. When WT HγD-Crys was exposed for 2 hours to 2 mW/cm^2 of UVR, solution turbidity rose dramatically after a lag period and then plateaued, consistent with previous studies and indicative of protein aggregation (Fig. 2.1). A lag period is often interpreted as evidence of a nucleation step in polymerization kinetics. However, we observed a shorter lag period when aggregation was monitored at 280 and 350 nm than those observed at 600 nm (Fig. 2.2a). This behavior suggests that the different lag times observed using different wavelengths of light represent detection of

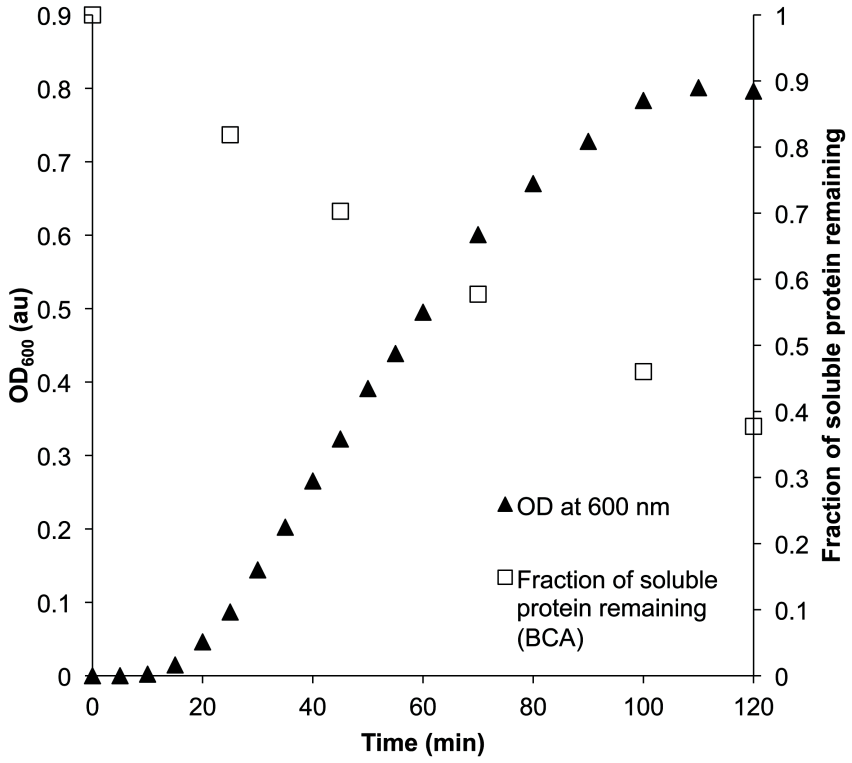

Figure 2.1 WT HγD-Crys Turbidity and Protein Concentration Over UVR Exposure. Changes in solution turbidity measured at OD_{600} (solid triangles, left axis) and changes in soluble protein concentration measured using the BCA assay on samples (open squares, right axis) as a function of UVR exposure time (2 mW/cm^2). Samples contained 0.25 mg/ml of WT HγD-Crys in sample buffer, and were incubated at 25 °C.

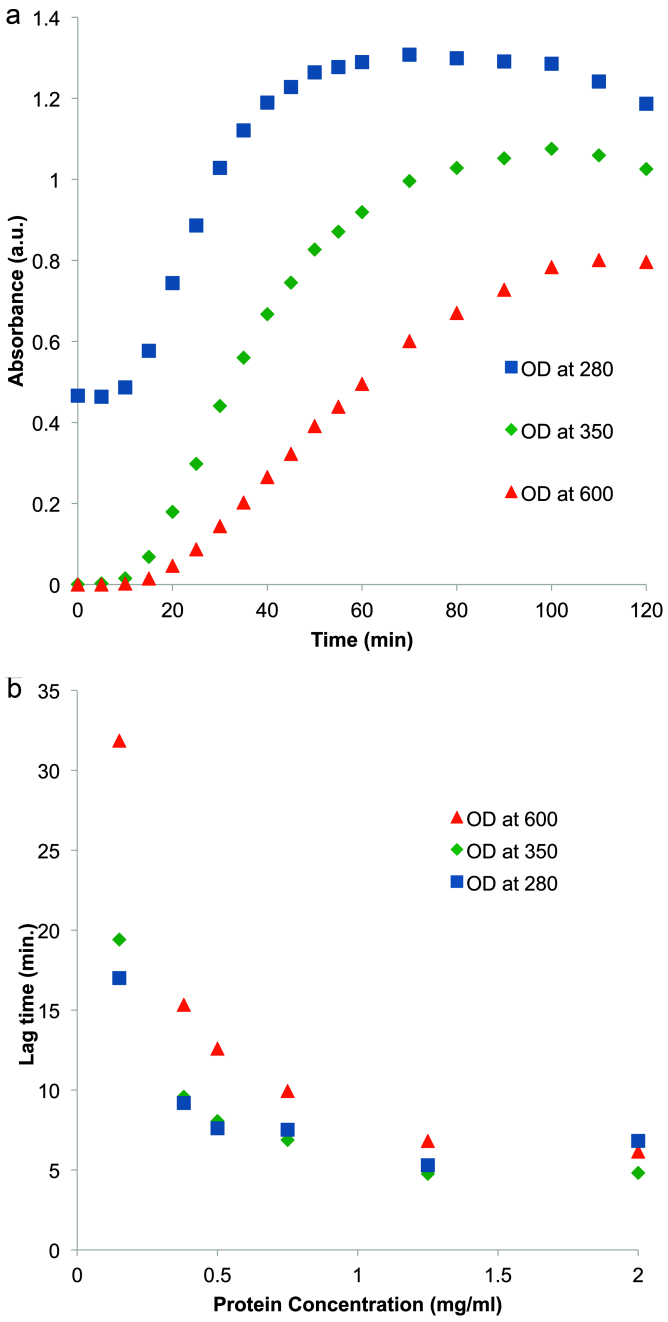

Figure 2.2. Light Scattering Monitored at 280, 350, and 600 nm. (a) Changes in solution turbidity measuring OD_{600} (red triangles), OD_{350} (green diamonds), and OD_{280} (blue squares) over UVR exposure time. Samples contained 0.25 mg/ml WT HγD-Crys in sample buffer. (b) Lag time to turbidity development versus concentrations of WT HγD-Crys observed via OD_{600} (red triangles), OD_{350} (green diamonds), and OD_{280} (blue squares). Turbidity data were fit to sigmoidal curves and the time to increase to 0.05 au above baseline OD at time 0 was calculated as the lag time.

differently sized aggregates, and that, for the reaction under study, the apparent lag period is a consequence of initial aggregating species being too small to scatter light significantly.

As an additional approach to whether the lag phase represents a true nucleation step, we examined the lag time versus HγD-Crys concentration (Fig. 2.2b). Unlike well-documented nucleation reactions, the lag time was relatively insensitive to protein concentration (221).

At longer exposure times, the dose of UVR delivered to the sample may be lower than initially measured due to scattering in the sample. However, the OD_{600} continued to rise steadily even after the OD_{280} plateaued (Fig. 2.2a), indicating continuing photo-aggregation despite potentially lower dose delivered.

The concentration of soluble WT HγD-Crys detected dropped steadily throughout UVR exposure to less than 40% its original concentration (Fig. 2.1), indicating more than 60% of the original sample's protein had entered an aggregated state by the time the OD_{600} had ceased increasing, while a significant population remained in solution.

Properties of the Photo-aggregation Reaction

To understand the parameters governing the photo-aggregation of HγD-Crys, the irradiation and turbidity monitoring experiment was repeated, varying the concentration of WT HγD-Crys (Fig. 2.3a) and the dose of UVR (Fig. 2.3b). Increased rate of photo-aggregation correlated with increased concentration of WT HγD-Crys and with UVR dose. The dependence of aggregation on

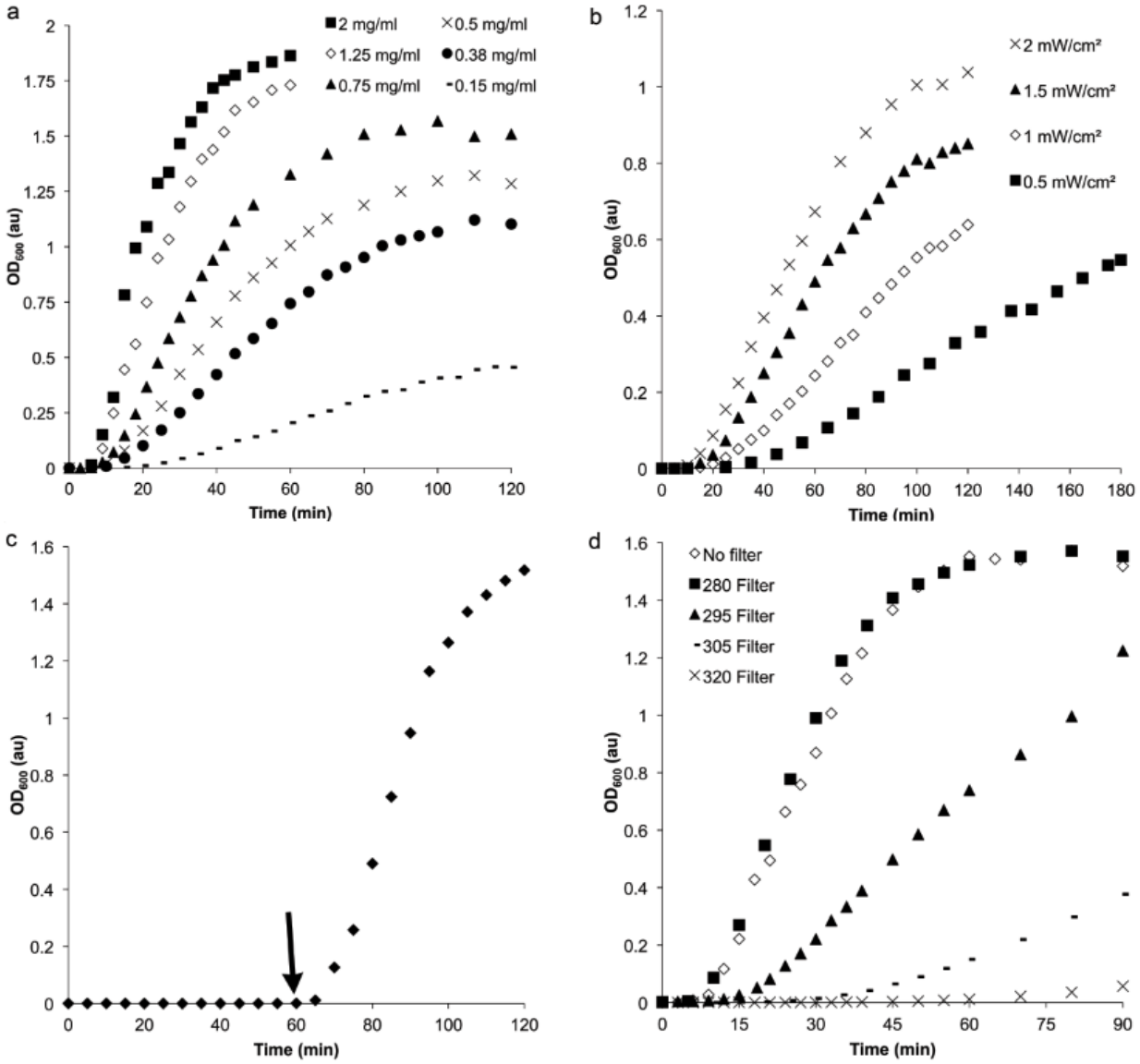

Figure 2.3 Parameters Governing Photo-aggregation. Parameters of UVR-induced protein aggregation of WT HγD-Crys observed using OD_{600}: (a) Irradiation of varying concentrations of WT HγD-Crys: 2 mg/ml (solid squares), 1.25 mg/ml (open diamonds), 0.75 mg/ml (solid triangles), 0.5 mg/ml (X's), 0.38 mg/ml (solid circles), 0.15 mg/ml (dashes). (b) UVR-induced aggregation of 0.25 mg/ml WT HγD-Crys samples using varying doses of UVR as measured via radiometer: 2 mW/cm^2 (X's), 1.5 mW/cm^2 (solid triangles), 1 mW/cm^2 (open diamonds), 0.5 mW/cm^2 (solid squares). (c) UVR exposure of a 1 mg/ml WT HγD-Crys sample in the absence or presence of atmospheric oxygen. Protein and buffer samples prepared anaerobically were irradiated, then opened to the atmosphere at 60 minutes (denoted by arrow). (d) Exposure of 1 mg/ml WT HγD-Crys samples to decreasing ranges of the UV lamp's emission spectrum using glass filters blocking all light shorter than a wavelength cutoff: no filter (open diamonds), 280 nm filter (solid squares), 295 nm filter (solid triangles), 305 nm filter (dashes), 320 nm filter (X's).

temperature and pH was also examined. Photo-aggregation did not show any distinctive dependence on either parameter (Fig. 2.4 and 2.5).

To determine whether oxygen played a role in the *in vitro* photo-aggregation of HγD-Crys, buffer and protein samples were prepared anaerobically and then exposed to UVR doses as before (Fig. 2.3c). No change in turbidity was observed over an hour of UVR exposure under anaerobic conditions. At 60 minutes, oxygen was reintroduced to the reaction. As UVR exposure continued, solution turbidity developed robustly. These results indicated oxygen is required to mediate photo-damage for the *in vitro* photo-aggregation of HγD-Crys.

Glass filters that sharply block all wavelengths shorter than specific thresholds were used to determine the action spectrum of photo-aggregation (Fig. 2.3d). When wavelengths below 280 nm were blocked, there was no difference observed in the development of turbidity with exposure time. However, cutting off UVR at 295 nm and below, 305 nm and below, and 320 nm and below progressively and dramatically slowed photo-aggregation. This indicated an action spectrum encompassing the UVB range of approx. 280-320 nm, but not the UVA range; this overlapped with the Tyr and Trp absorption spectra, as well as that of Trp photo-products like kynurenine.

HγD-Crys photo-aggregate structure

WT HγD-Crys photo-aggregates were visualized using uranyl-acetate negative stain transmission electron microscopy (TEM) (Fig. 2.6). Aggregates observed

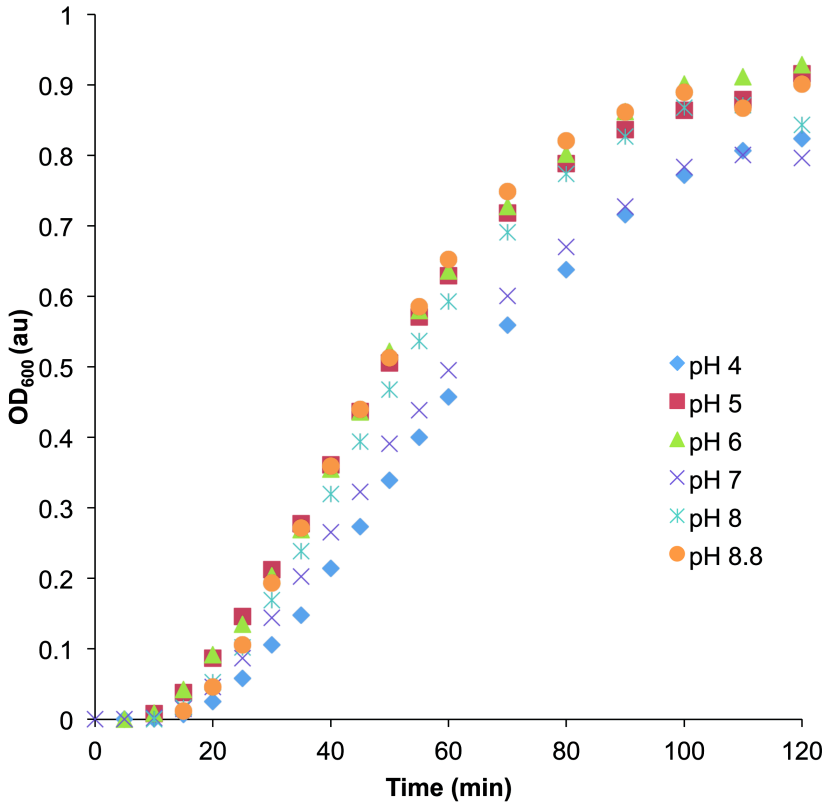

Figure 2.4 Photo-aggregation and pH. Changes in solution turbidity measuring OD_{600} of samples at pH 4 (blue diamonds), pH 5 (red squares), pH 6 (green triangles), pH 7 (purple X's), pH 8 (turquoise hatches), and pH 8.8 (orange circles) over UVR exposure time. Samples contained 0.25 mg/ml WT HγD-Crys in sample buffer. Solutions at pH 4 and 5 were produced by adding concentrated HCl to sample buffer beforehand. Solutions pH's were determined using a Thermo Orion PerpHect LogR Meter (model 330) with 8156BNUWP probe.

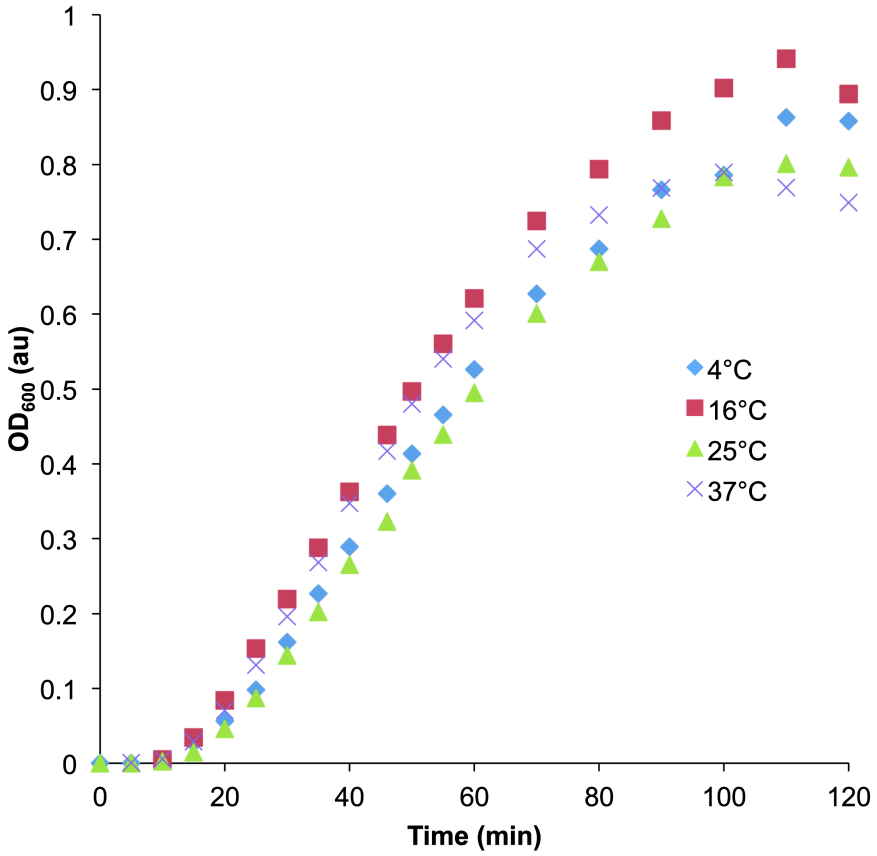

Figure 2.5 Photo-aggregation and Temperature. Changes in solution turbidity of 0.25 mg/ml WT HγD-Crys samples, measuring OD_{600}, of samples at 4°C (blue diamonds), 16°C (red squares), 25°C (green triangles), and 37°C (purple X's) over UVR exposure time.

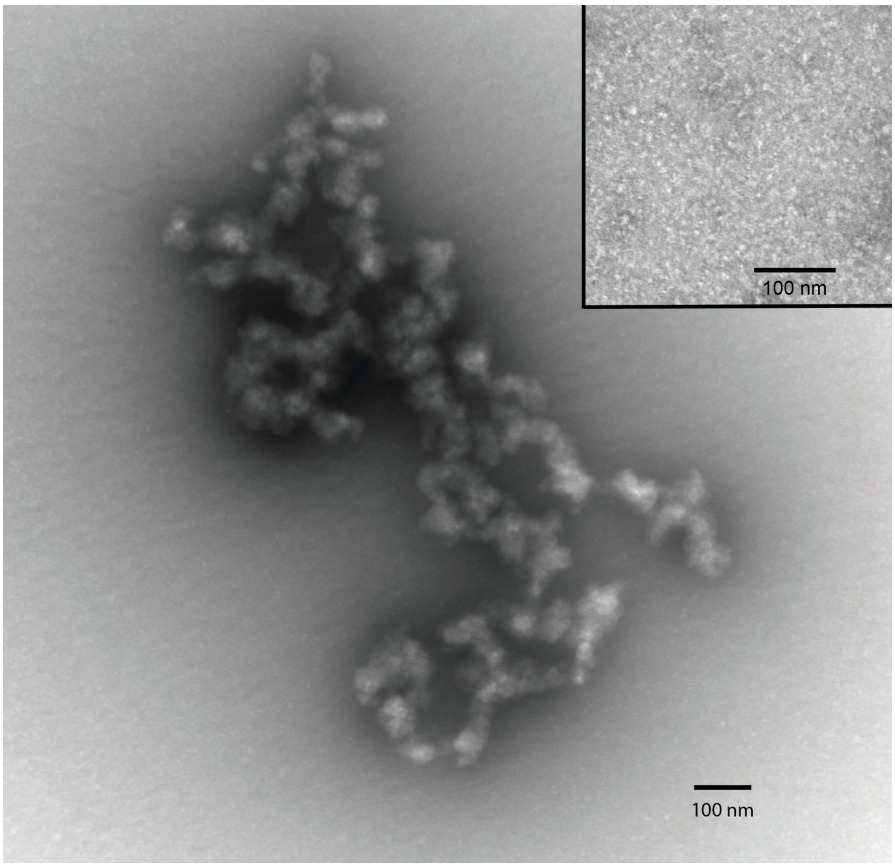

Figure 2.6 Electron Micrograph of HγD-Crys Photo-aggregate. Transmission electron micrograph of uranyl-acetate stained UVR-induced aggregate from a 1 mg/ml WT HγD-Crys sample at 30 minutes irradiation at 2 mW/cm^2. The inset is a negative control micrograph of unirradiated WT HγD-Crys.

were from 100 to ~1000 nm in length. They were non-amyloid in structure but, while irregularly arranged, appear to have a rough, globular repeating unit approximately 40-80 nm in size.

Samples of photo-aggregation reactions of WT HγD-Crys were collected as a function of irradiation time and were analyzed by SDS-PAGE (Fig. 2.7a). All the samples exhibited a strong 20 kDa band, representing monomeric WT HγD-Crys (iv). After 25 minutes of UVR exposure an ~40 kDa band could be seen (iii) appropriate in size to be a HγD-Crys dimer. In addition a series of high molecular weight bands (ii) appeared near the top of the gel, presumably multimeric species. By 45 minutes, a thin band at the top edge of the resolving gel could be seen, indicative of species too large to enter the gel (i). A series of lower molecular weight degradation products can be seen below the monomer band (v). Image analysis was used to quantify changes in band density between lanes, and showed that the monomer band diminished over time to half its original intensity over exposure time, while the dimer band increased until ~45 minutes then diminished (Fig. 2.7b). This is consistent with the formation of an initial covalent dimeric cross-linked photo-product that accumulates but is consumed by further photo-cross-linking and incorporated into larger aggregates

When the density of the dimer band was examined at earlier UVR exposure times and compared with solution turbidity, we saw that the dimer appeared before OD_{600} increased, and began to wane as turbidity plateaued (Fig. 2.8a). At the earliest time points, with only 2 minutes of UVR exposure, the dimer band was detected (Fig. 2.8b). This suggests the formation of a covalent dimer is

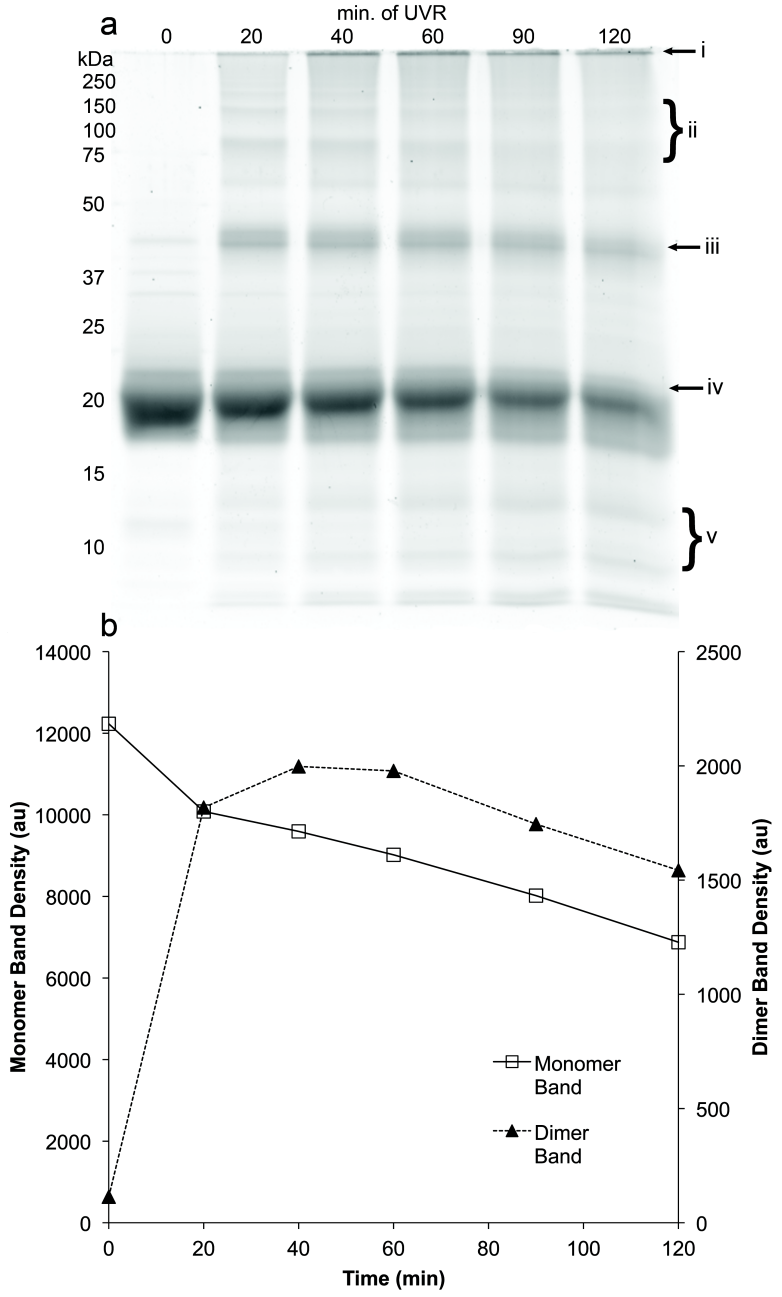

Figure 2.7 SDS-PAGE of Photo-aggregated HγD-Crys. (a) Scanned image of a krypton-stained gel from SDS-PAGE of UVR-induced aggregate samples from a 1 mg/ml WT HγD-Crys sample taken at a series of UVR exposure times: 0 min (lane 1), 25 min (lane 2), 45 min (lane 3), 70 min (lane 4), 100 min (lane 5), 120 min (lane 6). Marked sites: large protein aggregates unable to enter gel (i), high molecular weight species (ii), HγD-Crys dimer-sized band (iii), monomeric HγD-Crys band (iv), lower molecular weight degradation products (v). (b) Graphs of quantification of band density for the monomeric approx. 20 kDa band (left axis) and the dimeric approx. 40 kDa band (right axis) from the gel image in (a).

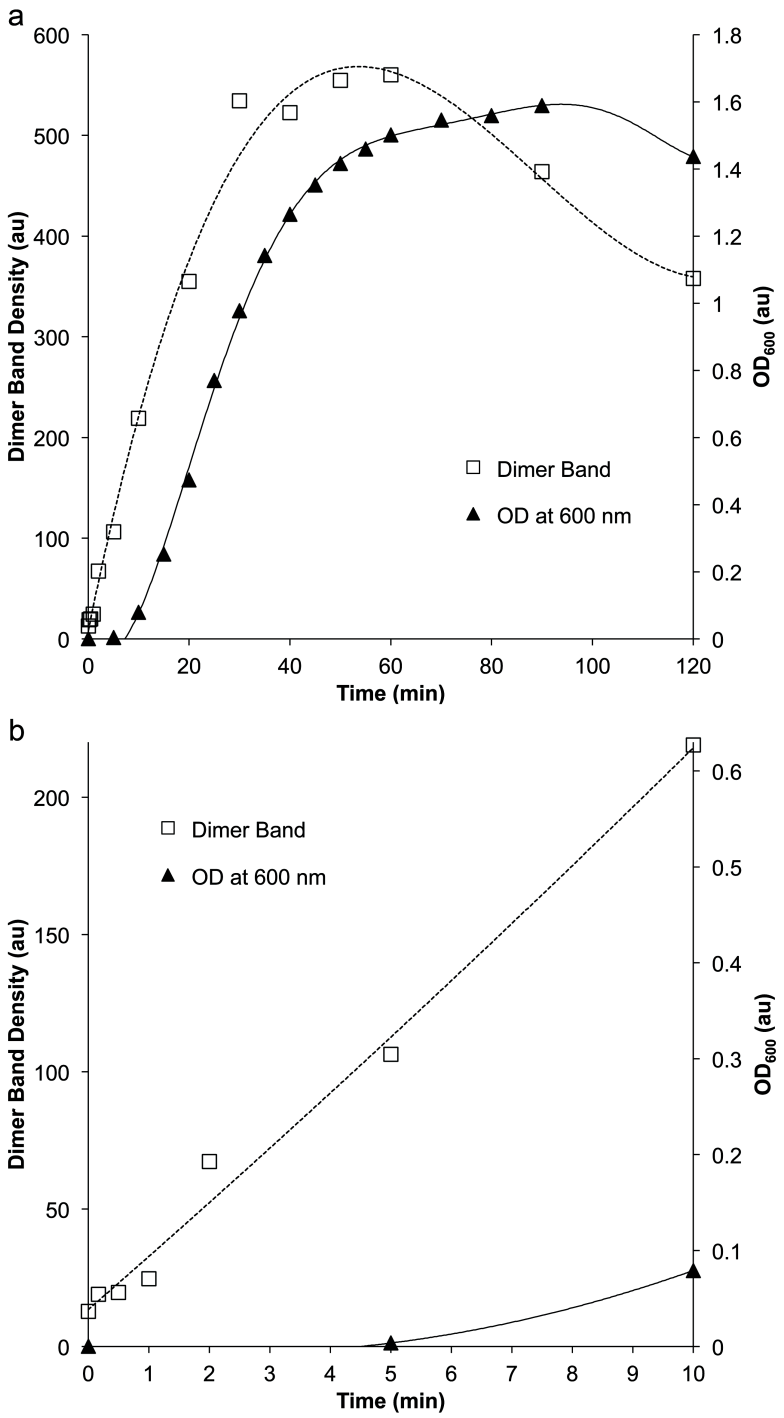

Figure 2.8 Comparing Turbidity to Dimeric Product Formation. (a) Turbidity development at OD_{600} of 1 mg/ml WT HγD-Crys sample (black triangles and solid line, right axis) and dimer gel band density quantification from SDS-PAGE of the same WT HγD-Crys sample (open squares and dotted line, left axis) versus UVR exposure time. Curves were generated using polynomial fits. (b) The same data is presented from (a), examining just the earliest time points from 0 to 10 minutes of UVR exposure.

an early step in the photo-aggregation of HγD-Crys, and that solution turbidity measurements monitor the presence of later aggregation products.

The role of aromatic residues in photo-aggregation

We initially assumed that UVR absorption by tryptophans was a key step in photo-damage, and that the photo-oxidized indole moiety was participating in free-radical polymerization. We therefore examined the absorbance spectra of HγD-Crys samples after varying UVR exposure times to assess whether photo-damage occurred to aromatic residues (Fig. 2.9a). We observed no significant change in absorbance spectra in samples from 0 minutes to 36 minutes. However, over that same time period, aggregation proceeded robustly (Fig. 2.9b). The lack of significant changes in the absorbance spectra indicates an overall lack of damage to HγD-Crys's Trp's and Tyr's during photo-aggregation.

To determine the role of Trp residues in photo-aggregation we examined triple and quadruple W:F mutant constructs of HγD-Crys, with a single Trp remaining or no Trp's remaining, respectively. Previous studies established that these mutants folded into native-like structures (108). We confirmed that the mutant HγD-Crys proteins were stably folded by measuring far UV circular dichroism as a function of increasing temperature. Though all the mutant proteins were less stable than wildtype, they retained their folded conformation to 60°C or above (Table 2.1).

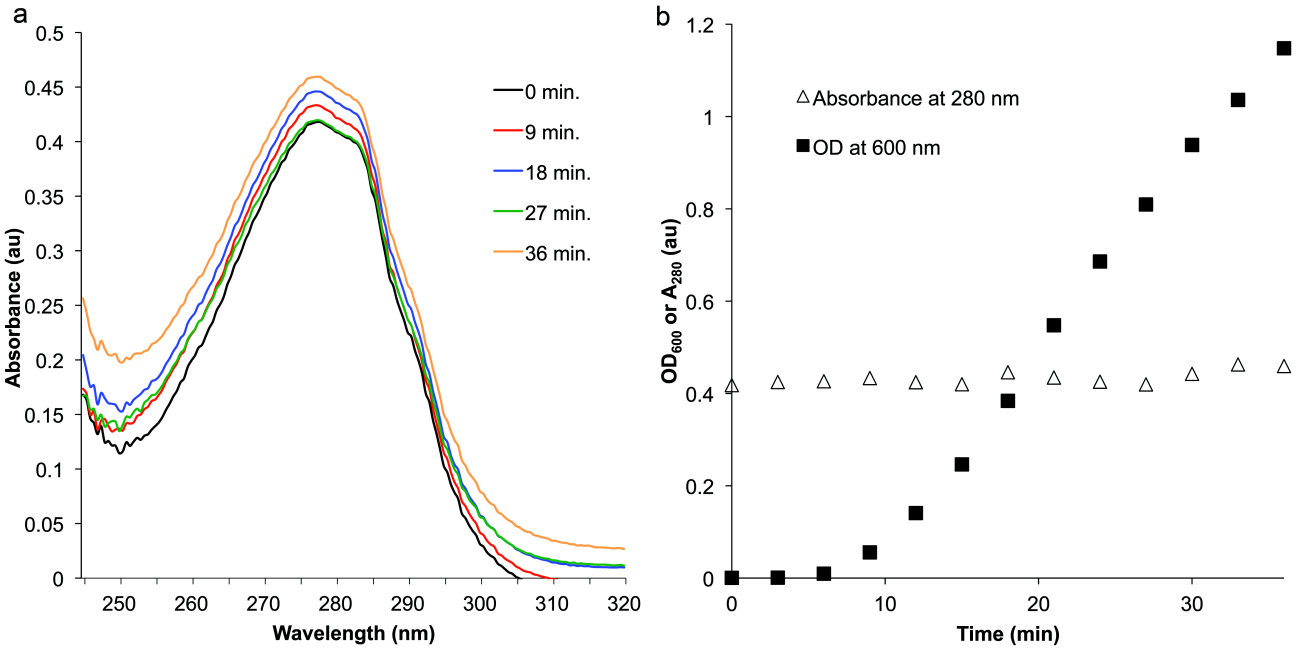

Figure 2.9 HγD-Crys Absorbance Spectra Over UVR Exposure. (a) Absorbance spectra of WT HγD-Crys at increasing UVR exposure times, taken from 1 mg/ml samples diluted to 0.1 mg/ml into GuHCl to minimize aggregate light scattering: 0 min (black), 9 min (red), 18 min (blue), 27 min (green), 36 min (orange). (b) Graph of the change in solution turbidity at 600 nm (solid squares) and absorbance at 280 nm (open triangles) over UVR exposure time of the same WT HγD-Crys samples exposed to UVR as in (a).

Table 2.1 Circular Dichroism Thermal Unfolding Data for HγD-Crys Mutant Constructs

Construct	*Melting Temperature (°C)*	*Standard Deviation (°C)*
WT	82.1	0.4
W42-only	68.85	0.163
W68-only	67.46	0.0234
W130-only	65	0.146
W156-only	65.1	0.089
NoTrp	61	0.11

In photo-aggregation experiments with all four triple mutants and the NoTrp quadruple mutant, turbidity rose dramatically faster and reached a higher plateau than WT. This indicated the W:F mutations made HγD-Crys more vulnerable to UVR-induced photo-aggregation, not less, and that the absence of Trp residues did not retard photo-aggregation (Fig. 2.10a).

We examined the concentration dependence of the rate of photo-aggregation for WT and mutant HγD-Crys and found that the multiple W:F mutant HγD-Crys's diverge significantly in the concentration dependence of their photo-aggregation rate (Fig. 2.10b). This implied that the W:F mutations significantly alter the photo-aggregation pathway with respect to wildtype.

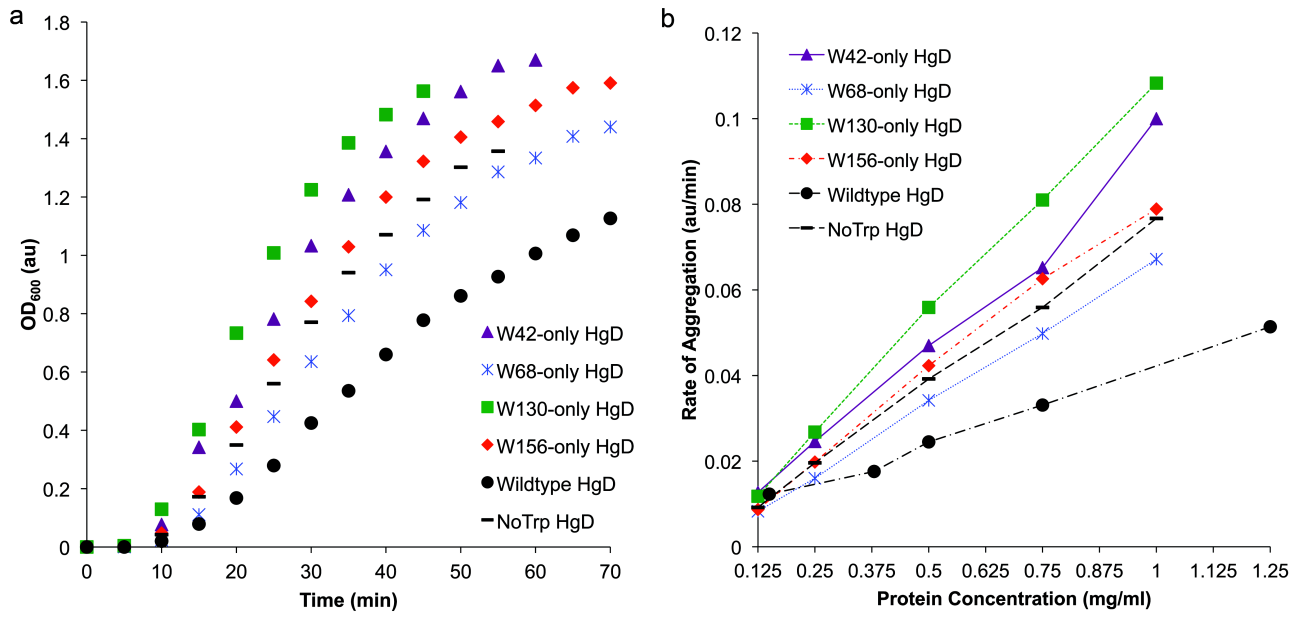

Figure 2.10 Comparing W:F Mutants to WT HγD-Crys Photo-aggregation. (a) Comparison of UVR-induced aggregation of W:F mutant constructs of HγD-Crys by monitoring OD_{600} of 0.5 mg/ml protein solutions in sample buffer over irradiation time. (b) Comparison of the concentration dependences of UVR-induced aggregation of W:F mutant HγD-Crys constructs by analyzing the apparent rate of aggregation (steepest linear slope of OD_{600} curves) versus protein concentration. W42-only HγD-Crys (purple triangles), W68-only HγD-Crys (blue hatches), W130-only HγD-Crys (green squares), W156-only HγD-Crys (red diamonds), WT HγD-Crys (black circles), NoTrp HγD-Crys (black dashes).

DISCUSSION

The γD-crystallins are very stable, resistant to denaturation both by chemical denaturants and heat, and are among the longer-lived proteins in the human body (66). However, exposure to UVR *in vitro* results in rapid aggregation into high molecular weigh complexes. Since this reaction requires oxygen, it presumably involves photo-oxidation of certain residues.

HγD-Crys contains many aromatic amino acids capable of UVR absorption and radical photochemistry - four tryptophans, fourteen tyrosines and six phenylalanines. Tryptophan has the highest specific absorption of protein amino acids at 280 nm, and HγD-Crys' 4 highly conserved Trp residues contribute 51.3% of its absorptivity, the remaining 48.7% coming from its 14 tyrosines (222, 223). The Trp excited state can transfer its energy to other side chains or the peptide backbone, or scission of the indole ring of the excited residue can occur creating photo-products, among them, kynurenine (17). In either path, absorption of UV photons by tryptophan could be an initial step in UVR-induced photo-damage.

We monitored photo-aggregation of HγD-Crys by two main methods, turbidity and SDS-PAGE. The inability to dissociate the aggregated state by boiling in SDS in the presence of reducing agents suggests covalent bonds between the subunits in the aggregated state. This suggests that aggregation of HγD-Crys was occurring via a radical polymerization mechanism (222). Such a model would also account for the small effects of temperature on aggregation.

SDS-PAGE revealed the formation of covalent dimeric photo-products immediately after UVR exposure began. These subsequently decreased in intensity, consistent with a role as intermediates in the polymerization reaction. When aggregation was monitored by turbidity, an apparent lag phase was present. While a lag in an aggregation reaction could be indicative of a nucleation step in the aggregation mechanism (221), it was more likely a consequence of early aggregates being too small to scatter light at 600 nm; this is supported by the shorter lag times when turbidity was monitored at shorter wavelengths, as well as the absence of a lag in production of dimeric photo-products.

The presence of distinct lower molecular weight bands of photo-products suggests that photochemical scission of particular peptide bonds is also occurring. UVR-induced photochemical scission of peptide bonds (224) and degradation of crystallins (145) have been described previously. Though we cannot exclude the possibility that the fragments are incorporated into the covalent aggregated state, their steady increase during the course of UVR exposure is consistent with a photo-product that is off the aggregation pathway.

We were surprised to find that in NoTrp HγD-Crys, the quadruple W:F mutant, photo-aggregation occurred; this indicated that Trp was not necessary for UVR-induced aggregation, despite being the strongest UVR absorber in HγD-Crys. Counter-intuitively, removing half the UVR absorbing capacity of HγD-Crys actually increased the rate of photo-aggregation. This suggests that the Trp residues, which are highly conserved among β/γ-crystallins (66), have a photo-protective role in HγD-Crys, and their replacement with Phe made HγD-Crys

more vulnerable to photodamage. It also implicates the tyrosines of HγD-Crys, the remaining significant UVR absorbers, as playing a role in photo-aggregation.

Such a photoprotective mechanism had been proposed to account for the super-quenched fluorescence emission found for the tryptophans of HγD-Crys as well as other crystallins (118). The human retina is very sensitive to UVR and the lens acts as a UV filter protecting the retina (84, 225). Bova et al proposed that kynurenine and related metabolites served as UVR filters in the lens (83). The work of Chen et al. makes the point that the β/γ-crystallins themselves--with their four conserved buried tryptophans – would also serve as UVR filters (120). The rapid quenching would then represent protection of the protein itself from UVR photo-damage.

The occurrence of photo-aggregation in the absence of Trp at first may appear inconsistent with several previous studies linking Trp photo-oxidative damage with the development of aggregation and/or cataract (191, 198, 226, 227). Previous studies, however, often examined protein mixtures from human or animal lenses, or purified tryptophan in solution as opposed to a single recombinantly purified γ-crystallin protein. Such situations differ from the conditions under study here in their oxygen levels, the presence of other proteins, and redox regulators. Other studies have also utilized photo-sensitizers to produce ROS and initiate oxidative damage to crystallins (217, 218). UVR-induced damage has also been studied using laser radiation sources at differing wavelengths and sometimes of much higher power than the comparably physiological UVR dose being administered here (226, 228). It is thus reasonable

to expect a different photo-damage pathway(s) to be encountered under the experimental conditions used here.

Interestingly, adding Trp's 42, 130, and 156 back (by examining triple W:F mutants with a single Trp remaining) slightly increased photo-aggregation rates relative to NoTrp HγD-Crys, with W156 increasing the least and W130 the most, while adding W68 back slightly decreased the rate of photo-aggregation. It would seem, overall, that having one Trp of the four is more deleterious for HγD-Crys photo-aggregation vulnerability than having none at all. The photo-protective effect may require more than one Trp to be present, and there may be differences in the photo-damage vulnerability and photo-protection contributed by the different Trp's.

The two triple W:F mutant HγD-Crys constructs with only a moderately fluorescent Trp remaining (W42 or W130) photo-aggregated more rapidly than those with only a quenched Trp remaining (W68 or W156). This seems consistent with the analysis of Chen et al., and suggests that the presence of a stronger fluorophore, and thus perhaps a longer-lived photochemically active species, conveys stronger photo-aggregation propensity than a weak fluorophore, which is photochemically active for a far shorter duration (119). Future experiments will address the effects of combinations of W:F mutations on photo-aggregation.

An alternative explanation for the behavior of these multiple mutant HγD-Crys constructs is that, by modifying the hydrophobic core, the mutants proteins are destabilized or have taken on a non-native conformation relative to WT.

Assuming the mechanism of the observed photo-aggregation involves an unfolding or partial unfolding step, these folding or structural changes would be responsible for the apparent photo-aggregation rate change. However, previous experiments have characterized the multiple W:F mutant HγD-Crys constructs and found they adopted stable, WT-like structures (108). CD thermal denaturation experiments showed that the mutants are, indeed, somewhat destabilized compared to WT (Table 1) but still unfold about 40°C above room temperature. Together, these suggest the changes in photo-aggregation behavior result from phenomenon other than destabilization.

Another explanation for the differences in photo-aggregation between WT and W:F mutants could be intra-protein cross-linking. If the conserved Trp residues become photo-excited and cross-linked to other sites within an individual HγD-Crys, such a reaction could compete with inter-protein cross-linking and thus slow the observed aggregation with the formation of photo-products with near identical molecular weights to monomeric HγD-Crys. Inserting W:F mutations would then be removing a competing chemical reaction pathway, not disrupting an energy transfer mechanism. However, this scenario is unlikely given the current data. Significant Trp-based intra-protein cross-links would cause a change in the absorbance spectra of the samples, which was not detected. Intra-molecular cross-links, while not creating a significant difference in molecular weight between uncross-linked and cross-linked proteins, would also create small differences in their mobility in an SDS-PAGE gel, which were not seen.

From the current study, tryptophan is unlikely to be the site of photo-damage, raising questions about which sites in HγD-Crys play key roles in UVR-induced photo-aggregation. Excited state energy transfer occurs from tyrosine to tryptophan (17), and the current results suggests one or a set of HγD-Crys' 14 tyrosines could be an important site of absorption and/or photo-damage. Besides Trp, a number of amino acids, including Cys, Tyr, and His, can participate in excited state radical chemistry that could lead to photochemical covalent cross-linking (15).

It seems likely that the mechanism of the observed photo-aggregation involves absorption at a non-Trp aromatic site, the generation of a free radical on a residue of HγD-Crys, followed by several steps of covalent cross-linking to other HγD-Crys subunits. The absorption and reaction steps of this mechanism could proceed through an array of sites on the protein, or be very specific and involve a small number of residues. Preliminary analysis using mass spectrometry has not found evidence for a single dominant covalent cross-link, suggesting that cross-links are occurring at a diverse set of sites across HγD-Crys. The initial results have, however, identified significant oxidation of Cys18 in irradiated samples, consistent with previous reports on lens protein oxidation (41, 229). This residue is solvent exposed and could be involved in a free radical polymerization.

CHAPTER 3:

Key Residues Sensitizing Human γD-Crystallin to Ultraviolet Radiation-Induced Photo-Aggregation *In vitro**

*This research is in preparation for submission for publication to Protein Science. Nathaniel Schafheimer, Zhen Wang, Kevin Schey, and Jonathan King. *In preparation* Key Residues Sensitizing Human γD-Crystallin to Ultraviolet Radiation-Induced Photo-Aggregation In vitro.

INTRODUCTION

The β/γ-crystallins contain a number of highly conserved aromatic residues. An extensive literature exists documenting the importance of aromatic residues to protein stability and folding (101, 152, 230). Clustering of aromatic and other hydrophobic amino acids drives the folding of polypeptide chains, and aromatics are key components of the water-tight hydrophobic core of many proteins. But these residues also absorb light in the UV range, entering into short-lived singlet excited states from which they can fluoresce or undergo intersystem crossing, converting to longer lived triplet excited states that can participate in radical chemistry leading to covalent damage and protein cross-linking (15). In both excited states, tryptophan, tyrosine, and phenylalanine have been shown to transfer excited state energy non-radiatively to other aromatics in close proximity (5-10 angstroms) (17, 19), and in the triplet state to molecular oxygen, generating singlet oxygen (14, 15). Singlet oxygen, like other reactive oxygen species (ROS), can react and cause oxidative damage to many biological targets, including the amino acids tryptophan, tyrosine, lysine, histidine, and cysteine (15).

Previous work has investigated the effect of UVR on extracted lenses and lens proteins, as well as ROS generated using photo-sensitizers. Bovine crystallin solutions exposed to photodynamically generated ROS became cloudy, and exposed proteins partitioned to the insoluble fraction (198). Human and bovine crystallin solutions exposed to UVR also displayed a rise in turbidity, non-Trp fluorescence, and protein cross-linking (194, 197). UVR has been found to

cause cataract in a number of animal models, including guinea pig, squirrel, rat, and rabbit (179, 186, 189, 195).

Human γD-Crystallin (HγD-Crys), one of the more abundant γ-crystallins in the nucleus of the human lens, is a 173 amino acid protein and contains 4 tryptophans, 14 tyrosines, and 6 phenylalanines. The tryptophan residues are highly conserved across vertebrate β/γ-crystallins and arranged in homologous pairs. Previous work on HγD-Crys has explored the contributions of its high number of aromatic residues to folding and long term stability (108, 115, 117). Recent work by Chen et al. characterized an energy transfer mechanism between tryptophan residues within a pair that rapidly dissipated excited state energy down the protein backbone (118, 120). This was hypothesized to play a photo-protective role, given the lens' chronic exposure to light. *In silico* work by Xia et al. simulated the effect of photo-damage to the tryptophans, replacing the buried tryptophan with kynurenine, its photo-damaged product (201). Kynurenine replacement loosened the hydrophobic core of HγD-Crys, destabilizing the protein and speeding unfolding.

Experiments in Chapter 2 showed that HγD-Crys photo-aggregated when exposed to UVR *in vitro* (231). By examining the photo-aggregation of W:F mutants of HγD-Crys, I presented evidence that the tryptophan energy transfer mechanism played a protective role, and also suggested that tryptophan was not a site of photo-damage or cross-linking when HγD-Crys photo-aggregated *in vitro*.

If the tryptophan pairs act photo-protectively and are not major sites of photo-damage, then some set of the remaining aromatic residues must

participate as UVR absorbers and/or photo-damage sites. Six pairs of interacting tyrosines and phenylalanines also exist across HγD-Crys (Fig. 1.11). Four of these, Y6/F11, Y45/Y50, and Y92/Y97, Y133/Y138 are Greek Key pairs, conserved between HγD-Crys' two domains in homologous positions at β-hairpins (115). Two pairs, Y16/Y28 and F115/F117, are non-Greek Key pairs, positioned at non-homologous locations. In addition individual tyrosines Y62 and Y150 are also important as the Greek Key signature tyrosine corners, making structurally key hydrogen bonds with the peptide backbone of the next β-strand (101). The tyrosine corners also form three-residue clusters with W68 and Y55 in the N-terminal domain and W156 and Y143 in the C-terminal domain. Recent work has examined the structural and folding roles of the tyrosine and phenylalanine pairs, showing that mutation of pairs to alanine significantly disturbs folding and stability for a given HγD-Crys domain (115). *In silico* molecular dynamics experiments by Yang et al. have also shown that Y:A mutation of the tyrosine pairs destabilizes HγD-Crys, opening the hydrophobic cores to water (personal communication).

In this chapter, we set out to study whether the aromatic pairs of HγD-Crys play a role in UVR-induced aggregation *in vitro*, and what types of photo-damage occur during UVR exposure. We used double alanine mutant HγD-Crys constructs targeting the aromatic pairs, and examined their photo-aggregation behavior using light scattering to monitor the development of larger, late stage aggregates, and SDS-PAGE to monitor initial dimeric/multimeric photo-products. We also used liquid chromatography electrospray ionization tandem mass

spectrometry followed by multiple reaction monitoring mass spectrometry to search directly for photo-damaged sites, identifying several cysteines as sites of oxidation, and examined the photo-aggregation behavior of cysteine to serine mutant constructs. Using this data, we propose a mechanism for photo-aggregation of HγD-Crys.

MATERIALS AND METHODS

Mutagenesis, Expression, and Purification of HγD-Crys: N-terminally 6x-His tagged wild-type (WT) HγD-Crys expression constructs were modified via site-directed mutagenesis to introduce Y:A, F:A, and C:S substitutions as described previously (108, 115). All constructs were confirmed via sequencing (Genewiz).

Recombinant WT HγD-Crys and mutant proteins were expressed and purified as described previously (108) with several modifications. Cells were grown to OD_{600} ~1 in Super broth media at 37 °C with shaking. IPTG was added to 1 mM and cultures were transferred to 18 °C followed by shaking overnight. Cells were pelleted by centrifugation for 20 minutes at 17000 *x g* and resuspended in 30 ml Ni-NTA Lysis Buffer (300 mM NaCl, 50 mM $NaPO_4$, 18 mM imidazole, pH 8) containing 2 tablets of Roche Complete EDTA-free protease inhibitor. After addition of lysosome to 3 mg/ml and DNAse to 3 µg/ml of lysate, pellets were lysed via ultrasonication, and centrifuged at 17000 *x g* for 45 minutes. Supernatants were filtered and applied to a Ni-NTA column (GE Healthcare). Protein was eluted using a linear gradient of increasing imidazole concentration. Fractions containing the protein of interest were pooled and

dialyzed three times against storage buffer (10 mM ammonium acetate, pH 7.0). HγD-Crys was concentrated using 10,000 MWCO Vivaspin 20 concentrator (Sartorius Stedim Biotech).

Expression and Purification of HαB-Crys:

HαB-Crys was expressed and purified as described previously (105). In brief, HαB-Crys was expressed in BL21 Gold (DE3) *E. coli* cells (Stratagene). Cleared cell lysates underwent two rounds of ion-exchange chromatography using a HiPrep 16/10 Q Sepharose FF column (GE Lifesciences) followed by size exclusion chromatography (SEC) in a Superose 6 10/300 GL SEC column (GE Lifesciences). Protein was kept in 50 mM sodium phosphate pH 7, 150 mM NaCl until needed. HαB-Crys was dialyzed into storage buffer and concentrated using a 10,000 MWCO Vivaspin 20 concentrator (Sartorius Stedim Biotech).

Protein Concentration Measurement: Stock protein sample concentration was determined using absorbance at 280 nm with the following extinction coefficients (determined using SIB's ProtParam): WT, single C:S, NoCys, and double F:A HγD-Crys 42,860 M^{-1} cm^{-1}, double Y:A HγD-Crys 39,880 M^{-1} cm^{-1}, single Y:A HγD-Crys 41,370 M^{-1} cm^{-1}, quadruple W:F HγD-Crys 20,860 M^{-1} cm^{-1}, HαB-Crys 13,980 M^{-1} cm^{-1}.

Photo-aggregation Experiments*:* Samples of HγD-Crys were prepared at 1 mg/ml in 1x Reaction Buffer (100 mM Na_2PO_4, 1 mM EDTA, pH 7). Samples

were irradiated at room temperature in a quartz cuvette (Starna Group) using a UVP Inc. UVLMS-38 lamp equipped with a 302 nm midrange bulb delivering a range of UVA/UVB light. UVR dose delivery was set to 2 mW/cm^2 by adjusting the cuvette's distance to the lamp, and determined before each experiment by a UVX Radiometer with midrange UVX-31 sensor. Turbidity readings at OD_{600} on a Cary UV/Vis Spectrometer were taken at regular time points during irradiation. Samples removed and analyzed via SDS-PAGE were reduced and boiled and electrophoresed through 14% acrylamide gels at 170 V for 1 hour; gels were stained using Krypton Fluorescent Protein Stain (Thermo Fisher Scientific) and imaged on a Typhoon 9400 (Amersham Biosciences). Gel band quantification was performed using ImageJ.

HαB-Crys photo-aggregation experiments were performed as above, with the following modifications. 1 ml HγD-Crys samples were prepared at 1 mg/ml, and 1 ml HαB-Crys samples were prepared at 2 mg/ml or 5 mg/ml, both in Reaction Buffer. 1 ml HγD-Crys and HαB-Crys samples were mixed together to produce 1:2 or 1:5 HγD-Crys:HαB-Crys samples (by mass and molarity). These mixed samples then proceeded through UVR exposure, turbidity readings, and gel sample removal as described above.

Western Blot Analysis: HαB-Crys monomers are similar in molecular weight to HγD-Crys, thus Western blotting was used to visualize HγD-Crys bands during aggregation suppression experiments. Transfer from unstained SDS-PAGE gels was conducted overnight at 4°C using 15 mA in SDS-PAGE Run Buffer (1% SDS,

25 mM Tris, and 192 mM glycine) onto 0.45 µm polyvinylidene difluoride membranes (Millipore).

The primary antibodies used for HγD-Crys and HαB-Crys were from Santa Cruz Biotechnology: HγD-Crys, sc-100697; HαB-Crys, sc-53919. The secondary antibodies were alkaline phosphatase (AP)-conjugated (BioRad) and the membranes were visualized using the AP-conjugate substrate kit (BioRad).

Mass Spectrometry Measurements: HγD-Crys samples for LC-MS/MS were prepared and irradiated as described in the photo-aggregation section. 0 and 60 minute exposed samples were mixed with SDS Load Buffer lacking BME (to final concentration 333 mM Tris pH 6.8, 2% SDS, 30% glycerol). DTT was added to 10 mM and samples were incubated for 1 hour at 37°C. Iodoacetamide was added to 55 mM and samples were incubated for an additional hour in the dark at 37°C.

Samples then underwent SDS-PAGE through a 14% acrylamide gel at 170V for 1 hour. The monomer and dimer gel bands were excised and destained with three consecutive washes of 50 mM ammonium bicarbonate/acetonitrile (ACN) (1/1, v/v) for 10 min. 20 µL 10 mM DTT was added to each sample and the gel bands were incubated at 56 °C for one hour. 20 µL 55 mM iodoacetamide was then added and the gel bands were incubated at room temperature in the dark for 30 min. The gel bands were then washed three times with 50 mM ammonium bicarbonate/ACN (1/1, v/v) for 10 min. each. The dehydrated gel bands were completely dried by SpeedVac. Each sample containing an individual

band was rehydrated in 10-15 µL of solution containing 10 ng/µL trypsin or chymotrypsin (Promega) in 50 mM ammonium bicarbonate for 15 min. 50 µL of 50 mM ammonium bicarbonate buffer was added to each sample and the samples were incubated at 37°C for 18 hours. Peptides were extracted using 20% ACN/0.1% formic acid (FA) once, 60% ACN/0.1% FA twice, and 80% ACN/0.1% FA once. The extract solutions were pooled and dried in by SpeedVac and reconstituted in 0.1% formic acid for subsequent LC-MS/MS analysis.

Peptides were separated on a one-dimensional fused silica capillary column (150 mm x 100 mm) packed with Phenomenex Jupiter resin (3 mm mean particle size, 300 Å pore size) using the following gradient at a flow rate of 0.5 mL/min: 0-10 min: 2% ACN (0.1% formic acid), 10-50 min: 2-35% ACN (0.1% formic acid), 50-60 min: 35-90% ACN (0.1% formic acid) balanced with 0.1% formic acid. The eluate was directly infused into a Velos Pro mass spectrometer or a Velos Orbitrap mass spectrometer (ThermoScientific) equipped with a nanoelectrospray source. Dynamic exclusion (repeat count 2, exclusion list size 300, and exclusion duration 60s) was enabled to allow detection of less abundant ions for all LC-MS/MS analyses.

HγD-Crys samples for Multiple Reaction Monitoring (MRM) mass spectrometry were prepared at 2 mg/ml in 1x Reaction Buffer and exposed to 2 mW/cm^2 UVR as in the photo-aggregation experiments. 200 µl time samples were removed at 0, 10, 20, 30, 40, 50, and 60 minutes of UVR exposure. Time samples were centrifuged at 4°C for 30 minutes at 17,000 *x g*, then the supernatant was removed and diluted tenfold into guanidine HCl (GuHCl) buffer

(final concentrations 5.5 M GuHCl, 100 mM sodium phosphate pH 7, 1 mM EDTA); these were labeled “Soluble Fraction.” The pellets were resuspended in 100 μl GuHCl buffer and labeled “Pellet Fraction.” Soluble and Pellet fraction time samples were incubated overnight at 37°C, followed by sequential addition of DTT to 10 mM and 1 hour incubation at 37°C, and iodoacetamide to 55 mM and 1 hour incubation at 37°C in the dark. Soluble and Pellet fraction time samples were then precipitated using a methanol/chloroform protocol to separate protein from GuHCl. After pellets were separated from supernatants, sample pellets were dried, and rehydrated and suspended in 30 μl of 2M urea, 100 mM Tris HCl (pH 8.5). Porcine trypsin (Promega) was added to all samples to a final concentration of 16.7 ng/μl, and samples were incubated over night at 37°C. Digestions were stopped by adding 1.5 μl of 1% trifluoroacetic acid to each sample.

Samples were analyzed by Multiple Reaction Monitoring (MRM) on a TSQ Vantage mass spectrometer (ThermoScientific, San Jose, CA). After an unscheduled run to determine retention times for peptides of interest, a scheduled MRM method was created using Skyline (https://brendanx-uw1.gs.washington.edu/labkey/project/home/software/Skyline/begin.view) to include a 10 minute window around the measured peptide retention time along with calculated optimum collision energies. Q1 peak width resolution was set to 0.7, collision gas pressure was 1 mTorr, and an EZmethod cycle time of 5 seconds was utilized. The resulting RAW instrument files were imported into Skyline for peak-picking and quantitation. For relative quantitation of C18

trioxidation, the peak area for trioxidized peptide 15-31 was compared to the summed intensity of two peptides determined to be unchanged by UV irradiation: peptide 3-9 and peptide 169-173.

Circular Dichroism Thermal Unfolding Measurements: CD spectra of the WT and mutant proteins were obtained using an AVIV model 202 CD spectrometer (Lakewood, NJ). Protein samples were prepared at a concentration of 0.1 mg/ml in 10 mM sodium phosphate, pH 7.0. Data were collected at 218 nm in a 1 cm quartz cuvette. Sample temperature was increased from 25°C to 95°C in 1°C steps with 1 minute of equilibration time per °C, followed by 5 second reads. Data were corrected for buffer blank readings, and mean residue ellipticity was calculated. The mean residue ellipticity versus temperature data were fit to a sigmoidal curve using Kaleidagraph (Synergy Software), and the unfolding midpoints were calculated. The unfolding temperatures reported are averages of 3 thermal unfolding experiments.

RESULTS

Photo-Aggregation of Aromatic Pair Mutants

To investigate the potential roles of the aromatic pairs in the photo-aggregation of HγD-Crys, we employed HγD-Crys double mutant proteins in which both members of an aromatic pair were mutated to alanine. We exposed these mutant HγD-Crys proteins to 2 mW/cm^2 UVR for 60 minutes while

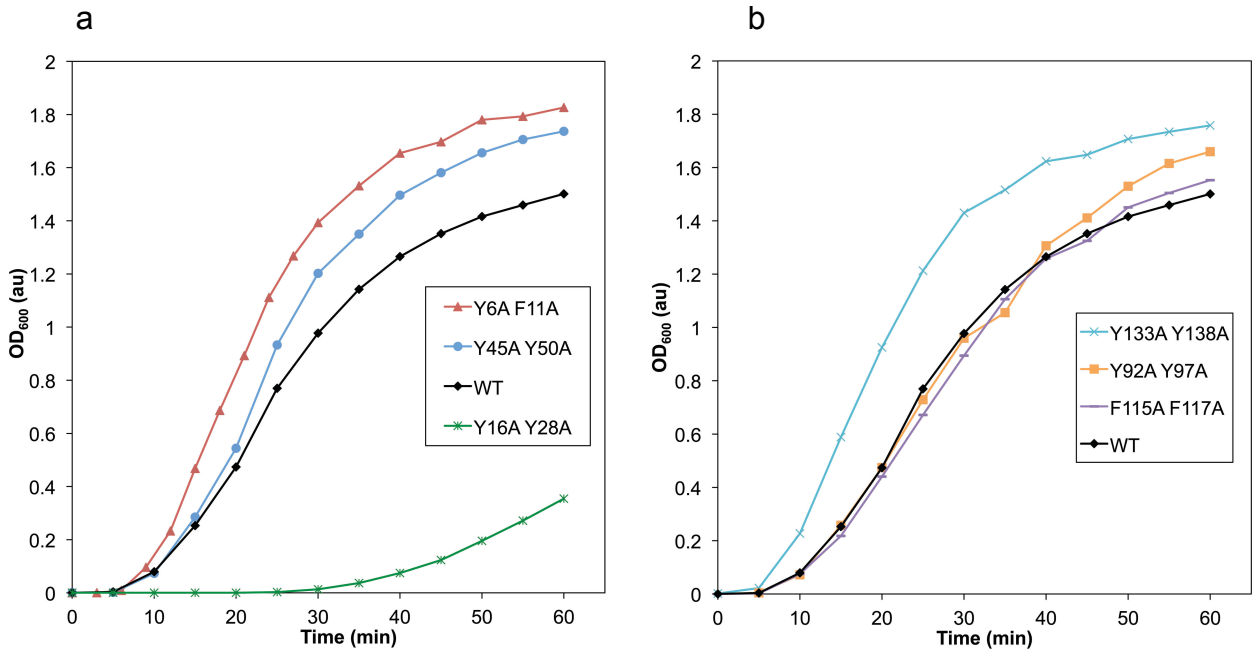

Figure 3.1 Comparing Y:A, F:A Mutants to WT HγD-Crys Photo-aggregation. Comparison of UVR-induced aggregation of HγD-Crys constructs with aromatic pairs replaced by alanine. Samples were made at 1 mg/ml in reaction buffer, and light scattering was monitored at 600 nm over UVR exposure time. (a) N-terminal pairs: WT (black diamonds), Y6A/F11A (red triangles), Y16A/Y28A (green hashes), and Y45A/Y50A (blue circles). (b) C-terminal pairs: WT (black diamonds), Y92A/Y97A (orange squares), F115A/F117A (lavender dashes), Y133A/Y138A (turquoise X's).

monitoring aggregation using light scattering at 600 nm (Fig. 3.1a and 3.1b). Two of the three N-terminal mutant pairs, Y6A/F11A, Y45A/Y50A, and one of the C-terminal mutant pairs, Y133A/Y138A, photo-aggregated slightly more quickly than WT, indicating their loss likely made HγD-Crys slightly more vulnerable to UVR. Two of the C-terminal mutants, Y92A/Y97A and F115A/F117A, behaved similarly to WT, indicating they had no effect on HγD-Crys photo-aggregation. One N-terminal pair mutant, Y16A/Y28A, photo-aggregated significantly slower than WT, suggesting that one or both residues are important participants in photo-damage.

The differences in photo-aggregation between the aromatic pair mutants suggested that specific tyrosines and phenylalanines of HγD-Crys are distinct in their absorptive and photochemical properties. Because absorbed energy can be transferred between nearby aromatic amino acids, the pair mutants that photo-aggregated more significantly than WT could have roles transferring energy to the highly conserved tryptophan pairs, previously suggested to play a protective role (118, 121). Interestingly, light scattering eventually developed at longer UVR exposure times in the Y16A/Y28A samples, suggesting that other photo-damage sites must still be operating in the absence of these tyrosines.

Photo-Aggregation of C:S Mutant HγD-Crys

Mass spectrometry by Schey and coworkers identified C18, and to a much lesser extent C78 and C108, as sites of oxidative damage after UVR exposure. Cysteine thiols were oxidized to sulfinic and sulfonic acid (Fig. 1.3). To determine

the importance of the individual cysteine residues identified via mass spectrometry in photo-aggregation, we constructed HγD-Crys mutant constructs with cysteines of interest mutated to serines. We exposed the purified proteins to UVR, monitoring turbidity as with the aromatic pairs (Fig. 3.2). C78S HγD-Crys and C108S HγD-Crys both behaved similarly to WT or aggregated slightly more quickly, suggesting their oxidation might have been unrelated to aggregation..

C18S HγD-Crys photo-aggregated much slower than WT, suggesting that C18 played an important role in HγD-Crys photo-aggregation. This is consistent with the mass spectrometry data, which showed a much higher abundance of C18 oxidation than C78 or C108 in both fractions, suggesting it more readily reacts with ROS. It seems unlikely that the oxidation of C18 by itself is important for aggregation, given that it does not produce a covalent photo-crosslink. The complete oxygen dependence of *in vitro* photo-aggregation tells us that ROS are present during UVR exposure and implies that C18 oxidation is an off-pathway photo-damage reaction in competition with C18's aggregation-relevant role.

Cysteine thiol groups have been shown to participate in radical photochemistry that produces cross-links to a variety of chemical groups (22, 232, 233). Given the oxidation of C18, it seems likely that cysteine radicals would also be produced. These might be expected to form thio-ether cross-links to many residues on the surface of HγD-Crys. The heterogeneity of said cross-links would make them difficult to identify by mass spectrometry.

To determine whether photo-aggregation of HγD-Crys can occur in the absence of cysteine, we created a multiple mutant HγD-Crys construct, NoCys,

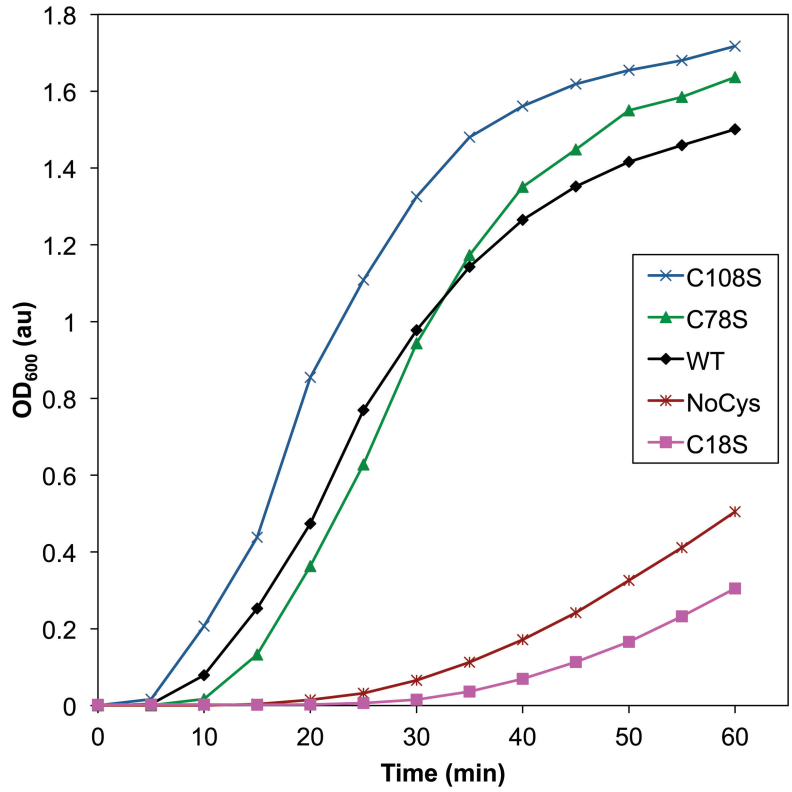

Figure 3.2 Comparing C:S Mutants to WT HγD-Crys Photo-aggregation. Comparison of UVR-induced aggregation of HγD-Crys constructs with select cysteine residues replaced with serine. Samples contained protein at 1 mg/ml in reaction buffer, and light scattering was monitored at 600 nm as a function of UVR exposure time. WT (black diamonds), C18S (magenta squares), C78S (green triangles), C108S (indigo X's), NoCys (maroon hashes).

with all 6 cysteines mutated to serine. When exposed to UVR, the NoCys HγD-Crys protein photo-aggregated, but the rate of photo-aggregation was slowed as compared to WT, similar to C18S HγD-Crys. This suggested that C18 may be the only important cysteine in HγD-Crys, as removing all cysteines retarded photo-aggregation to a similar extent as mutating C18.

The fact that the NoCys HγD-Crys protein still exhibited photo-aggregation demonstrated that even if thiol chemistry is involved in the photo-aggregation of WT, as mass spectrometry experiments with C18 suggested, other sites in HγD-Crys must also be involved in photo-aggregation. NoCys HγD-Crys was extremely destabilized relative to WT HγD-Crys (Table 3.1), but still photo-aggregated much more slowly than WT, demonstrating that overall thermodynamic stability does not appear to play a significant role in photo-aggregation propensity.

Analyzing Mutants of the Y16/C18/Y28 Cluster

In the high resolution HγD-Crys crystal structure by Slingsby and coworkers, the thiol group of C18 is directly contacting the aromatic ring of Y16, itself stacked in a pair with Y28 (112). To investigate the relationships among these three residues implicated in photo-aggregation, we made different individual and combination mutant HγD-Crys constructs of the three sites and compared the mutant protein photo-aggregation behavior by monitoring turbidity (Fig. 3.3a and 3.3b).

Table 3.1 Circular Dichroism Thermal Unfolding Data for HγD-Crys Mutant Constructs

Construct	*Melting Temperature (°C)*	*Standard Deviation (°C)*
WT	82.1	0.4
Y16A	77.3	0.07
Y28A	76.9	0.04
C18S	72.5	0.3
Y16A Y28A	75.3	0.07
Y16A C18S	73.2	0.13
C18S Y28A	73.3	0.1
Y16A C18S Y28A	72.3	0.06
NoCys	59.6	0.08

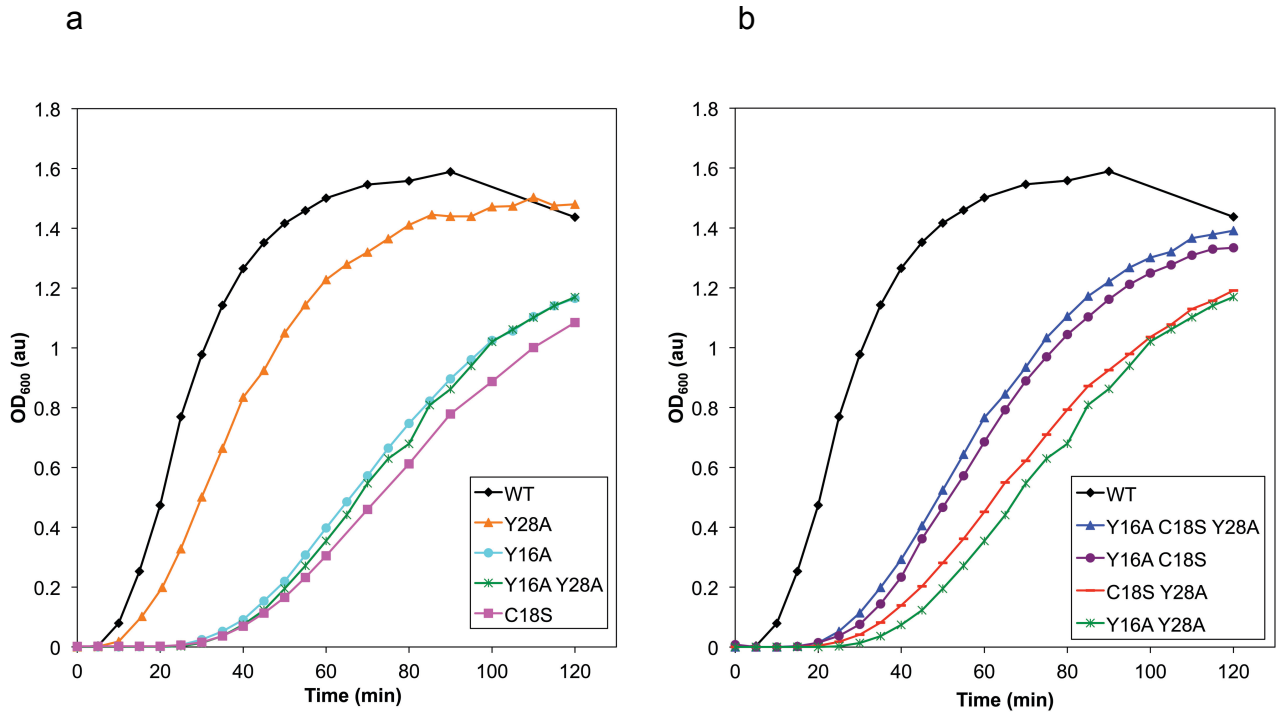

Figure 3.3 Y16A, Y28A, C18S Combination Mutant Photo-aggregation. Comparison of UVR induced aggregation of HγD-Crys constructs with individual or combination mutations of C18 to serine, Y16 to alanine, and Y28 to alanine. Samples were made at 1 mg/ml in reaction buffer, and light scattering was monitored at 600 nm over UVR exposure time. (A) WT (black diamonds), Y16A (turquoise circles), C18S (magenta squares), Y28A (orange triangles), Y16A/Y28A (green hashes). (B) WT (black diamonds), Y16A/Y28A (green hashes), Y16A/C18S (purple circles), C18S/Y28A (maroon dashes), Y16A/C18S/Y28A (beige triangles).

The Y16A HγD-Crys single mutant displayed retarded photo-aggregation as compared to WT, similar to C18S and Y16A/Y28A HγD-Crys. Y28A HγD-Crys photo-aggregation was only mildly delayed and much more similar to WT. This suggested that for photo-aggregation, Y16 is the important tyrosine of the Y16A/Y28A pair tested earlier (Fig. 3.1a). Due to the similarity in photo-aggregation rates of Y16A and C18S HγD-Crys, it is likely that the slowing of photo-aggregation in each single mutant was due to removal of a shared activity dependent on the presence of both residues. Therefore, we postulate that mutating one residue would be sufficient to abolish the relevant photochemical activity of both. Additionally, Y28A HγD-Crys' mild photo-aggregation retardation as compared to WT, may have nothing to do with its own participation in photochemistry and simply be a product of Y28's effect on Y16 and C18.

Y16A/C18S HγD-Crys, C18S/Y28A HγD-Crys, and the triple mutant Y16A/C18S/Y28A HγD-Crys were exposed to UVR and compared to Y16A/Y28A HγD-Crys and WT to investigate the interplay between the three residues. C18S/Y28A HγD-Crys behaved similarly to C18S and Y16A/Y28A, suggesting again that Y28 is not important for photo-aggregation and that the mutation of C18 or Y16 is sufficient to produce the observed retardation.

Curiously, the Y16A/C18S double mutant HγD-Crys and the triple mutant Y16A/C18S/Y28A HγD-Crys photo-aggregated at an intermediate rate between Y16A/Y28A and WT HγD-Crys. The simple lack of an additive delay when Y16 and C18 were both mutated away is further evidence that they participate in a single photochemical process. But the moderate increase in photo-aggregation

rate over the single mutants when the Y16A and C18S mutations are put together suggested that while the double mutation abolishes the photochemistry Y16 and C18 are involved in, it increases the rate of some other photo-aggregation related reaction, perhaps by subtly perturbing the structure of the N-terminal domain. A similar analysis applies to the Y16A/C18S/Y28A triple mutant HγD-Crys, and its similar intermediate behavior to Y16A/C18S HγD-Crys is further evidence of the peripheral photo-aggregation activity of Y28.

MRM Mass Spectrometric Analysis of C18 Tri-oxidation

To test the hypothesis that Y16 and C18 are involved in the same photochemical damage mechanism, MRM mass spectrometric analysis was performed comparing UVR-exposed WT and Y16A HγD-Crys (Fig. 3.4). The Schey group measured the abundance of the tri-oxidized tryptic HγD-Crys peptide 15-31 from soluble or pelleted photo-aggregate samples as a function of UVR-exposure time. The amount of peptide with C18 oxidized to sulfonic acid rose in a UVR exposure time dependent manner for both WT and Y16A HγD-Crys soluble protein samples, while the pelleted samples were steadily much higher than the soluble samples. However, the amount of tri-oxidized peptide in the Y16A samples was much lower than in WT, and rose more slowly in the soluble samples. This supports the idea that Y16 and C18 are a single photochemically linked site. Disrupting one residue disrupted both the photochemistry and photo-aggregation effect of the site.

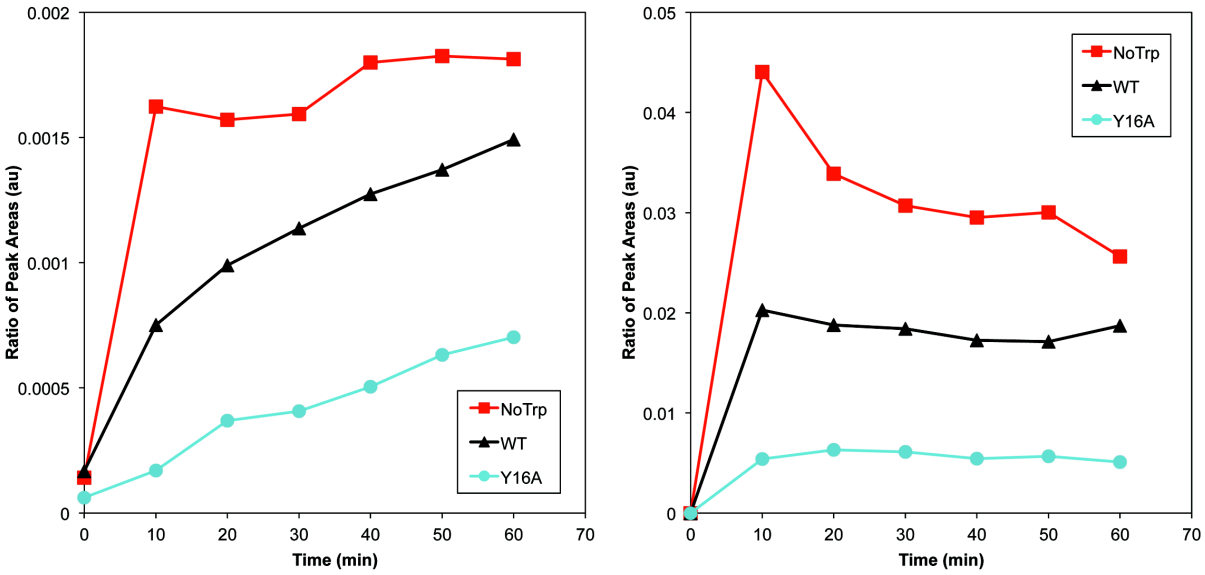

Figure 3.4 MRM Mass Spectrometry Monitoring C18 Tri-oxidation. Quantitation of tri-oxidized peptide 15-31 for UVR-exposed WT, Y16A, and NoTrp HγD-Crys as a function of exposure time. The y-axis plots the 15-31 peptide peak area divided by peak areas for peptides 3-9 and 169-173 for internal protein loading control. (a) Soluble UVR-exposed protein samples, (b) Pelleted photo-aggregated protein samples, with squares (NoTrp), triangles (WT), and circles (Y16A).

In chapter 2, we saw evidence that the 4 tryptophans of HγD-Crys played a protective role against photo-aggregation. It seemed likely that that protective role involved minimizing photochemical damage to the aromatic residues, but it is also possible that the tryptophan energy transfer mechanism could be protective against other types of photo-damage. To test whether the tryptophans played a role in C18 oxidation, we examined UVR-exposed NoTrp HγD-Crys via the same MRM mass spectrometry experiment as WT and Y16A HγD-Crys. NoTrp HγD-Crys showed higher amounts of C18 oxidation to sulfonic acid, and oxidation appeared more rapidly than WT or Y16A, suggesting that the photo-protective effect of the tryptophans extends to C18 oxidation.

Early- vs. Late-Stage Photo-Aggregation

Previously, we used SDS-PAGE to monitor the development of initial cross-linked photo-products of WT HγD-Crys. This early dimerization was differentiated from the later rise in larger, visible light scattering aggregates (231). In this chapter, we used the same comparison to determine whether the Y16A, C18S, and NoCys mutations affect early- or late-stage photo-aggregation (Fig. 3.5a and 3.5b). When WT HγD-Crys was exposed to UVR, dimers appeared quickly, before light scattering. Despite the significant delay in light scatter development seen with the Y16A, C18S, and NoCys mutants, all three developed photo-dimers at early times, similar to WT. This indicated that the photochemical process (or possibly processes) that involve C18 and Y16 influence the light scattering, late-stage of photo-aggregation, but not the early-

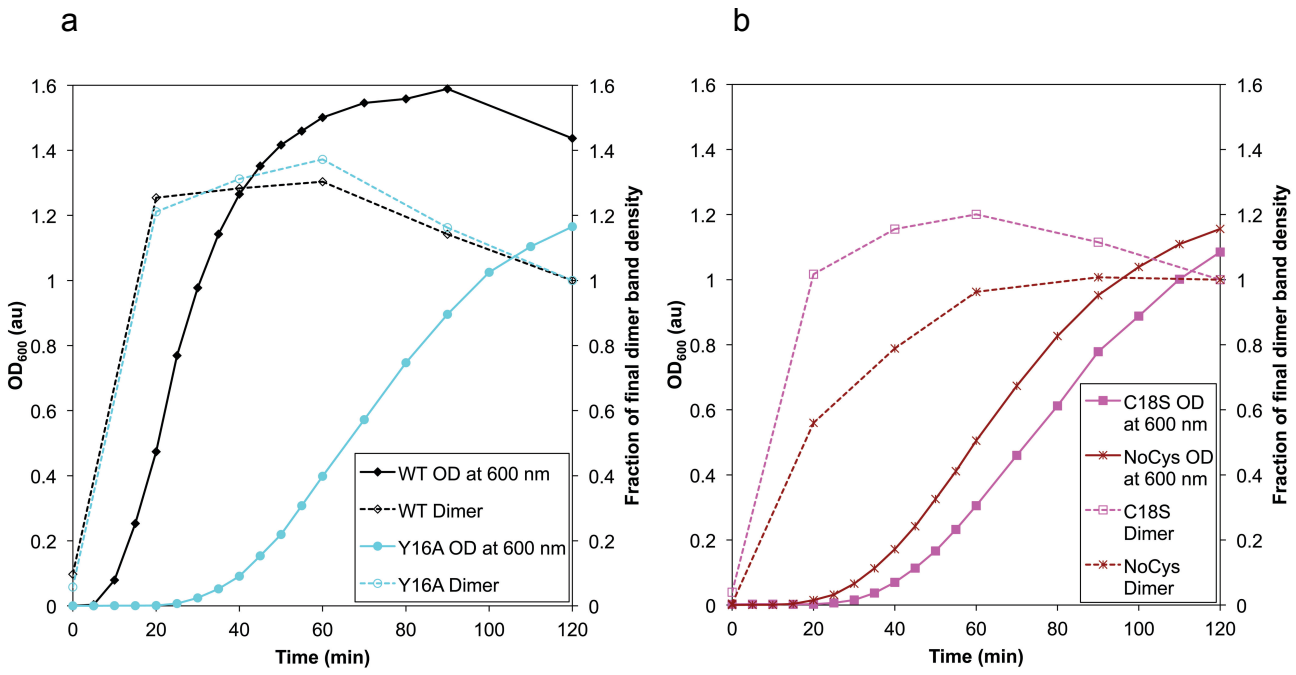

Figure 3.5 Comparing Turbidity to Dimeric Product Formation with Y16A, C18S, NoCys, and WT HγD-Crys. Comparison of turbidity development at 600 nm (left axis, solid lines and closed symbols) and density of dimer gel band (right axis, dotted lines and open symbols) versus UVR exposure time for 4 HγD-Crys constructs. Samples were made at 1 mg/ml in reaction buffer. 20 μl of samples were added to 10 μl of 3x gel loading buffer, boiled, and then 15 μl were electrophoresed. Dimer band density was normalized to final dimer band density to give the fraction of final dimer band density.
a) WT (black diamonds), Y16A (turquoise circles)
b) C18S (magenta squares), NoCys (maroon hashes).

stage dimer formation. The formation of dimeric photo-products when NoCys HγD-Crys protein was exposed to UVR also conclusively demonstrated that the dimer-producing cross-link does not involve cysteine.

Chaperone Suppression of HγD-Crys Photo-Aggregation

In the lens, chaperones decrease protein aggregation by recognizing misfolded proteins and binding to them. To understand whether the early-stage dimer was on pathway to aggregation and whether the late-stage of photo-aggregation was physiologically relevant, we added the lens chaperone human αB-crystallin (HαB-Crys) to the HγD-Crys UVR reaction. When exposed to UVR, HγD-Crys photo-aggregation, as observed by light scattering, was suppressed in a HαB-Crys concentration dependent fashion (Fig. 3.6a). HαB-Crys' suppression of late-stage, light scattering aggregation suggested this *in vitro* process is similar to aggregation that occurs *in vivo*.

We then went on to determine whether early-stage dimer formation was also suppressed in the presence of HαB-Crys (Fig. 3.6b). With a 5:1 ratio of HαB-Crys:HγD-Crys, HγD-Crys photo-dimers appeared at early time points and higher order multimers appeared soon after. The lack of dimer and multimer formation suppression by HαB-Crys suggested HαB-Crys may not recognize the initial cross-linked products. This result also gave credence to the hypothesis that initial dimers are side reaction photo-products, potentially unrelated to the Y16- and C18-influenced later aggregation reactions.

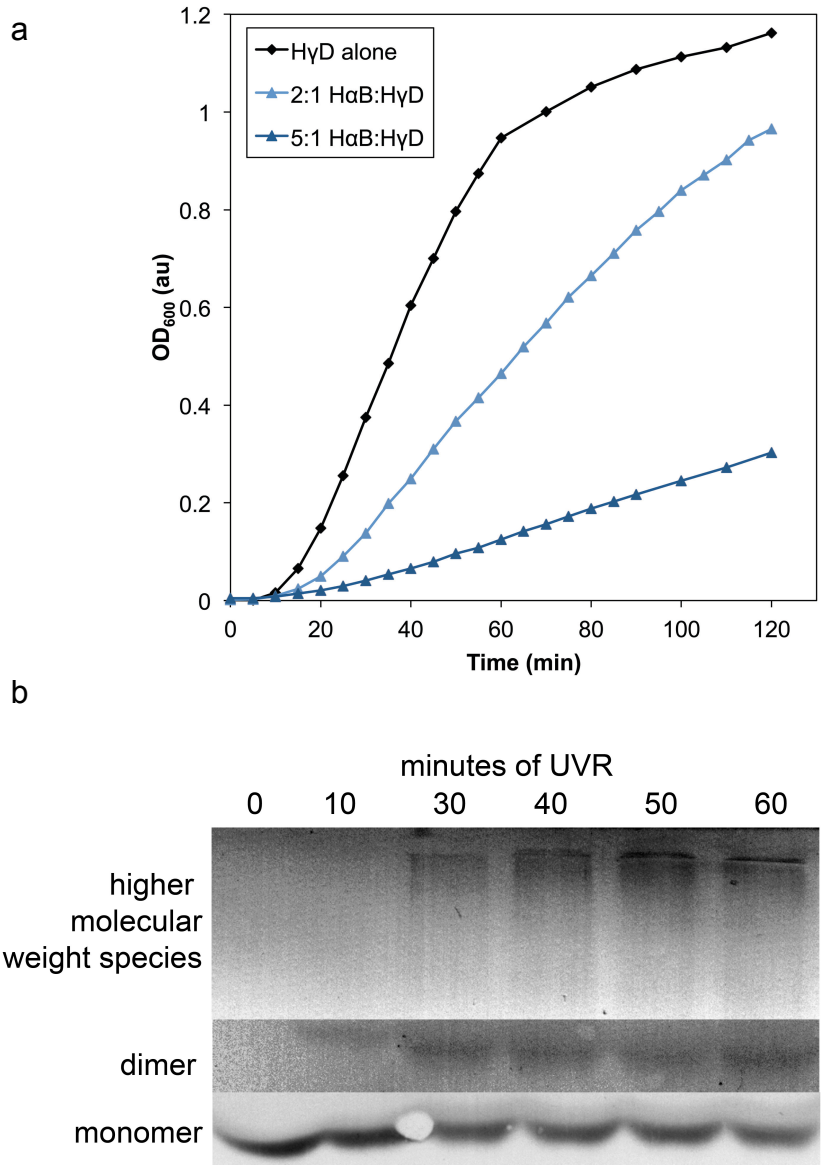

Figure 3.6 Photo-aggregation of HγD-Crys in the Presence of HαB-Crys. Monitoring photo-aggregation of 0.5 mg/ml HγD-Crys samples using light scatter at 600 nm over UVR exposure time and Western blotting to detect initial multimeric photo-products in the presence of varying amounts of HαB-Crys. a) Light scattering versus UVR exposure: HγD-Crys alone (black diamonds), HγD-Crys plus 1 mg/ml HαB-Crys at 2:1 HαB-Crys:HγD-Crys (light blue triangles), HγD-Crys plus 2.5 mg/ml HαB-Crys at 5:1 HαB-Crys:HγD-Crys (dark blue triangles). b) Western blot against HγD-Crys of 5:1 HαB-Crys:HγD-Crys samples from (a) exposed to UVR for varying times. Image is a composite of scanned sections of one developed membrane, each adjusted for ease of viewing.

An important control experiment for any aggregation suppression experiment is a sample in which a protein with no chaperone activity is included in place of the chaperone under study. Unfortunately, crystallin photo-aggregation suppression experiments present special challenges in this regard. HαB-Crys, unlike other readily available model proteins, does not photo-aggregate and scatter light upon UVR exposure (Fig. 3.7). Therefore, a satisfactory non-chaperone control protein would need to be similarly aggregation resistant. We have found no such protein, and have been unable to produce inactive soluble HαB-Crys by heating, extended UVR exposure, or freeze thawing (data not shown). Thus we are unable to control for the possibility that the observed HγD-Crys aggregation suppression is due simply to the presence of an aggregation resistant protein in solution.

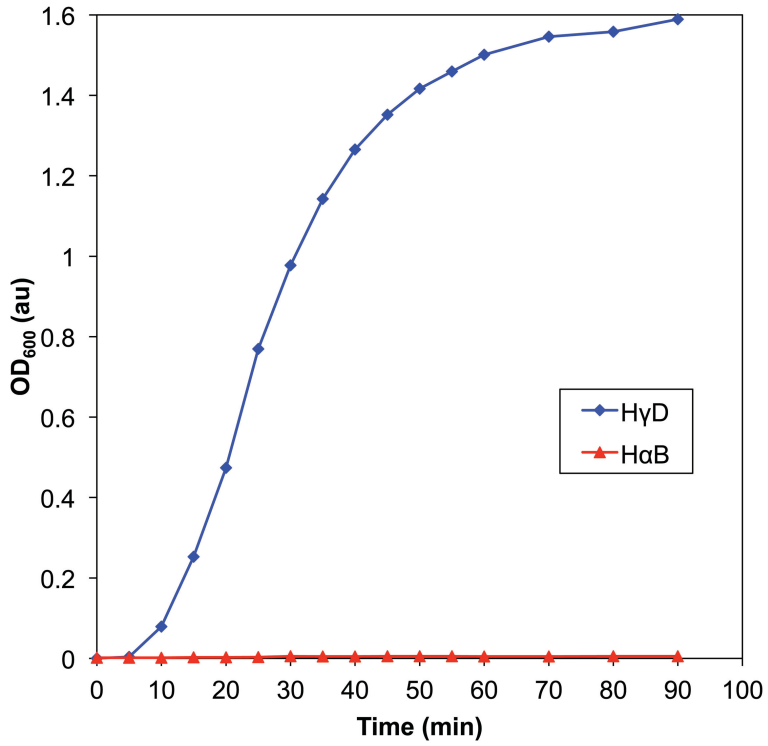

Figure 3.7 Comparing Photo-aggregation of HγD-Crys and HαB-Crys Alone. Monitoring photo-aggregation of 1 mg/ml solutions of HγD-Crys (blue diamonds) or HαB-Crys (red triangles) over UVR exposure time using OD at 600 nm.

DISCUSSION

Two aromatic residues, Y16 and C18, appear to be important to the photo-aggregation of the long-lived lens protein, HγD-Crys. One, Y28, could be involved, directly or peripherally. We further showed that these residues were involved in the later, light scattering steps of photo-aggregation. Combined with previous work analyzing the photo-aggregation behavior of W:F mutants of the conserved tryptophan pairs (231), 16 of HγD-Crys' 24 aromatic residues have been perturbed via site-directed mutagenesis and examined for their role in photo-aggregation. Several questions arise: first, what differentiates Y16, and potentially Y28, from the other UVR absorbing residues?

Solvent exposure and the proximity of amino acid side chains known to undergo radical chemistry mark Y16 and Y28 as different from other aromatic pairs (Fig. 3.8). In the HγD-Crys crystal structure, both Y16 and Y28 are surface exposed compared to other aromatic pairs, making it more likely for them to encounter molecular oxygen and that the photochemistry they undergo could result in an intermolecular cross-link. Additionally, the Y16/Y28 pair is the only pair in the HγD-Crys crystal structure with a cysteine thiol (C18) contacting an aromatic ring. There is also a histidine, H22, in close proximity to Y16 and Y28. Both thiol and imidazole side chains have been shown to participate in radical photochemistry, for example, in the cysteine-based variants of thiol-ene "click" chemistry, or in the formation of histidine-histidine or histidine-lysine cross-links via singlet oxygen (233, 234).

a b

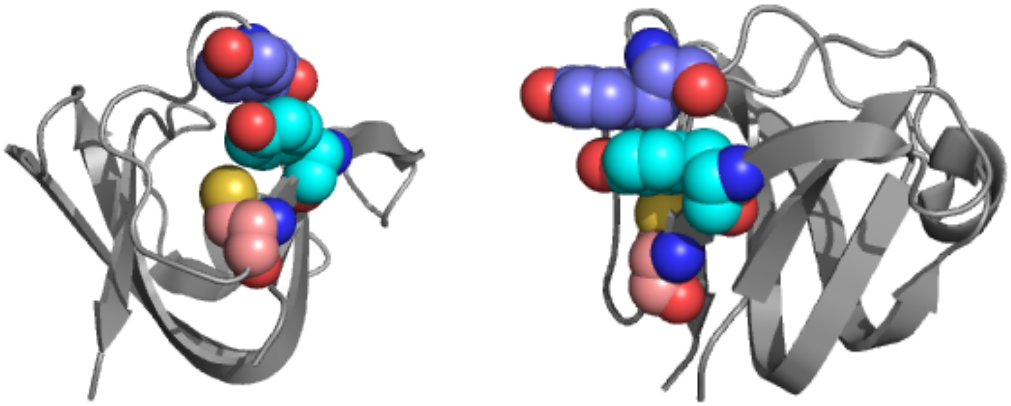

Figure 3.8 Three-dimensional Structure of HγD-Crys N-terminal Domain Highlighting Y16, Y28, and C18. Ribbon structure of the N-terminal domain of HγD-Crys highlighting the identified key residues for photo-aggregation as spheres: Y16 (turquoise carbons), Y28 (indigo carbons), and C18 (salmon carbons). (a) and (b) are approx. 90° rotations of the same structure, highlighting the positioning of the three residues relative to each other.

Y16 and Y28 are also members of the N-terminal “non-Greek Key” aromatic pair, and are not as strongly conserved across βγ-crystallins as the Greek Key pairs (115). Kong et al. aligned the sequences of 79 β/γ-crystallin protein sequences across 8 species, and found that Y16 and Y28 were only conserved across 44% of sequences, just in the γ-crystallins, whereas the Greek Key pairs were conserved across 82-100%. It is possible that selective pressures for structural stability and against photo-aggregation propensity are at odds over the advantage of the Y16/Y28 aromatic pair. The C-terminal “non-Greek Key” aromatic pair mutant, F115A/F117A HγD-Crys, although also poorly conserved, photo-aggregated similarly to WT, suggesting no similarity to its N-terminal counterpart in this regard.

Mass spectrometry has not identified cross-linked peptides or other photo-damage sites besides C18, C78, and C108. While we hesitate to extrapolate from negative results, this could suggest several explanations. ROS-mediated cross-links and oxidation can target a number of amino acids, and as such there could be many sites of photodamage such that most are too low in abundance to be detected by our methods (15). Photo-crosslinked species are likely resistant to protease digestion, as the native β/γ-crystallin family proteins have proven to be (data not shown); the denaturants present in our digestion reactions may be insufficient to produce a trypsin digestible substrate. This would explain why we observe complete peptide coverage but primarily undamaged peptide spectra. This could also explain why mass spectroscopic analysis of gel bands containing dimeric photo-products identify no cross-linked peptides.

Whether or not HγD-Crys contains many low frequency photo-damage sites, other photodamage sites besides the Y16/Y28 pair and C18 must exist, as photo-aggregation occurred in their absence. The oxygen dependence of the *in vitro* photo-aggregation of HγD-Crys strongly favors a mechanism of indirect photo-damage with singlet oxygen mediating cross-linking and photo-oxidation (14, 15). This expands the list of potential sites of damage from UVR absorbers, including the unexamined 5 unpaired tyrosine residues and the 3 unexamined phenylalanines, and other sites vulnerable to ROS like histidine and lysine, both shown to form cross-links when exposed to singlet oxygen. The phenylalanines, while shown to undergo direct photodamage when excited, do not react with singlet oxygen at rates that compete with other residues (15). Of the remaining tyrosines, none save one are significantly surface accessible; although two, Y62 and Y143, are tyrosine corners and important for HγD-Crys' Greek Key structural stability. The exception, Y153, seems a likely candidate for photo-damage based on our evaluation of the distinguishing characteristics of the Y16 Y28 pair: it is relatively exposed to solution and in close proximity to surface exposed H121.

The formation and molecular basis of the initial photo-dimer HγD-Crys remain a mystery. Because it presents as a distinct band after boiling, reduction, and SDS-PAGE, we can be reasonably sure that it is covalent, non-disulfide based, and arises from a particular cross-link, as a series of linkages would produce a number of similar bands. HαB-Crys has been shown to possess chaperone activities (88), and animal αB-crystallins have inhibited photo-aggregation *in vitro* (128, 235), but HαB-Crys did not suppress HγD-Crys photo-

dimer formation, so it is possible that the initial dimer is an off pathway photo-product without relevance to light scattering photo-aggregation. However the first step in a polymerization scheme is the linking of two individual monomers, and since initial dimer formation occurs before light scattering development, the dimer is still plausibly the first intermediate on the path toward photo-aggregation. Alternately, the fast-forming, gel-visible dimers could be protective "dead-ends," in which ROS cause cross-linking that lead to less photoaggregation prone species. This could explain HαB-Crys not suppressing dimer formation and the increase and decrease in the dimer's abundance over exposure time as the protective species is slowly incorporated into larger aggregates.

Examining the current study of the aromatic pairs, and the previously investigated protective role of the conserved tryptophan pairs (231), we can imagine a UVR-induced radical polymerization mechanism of HγD-Crys photo-aggregation as follows (Fig. 3.9). Y16 can absorb a UV photon, entering into an excited state. It can transfer its excited state energy nonradiatively to other aromatic residues, themselves excitable by UVR. Homotransfer of excited state energy between aromatic amino acids is well established (17, 19), and the high number of aromatic residues in HγD-Crys means no aromatic residue is more than ~10 Å from another. These excited aromatic residues can transfer their energy to the conserved tryptophan pairs, which have been shown to transfer energy very efficiently from W42 to W68 and W130 to W156, respectively, dissipating it without undergoing photochemistry (118-120). In this model, the tryptophan pairs act photoprotectively as a sink for excitation energy.

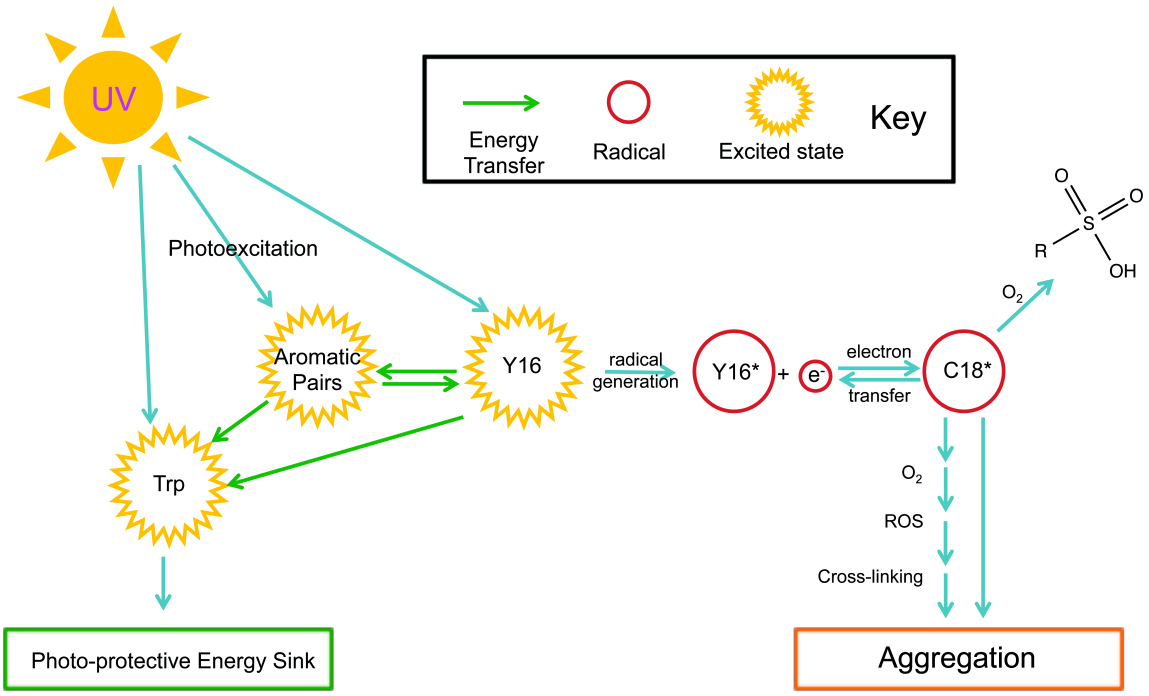

Figure 3.9 A Model for *In Vitro* Photo-aggregation of HγD-Crys. A proposed schematic for *in vitro* photo-aggregation of HγD-Crys incorporating current and previous data.

Y16 (or Y28), unlike the other aromatic residues examined, is on the surface of HγD-Crys and might transfer its excited state to molecular oxygen, generating singlet oxygen. Singlet oxygen can react at a number of sites on HγD-Crys, causing cross-linking leading to photo-aggregation. Y16 can also participate in radical chemistry while excited (14, 15), creating a tyrosyl radical and a free radical. C18's thiol group, in contact with Y16's aromatic ring, could react with Y16*, generating a thiol radical; if the exchange of the radical electron is reversible, this might stabilize these intermediate photo-products, increasing the likelihood of a damaging reaction or generation of ROS. Thiol and tyrosyl radicals can also interact with molecular oxygen, generating superoxide radical, which can, like singlet oxygen, target a number of sites on HγD-Crys, causing cross-linking and photo-aggregation. The exposure time dependent build up of C18 oxidation products observed via mass spectrometry indicates a competing side reaction where ROS oxidize C18. The reduction in this side reaction product as observed via MRM mass spectrometry when Y16 is mutated to alanine is strong evidence for photochemical interaction of C18 and Y16, and the significant increase in C18 tri-oxidation in the NoTrp mutant suggests a link between photo-damage to C18 and the tryptophan photo-protective role.

The lens is a very different environment from the test tube conditions here. Besides maintaining a protein concentration of 200-400 mg/ml (66), lens fiber cells have several defense mechanisms against photo-oxidative damage: free UV filter molecules consisting of kynurenine/tryptophan derivatives, the thioredoxin system, and the thioltransferase system (44, 65, 83). Additionally, the

lens, an avascular, blood-less tissue, maintains very low oxygen levels (32). Despite this, the oxygen dependent photo-crosslinking observed in this study, *in vitro*, is likely still very physiologically relevant to cataract. Protein damage leading to aggregation and cataract develops over the course of a human lifetime; on such a timeline, even relatively rare damage events such as those dependent on oxygen, as diagrammed here, can be significant to pathological outcomes. Additionally, eye injury or surgery drastically raises the oxygen level of the lens, likely making photo-oxidative damage a greater threat to lens proteins.

HαB-Crys' *in vitro* suppression of light scattering upon UVR exposure of HγD-Crys strongly indicates that photo-aggregation figures prominently in the range of threats facing lens protein homeostasis. As our understanding of protein photo-damage in the lens increases, so too do our options for cataract therapy. Giblin, Andley and colleagues have shown that UVR blocking contact lenses prevent the UVR-induced opacification of lab animal lenses (179, 180, 182). Carnosine, an inhibitor of ROS generating lipid peroxidation, shows promise as an anti-cataract drug (176, 177, 236). HαB-Crys peptide fragments injected into animal cataract models have been shown to suppress aggregation and protein oxidation (178). The identification of specific sites important to HγD-Crys photo-aggregation can continue to inform these efforts.

CHAPTER 4:

FINAL DISCUSSION

AND

FUTURE DIRECTIONS

FINAL DISCUSSION

This research was motivated by a desire to understand the mechanism of the UVR-induced damage to lens proteins that may lead to cataract. Eye researchers have suspected for decades that UVR was a contributing cause of age-related cataract (135, 189, 191, 197, 237). Experiments with UVR-exposed extracted human and animal lenses, as well as purified lens proteins, showed that many of the characteristics of cataracts found in extracted lenses (opacity, accumulation of insoluble proteins, disruption of lens fiber cell structure) could be recapitulated *in vitro* (238). But despite the suspicions of researchers, no epidemiological link was found between heightened solar UVR exposure and nuclear cataract, and only a weak association was found between UVR and cortical cataract (141, 172). As mentioned earlier, I believe this is due in part to the high variability of eye exposure to UVR between individuals (205), as well as challenges in accurately estimating or measuring the UVR dose received by the eye (204). It is also likely due to the multifactorial nature of the lens changes leading to age-related cataract (238).

Many of the earlier studies examining UVR-induced changes to lens proteins were performed before the widespread use of modern molecular biological advances in protein purification, site-directed mutagenesis, mass spectrometry, and computer simulation. It is only recently that these refinements have been brought to bear on the problem of UVR-induced cataract (107, 120, 227, 239). Recent work by Wang and Wen explored the effect of UVC on purified HγD-Crys (126), and found it formed covalent, cross-linked products while

showing a decrease in the number of free thiol groups. While an interesting study, UVC never reaches the lens *in vivo*, having been blocked by the ozone layer or cornea. I wanted to investigate how the physiologically relevant UV range, UVB/UVA, damaged HγD-Crys, and I wanted to harness the power of recombinant protein purification, mutant protein constructs, and mass spectrometry to do so.

I began, in chapter 2, with the initial hypotheses that UVA/UVB exposed HγD-Crys would photo-aggregate much like mixtures of lens proteins had before it, and that UVR-induced damage to HγD-Crys would proceed through its highly conserved tryptophan residues. This was a reasonable assumption; some of the earliest investigations of the response of lens proteins to UVR found that tryptophan fluorescence dropped after UVR exposure and new, non-tryptophan fluorescence developed, consistent with tryptophan's photochemical transformation into a product like N-formylkynurenine (197). By irradiating HγD-Crys *in vitro* under a variety of conditions, I found that the protein formed high molecular weight aggregates with a covalent nature in an oxygen dependent fashion, confirming many different previous observations from other experimental systems. I also found that my initial hypothesis was incorrect: HγD-Crys aggregated more severely in the absence of tryptophan, and restoring individual tryptophans via mutagenesis appeared to make HγD-Crys more photo-aggregation prone, while WT HγD-Crys showed no change in UVR absorbance as aggregation proceeded. This conclusively showed that aggregation could proceed in the absence of the tryptophans, the primary UVR absorbers, while

dovetailing with previous hypotheses that suggested the tryptophans' and their efficient energy transfer were a photo-protective mechanism (120).

In chapter 3, I addressed the question that arose immediately from chapter 2's results: if not the tryptophans, then what sites mediate UVR absorption and damage in HγD-Crys? Absorption is a prerequisite for photo-damage to occur, and so some subset of HγD-Crys' 14 tyrosines, the remaining strong UVR absorbers, were the next sites to rule out. Using Y:A and F:A double mutant constructs, I saw that most of the tyrosine/phenylalanine aromatic pairs, previously shown to play key roles in HγD-Crys' folding and structural stability, did not play important roles in photo-aggregation. However, mutation of Y16 and Y28 significantly reduced the rate of photo-aggregation relative to WT, suggesting they could be sites of absorption or photochemistry. Working with collaborators using LC MS/MS and MRM mass spectrometry, we identified cysteine 18 as a site of photo-oxidation, and found that its photochemistry is affected by the Y16A mutation and the absence of the 4 tryptophans. Combined with examination of a series of multiple mutant proteins, this data suggested that C18 and Y16, in contact in crystal structures of HγD-Crys, are likely involved in a photochemical process leading to aggregation.

The model I put forth at the end of chapter 3 (Fig. 3.9) is a combination of the experimental data of chapters 2 and 3, and the photochemistry and excited state behavior of the aromatic and cysteine residues described in the literature (14, 15, 17, 19). Rapid energy transfer is known to occur between aromatic amino acids within short distances in a protein, and both the relative energy level

of the first excited singlet states of the aromatics and the experimental data of chapter 2 and 3 are consistent with a model where the tryptophans act as a sink for photo-excitation. Most of the aromatic pair mutants in chapter 3 behaved similarly to WT in photo-aggregation experiments indicating no particular importance to photo-aggregation. Those that aggregated more quickly than WT may be especially important in funneling energy to the tryptophans, or maintaining the rigid conformation required for their quenching.

Y16 and Y28, based on data in chapter 3, likely mediate photo-damage. And given that aggregation of Y16A mutants were slowed to a similar extent to Y16A/Y28A compared to the more mild retardation of Y28A, it seems likely that Y16 is the primary participant and Y28 secondary in this damage pathway. Because of the tight stacking of Y16 and Y28, it is possible that the reason behind the Y28A mutant's slower photo-aggregation is not due to an associated incremental loss of photochemical activity inherent to Y28, but that it alters the position of Y16 to less favor photo-damage. Literature on excited state tyrosine's photochemistry suggests the formation of a tyrosyl radical, and radical electron's can be rapidly transferred to nearby amino acids (15). Cysteine 18, as mentioned above, is in direct contact with the Y16. Based on data from chapter 3, showing that C18S HγD-Crys displayed photo-aggregation retardation similar to Y16A and Y16A/Y28A HγD-Crys, as well as mass spectrometric data identifying it as a site of interaction with oxygen, C18 is a likely site of photo-crosslinking. It is still possible that Y16 plays a role in crosslinking instead or in addition to C18, but we have no evidence that it interacts with oxygen, a requirement for the observed

photo-aggregation, as of yet. Clearly, other sites must mediate photo-aggregation in addition to C18 and Y16.

FUTURE DIRECTIONS

The identification of potential roles of Y16 and C18 and the creation of this initial model for photo-aggregation raise many questions and suggests a number of future experiments. For example, despite knowing from the literature the types of chemistry cysteine thiol's are capable of, we do not know exactly how C18 is reacting to promote photo-aggregation, or how many steps and other residues might be involved. We can infer that off-pathway products are formed, since the sulfinic and sulfonic acid products identified via mass spectrometry are not plausible intermediates toward cross-links. Identifying the aggregation-promoting photochemistry C18, or Y16, undergoes, along with any intermediates, would be a key future experiment next step.

This question is part of a broader question: what sites on HγD-Crys participate in or are targets of radical photochemistry? Due to radical chemistry's wide range of targets and products and short intermediate lifetimes, this may be difficult to determine. A number of radical spin trap compounds have been studied for use in EPR that react to form stable covalent adducts at sites of radical generation (199, 240). Further advanced mass spectrometric analysis incorporating UVR exposure in the presence of the spin traps could identify more thoroughly all sites undergoing radical chemistry. Another option is ^{35}S methionine and cysteine labeling, which could identify/confirm (by electrophoretic

mobility shift assays coupled with autoradiography) which methionine or cysteine sites could be involved in a cross-link. Given that C18 has been shown to play an important role in photoaggregation, blocking free thiols with an alkylating agent, like iodoacetamide, should also, in theory, slow photoaggregation in a way similar to C18S HγD-Crys.

We know that oxygen is required for photo-aggregation, and that this almost certainly means the formation of an ROS. The site(s) where that ROS reacts to induce a covalent interprotein cross-link is also unknown, although C18 and potentially Y16 are candidates, and the spin trap method above could help identify other sites. There are several types of ROS, including hydroxyl radicals, hydrogen peroxide, singlet oxygen, and superoxide. A number of ROS quenching compounds exist, many of which are fluorescent and alter their fluorescence properties upon reaction with specific types of ROS (241, 242). By including them in the UVR photo-aggregation experiments described in chapters 2 and 3, the predominant type of ROS generated or the ROS most important to photo-aggregation could be determined. Similar to the possibility of a plethora of cross-link types precluding individual identification, it is possible that several ROS are generated upon irradiation of HγD-Crys, making it difficult to determine their relative importance using quenching compounds. Directly adding or generating specific ROS species, like hydrogen peroxide or singlet oxygen (via sensitizer or device (243, 244)) to HγD-Crys samples could also help answer this question.

I have addressed photochemical questions up until now, but structural questions abound as well. We currently have no understanding of the structure of

HγD-Crys within the photo-aggregated state. Previous work has suggested a partially folded conformation, in which the N-terminal domain is unfolded while the C-terminal domain remains folded, as the aggregation prone state when HγD-Crys refolds out of GuHCl (105, 107), and a domain swapping mechanism of aggregation has been proposed for HγD-Crys (245).

But a radical polymerization mechanism of aggregation, highly likely due to the covalent cross-linking and ready source of radicals, could occur in a partially/completely unfolded conformation or a near-native one. FTIR spectroscopy has been used extensively in the past to assay protein secondary structure, and can examine insoluble aggregated samples (246, 247). This technique would be a logical choice to characterize HγD-Crys' conformation within the aggregate.

To analyze the intermolecular architecture of the amorphous aggregates generated, cross-linking experiments could be conducted (248-251). A chemical cross-linker applied to earlier, soluble high molecular weight species could chemically link sites interacting within the aggregated state. When compared using mass spectrometry to native monomeric HγD-Crys exposed to cross-linker, cross-links unique to the UVR-exposed sample could identify sites near to each other within photo-aggregates.

Additional sites must participate in HγD-Crys' *in vitro* photo-aggregation, since the protein aggregated in the absence of C18, Y16, and Y28. Several tyrosine residues remain to be examined by mutagenesis and irradiation of the resulting mutant protein; these include those clustered with the HγD-Crys'

tryptophans, which could have photochemical significance, as well as the Greek Key tyrosine corners, already shown to be structurally important (115). Histidine residues are also capable of radical chemistry and cross-linking (15). HγD-Crys has 6 histidines, and the construct under study here contains an N-terminal 6xHis-tag, increasing the total to 12. Interestingly, H22 is very near to Y16, Y28, and C18, and exposed to the surface. These remaining tyrosines and histidines would be the first step in continuing to examine the photo-aggregation of HγD-Crys using mutant analysis.

CHAPTER 5:

REFERENCES

REFERENCES

1. Fu, Q., J. R. Holton, J. A. Curry and J. A. Pyle (2003) Radiation (Solar). In *Encyclopedia of atmospheric sciences*. pp. 1859-1863. Academic Press.
2. Standardization, I. O. f. (2007) Space environment (natural and artificial) -- Process for determining solar irradiances. pp. 1-20.
3. Cadet, J., S. Mouret, J. L. Ravanat and T. Douki (2012) Photoinduced Damage to Cellular DNA: Direct and Photosensitized Reactions†. *Photochem. Photobiol.* **88,** 1048-1065.
4. Creed, D. (1984) The photophysics and photochemistry of the near-UV absorbing amino acids--I. Tryptophan and its simple derivatives. *Photochem. Photobiol.* **39,** 537-562.
5. Creed, D. (1984) The photophysics and photochemistry of the near-UV absorbing amino acids--II. Tyrosine and its simple derivatives. *Photochem. Photobiol.* **39,** 563-575.
6. Creed, D. (1984) The photophysics and photochemistry of the near-UV absorbing amino acids--III. Cystine and its simple derivatives. *Photochem. Photobiol.* **39,** 577-583.
7. Chen, L., J. Y. Hu and S. Q. Wang (2012) The role of antioxidants in photoprotection: a critical review. *J. Am. Acad. Dermatol.* **67,** 1013-1024.
8. Goldblatt, C., T. M. Lenton and A. J. Watson (2006) Bistability of atmospheric oxygen and the Great Oxidation. *Nature* **443,** 683-686.
9. Cockell, C. S. (1998) Biological effects of high ultraviolet radiation on early earth--a theoretical evaluation. *J. Theor. Biol.* **193,** 717-729.
10. Cockell, C. (2000) Ultraviolet radiation and the photobiology of Earth's early oceans. *Origins Life Evol. Biospheres* **30,** 467-500.
11. Raven, J. A. (2011) The cost of photoinhibition. *Physiol. Plant.* **142,** 87-104.
12. Friedberg, E. C. (2001) How nucleotide excision repair protects against cancer. *Nat. Rev. Cancer* **1,** 22-33.
13. Duan, M.-R. and M. J. Smerdon (2010) UV damage in DNA promotes nucleosome unwrapping. *J. Biol. Chem.***,** 1-9.
14. Pattison, D. I., A. S. Rahmanto and M. J. Davies (2011) Photo-oxidation of proteins. *Photochem. Photobiol. Sci.* **11,** 38.
15. Davies, M. J. and R. J. Truscott (2001) Photo-oxidation of proteins and its role in cataractogenesis. *J. Photochem. Photobiol., B* **63,** 114-125.
16. Foote, C. S. (1991) Definition of type I and type II photosensitized oxidation. *Photochem. Photobiol.* **54,** 659-659.
17. Borkman, R. and S. Phillips (1985) Tyrosine-to-tryptophan energy transfer and the structure of calt gamma-II crystallin. *Exp. Eye Res.* **40,** 819-826.
18. Callis, P. R. (1997) 1La and 1Lb transitions of tryptophan: applications of theory and experimental observations to fluorescence of proteins. *Methods Enzymol.* **278,** 113-150.
19. Moens, P. D. J., M. K. Helms and D. M. Jameson (2004) Detection of tryptophan to tryptophan energy transfer in proteins. *Protein J.* **23,** 79-83.
20. Baugher, J. and L. Grossweiner (1977) Photolysis mechanism of aqueous tryptophan. *J. Phys. Chem.* **81,** 1349-1354.

21. Malencik, D. and S. Anderson (2003) Dityrosine as a product of oxidative stress and fluorescent probe. *Amino Acids* **25,** 233-247.
22. Reddie, K. G. and K. S. Carroll (2008) Expanding the functional diversity of proteins through cysteine oxidation. *Curr. Opin. Chem. Biol.* **12,** 746-754.
23. Bent, D. V. and E. Hayon (1975) Excited state chemistry of aromatic amino acids and related peptides. II. Phenylalanine. *J. Am. Chem. Soc.* **97,** 2606-2612.
24. Balasubramanian, D., X. Du and J. S. Zigler (1990) The reaction of singlet oxygen with proteins, with special reference to crystallins. *Photochem. Photobiol.* **52,** 761-768.
25. Berry, Y. and R. J. Truscott (2001) The presence of a human UV filter within the lens represents an oxidative stress. *Exp. Eye Res.* **72,** 411-421.
26. Ortwerth, B. J., S. H. Slight, M. Prabhakaram, Y. Sun and J. B. Smith (1992) Site-specific glycation of lens crystallins by ascorbic acid. *Biochim. Biophys. Acta* **1117,** 207-215.
27. Linetsky, M., H. L. James and B. J. Ortwerth (1999) Spontaneous generation of superoxide anion by human lens proteins and by calf lens proteins ascorbylated in vitro. *Exp. Eye Res.* **69,** 239-248.
28. Avila, F., A. Matus, D. Fuentealba, E. Lissi, B. Friguet and E. Silva (2008) Autosensitized oxidation of glycated bovine lens proteins irradiated with UVA-visible light at low oxygen concentration. *Photochem. Photobiol. Sci.* **7,** 718-724.
29. Aquilina, J. A., J. A. Carver and R. J. Truscott (1997) Oxidation products of 3-hydroxykynurenine bind to lens proteins: relevance for nuclear cataract. *Exp. Eye Res.* **64,** 727-735.
30. Korlimbinis, A., P. Hains, R. Truscott and J. Aquilina (2006) 3-Hydroxykynurenine oxidizes alpha-crystallin: potential role in cataractogenesis. *Biochemistry* **45,** 1852.
31. Sherin, P. S., J. Grilj, L. V. Kopylova, V. V. Yanshole, Y. P. Tsentalovich and E. Vauthey (2010) Photophysics and photochemistry of the UV filter kynurenine covalently attached to amino acids and to a model protein. *J. Phys. Chem. B* **114,** 11909-11919.
32. Siegfried, C. J., Y.-B. Shui, N. M. Holekamp, F. Bai and D. C. Beebe (2010) Oxygen Distribution in the Human Eye: Relevance to the Etiology of Open Angle Glaucoma after Vitrectomy. *Invest. Ophthalmol. Visual Sci.*
33. Gracanin, M., C. L. Hawkins, D. I. Pattison and M. J. Davies (2009) Singlet-oxygen-mediated amino acid and protein oxidation: Formation of tryptophan peroxides and decomposition products. *Free Radical Biol. Med.* **47,** 92-102.
34. Sheng, D. and M. H. Gold (1999) Oxidative polymerization of ribonuclease A by lignin peroxidase from Phanerochaete chrysosporium. Role of veratryl alcohol in polymer oxidation. *Eur. J. Biochem.* **259,** 626-634.
35. Tappel, A. and A. Tappel (2004) Oxidant free radical initiated chain polymerization of protein and other biomolecules and its relationship to diseases. *Med. Hypotheses* **63,** 98-99.

36. Thillet, J. and A. M. Michelson (1985) Oxidation and cross-linking of human hemoglobins by activated oxygen species. *Free Radical Res. Commun.* **1,** 89-100.
37. Delavoie, F., H. Li, M. Hardwick, J.-C. Robert, C. Giatzakis, G. Péranzi, Z.-X. Yao, J. Maccario, J.-J. Lacapère and V. Papadopoulos (2003) In Vivo and in Vitro Peripheral-Type Benzodiazepine Receptor Polymerization: Functional Significance in Drug Ligand and Cholesterol Binding. *Biochemistry* **42,** 4506-4519.
38. Takasaki, S., Y. Kato, M. Murata, S. Homma and S. Kawakishi (2005) Effects of peroxidase and hydrogen peroxide on the dityrosine formation and the mixing characteristics of wheat-flour dough. *Biosci., Biotechnol., Biochem.* **69,** 1686-1692.
39. Maiorino, M., A. Roveri, L. Benazzi, V. Bosello, P. Mauri, S. Toppo, S. C. E. Tosatto and F. Ursini (2005) Functional interaction of phospholipid hydroperoxide glutathione peroxidase with sperm mitochondrion-associated cysteine-rich protein discloses the adjacent cysteine motif as a new substrate of the selenoperoxidase. *J. Biol. Chem.* **280,** 38395-38402.
40. Sreekumar, P. G. (2011) Methionine sulfoxide reductase A: Structure, function and role in ocular pathology. *World J. Biol. Chem.* **2,** 184.
41. Garner, M. H. and A. Spector (1980) Selective oxidation of cysteine and methionine in normal and senile cataractous lenses. *Proc. Natl. Acad. Sci. U. S. A.* **77,** 1274-1277.
42. Karunakaran-Datt, A. and P. Kennepohl (2009) Redox Photochemistry of Methionine by Sulfur K-edge X-ray Absorption Spectroscopy: Potential Implications for Cataract Formation. *J. Am. Chem. Soc.* **131,** 3577-3582.
43. Brennan, L. A., W. Lee and M. Kantorow (2010) TXNL6 Is a Novel Oxidative Stress-Induced Reducing System for Methionine Sulfoxide Reductase A Repair of a-Crystallin and Cytochrome C in the Eye Lens. *PLoS One***,** 1-11.
44. Xing, K. and M. Lou (2010) Effect of age on the thioltransferase (glutaredoxin) and thioredoxin systems in the human lens. *Invest. Ophthalmol. Visual Sci.*
45. Zigler, J. S. and P. V. Rao (1991) Enzyme/crystallins and extremely high pyridine nucleotide levels in the eye lens. *FASEB J.* **5,** 223-225.
46. Wistow, G., B. Turnell, L. Summers, C. Slingsby, D. Moss, L. Miller, P. Lindley and T. Blundell (1983) X-ray analysis of the eye lens protein gamma-II crystallin at 1.9 A resolution. *J. Mol. Biol.* **170,** 175-202.
47. Craghill, J., A. D. Cronshaw and J. J. Harding (2004) The identification of a reaction site of glutathione mixed-disulphide formation on gammaS-crystallin in human lens. *Biochem. J.* **379,** 595-600.
48. Giblin, F. J., L. L. David, P. A. Wilmarth, V. R. Leverenz and M. F. Simpanya (2013) Shotgun proteomic analysis of S-thiolation sites of guinea pig lens nuclear crystallins following oxidative stress in vivo. *Mol. Vision* **19,** 267-280.
49. Roussel, X., A. Kriznik, C. Richard, S. Rahuel-Clermont and G. Branlant (2009) Catalytic mechanism of Sulfiredoxin from Saccharomyces

cerevisiae passes through an oxidized disulfide sulfiredoxin intermediate that is reduced by thioredoxin. *J. Biol. Chem.* **284,** 33048-33055.
50. Lee, W., T. Wells and M. Kantorow (2007) Localization and H2O2-specific induction of PRDX3 in the eye lens. *Mol. Vision* **13,** 1469-1474.
51. Murrow, L. and J. Debnath (2013) Autophagy as a Stress-Response and Quality-Control Mechanism: Implications for Cell Injury and Human Disease. *Annu. Rev. Pathol.: Mech. Dis.* **8,** 105-137.
52. Li, W.-w., J. Li and J.-k. Bao (2011) Microautophagy: lesser-known self-eating. *Cell. Mol. Life Sci.* **69,** 1125-1136.
53. Marques, C. (2004) Ubiquitin-dependent lysosomal degradation of the HNE-modified proteins in lens epithelial cells. *FASEB J.*
54. Shang, F. and A. Taylor (2011) Ubiquitin–proteasome pathway and cellular responses to oxidative stress. *Free Radical Biol. Med.* **51,** 5-16.
55. Pereira, P., F. Shang, M. Hobbs, H. Girão and A. Taylor (2003) Lens fibers have a fully functional ubiquitin-proteasome pathway. *Exp. Eye Res.* **76,** 623-631.
56. Dudek, E., K. J. Lampi, J. A. Lampi, F. Shang, J. A. King, Y. Wang and A. Taylor (2010) Ubiquitin proteasome pathway-mediated degradation of proteins: effects due to site-specific substrate deamidation. *Invest. Ophthalmol. Visual Sci.*, 1-10.
57. Liu, Z., A. Taylor, Y. Liu, M. Wu, X. Gong and F. Shang (2012) Enhancement of Ubiquitin Conjugation Activity Reduces Intracellular Aggregation of V76D Mutant D-Crystallin. *Invest. Ophthalmol. Visual Sci.* **53,** 6655-6665.
58. Oyster, C. W. (1999) *The Human Eye: Structure and Function.* Sinauer Associates, Inc., Sunderland, MA.
59. Lamb, T. D. and E. N. Pugh (2004) Dark adaptation and the retinoid cycle of vision. *Prog. Retinal Eye Res.* **23,** 307-380.
60. Navid, A., S. C. Nicholas and R. D. Hamer (2006) A proposed role for all-trans retinal in regulation of rhodopsin regeneration in human rods. *Vision Res.* **46,** 4449-4463.
61. Rózanowska, M. and T. Sarna (2005) Light-induced damage to the retina: role of rhodopsin chromophore revisited. *Photochem. Photobiol.* **81,** 1305-1330.
62. Beebe, D. C., N. M. Holekamp, C. Siegfried and Y.-B. Shui (2011) Vitreoretinal influences on lens function and cataract. *Philos. Trans. R. Soc., B* **366,** 1293-1300.
63. Bassnett, S. (2009) On the mechanism of organelle degradation in the vertebrate lens. *Exp. Eye Res.* **88,** 133-139.
64. Bassnett, S. (2002) Lens organelle degradation. *Exp. Eye Res.* **74,** 1-6.
65. Streete, I. M., J. F. Jamie and R. J. W. Truscott (2004) Lenticular levels of amino acids and free UV filters differ significantly between normals and cataract patients. *Invest. Ophthalmol. Visual Sci.* **45,** 4091-4098.
66. Bloemendal, H., W. de Jong, R. Jaenicke, N. H. Lubsen, C. Slingsby and A. Tardieu (2004) Ageing and vision: structure, stability and function of lens crystallins. *Prog. Biophys. Mol. Biol.* **86,** 407-485.

67. Morishita, H., S. Eguchi, H. Kimura, J. Sasaki, Y. Sakamaki, M. L. Robinson, T. Sasaki and N. Mizushima (2013) Deletion of Autophagy-related 5 (Atg5) and Pik3c3 Genes in the Lens Causes Cataract Independent of Programmed Organelle Degradation. *J. Biol. Chem.* **288,** 11436-11447.
68. Augusteyn, R. C. (2008) Growth of the lens: in vitro observations. *Aust. J. Optom.* **91,** 226-239.
69. Cvekl, A., Y. Yang, B. K. Chauhan and K. Cveklova (2004) Regulation of gene expression by Pax6 in ocular cells: a case of tissue-preferred expression of crystallins in lens. *Int. J. Dev. Biol.* **48,** 829-844.
70. Ogino, H., H. Ochi, H. M. Reza and K. Yasuda (2012) Transcription factors involved in lens development from the preplacodal ectoderm. *Dev. Biol.* **363,** 333-347.
71. Donner, A., S. Lachke and R. Maas (2006) Lens induction in vertebrates: variations on a conserved theme of signaling events. *Semin. Cell Dev. Biol.* **17,** 676-685.
72. Mathias, R. T., J. L. Rae and G. J. Baldo (1997) Physiological properties of the normal lens. *Physiol. Rev.* **77,** 21-50.
73. Gao, J., X. Sun, L. C. Moore, T. W. White, P. R. Brink and R. T. Mathias (2011) Lens intracellular hydrostatic pressure is generated by the circulation of sodium and modulated by gap junction coupling. *J. Gen. Physiol.* **137,** 507-520.
74. Donaldson, P. J., L. S. Musil and R. T. Mathias (2010) Point: A critical appraisal of the lens circulation model--an experimental paradigm for understanding the maintenance of lens transparency? *Invest. Ophthalmol. Visual Sci.* **51,** 2303-2306.
75. Beebe, D. and R. J. W. Truscott (2010) Counterpoint: The Lens Fluid Circulation Model--A Critical Appraisal. *Invest. Ophthalmol. Visual Sci.* **51,** 2303-2306.
76. Donaldson, P. J., L. S. Musil and R. T. Mathias (2010) Reply to: The Lens Fluid Circulation Model--A Critical Appraisal. *Invest. Ophthalmol. Visual Sci.*, 1-3.
77. Beebe, D. and R. J. W. Truscott (2010) Reply to: A Critical Appraisal of the Lens Circulation Model--An Experimental Paradigm for Understanding the Maintenance of Lens Transparency. *Invest. Ophthalmol. Visual Sci.* **51,** 2310-2312.
78. Candia, O. A., R. Mathias and R. Gerometta (2012) Fluid Circulation Determined in the Isolated Bovine Lens. *Invest. Ophthalmol. Visual Sci.* **53,** 7087-7096.
79. Beebe, D. C. (2008) Maintaining transparency: a review of the developmental physiology and pathophysiology of two avascular tissues. *Semin. Cell Dev. Biol.* **19,** 125-133.
80. Bjorn, L. O. (2007) The Nature of Light and Its Interaction with Matter. In *Photobiology: The Science of Life and Light*. (Edited by L. O. Bjorn), pp. 14-15. Springer Science+Business Media, LLC.

81. Vérétout, F. and A. Tardieu (1989) The protein concentration gradient within eye lens might originate from constant osmotic pressure coupled to differential interactive properties of crystallins. *Eur. Biophys. J.* **17,** 61-68.
82. Zhao, H., P. H. Brown and P. Schuck (2011) On the Distribution of Protein Refractive Index Increments. *Biophys. J.* **100,** 2309-2317.
83. Bova, L. M., A. M. Wood, J. F. Jamie and R. J. Truscott (1999) UV filter compounds in human lenses: the origin of 4-(2-amino-3-hydroxyphenyl)-4-oxobutanoic acid O-beta-D-glucoside. *Invest. Ophthalmol. Visual Sci.* **40,** 3237-3244.
84. Ham, W. T., H. A. Mueller, J. J. Ruffolo, D. Guerry and R. K. Guerry (1982) Action spectrum for retinal injury from near-ultraviolet radiation in the aphakic monkey. *Am. J. Ophthalmol.* **93,** 299-306.
85. Bova, L. M., M. H. Sweeney, J. F. Jamie and R. J. Truscott (2001) Major changes in human ocular UV protection with age. *Invest. Ophthalmol. Visual Sci.* **42,** 200-205.
86. Mirarefi, A. Y., S. Boutet, S. Ramakrishnan, A. J. Kiss, C.-H. C. Cheng, A. L. DeVries, I. K. Robinson and C. F. Zukoski (2010) Small-angle X-ray scattering studies of the intact eye lens: Effect of crystallin composition and concentration on microstructure. *Biochim. Biophys. Acta, Gen. Subj.* **1800,** 556-564.
87. Horwitz, J. (1992) Alpha-crystallin can function as a molecular chaperone. *Proc. Natl. Acad. Sci. U. S. A.* **89,** 10449-10453.
88. Horwitz, J. (2003) Alpha-crystallin. *Exp. Eye Res.* **76,** 145-153.
89. Wistow, G. (2012) The human crystallin gene families. *Hum. Genomics* **6,** 26.
90. Laganowsky, A., J. L. P. Benesch, M. Landau, L. Ding, M. R. Sawaya, D. Cascio, Q. Huang, C. V. Robinson, J. Horwitz and D. Eisenberg (2010) Crystal structures of truncated alphaA and alphaB crystallins reveal structural mechanisms of polydispersity important for eye lens function. *Protein Sci.* **19,** 1031-1043.
91. Raman, B. and C. M. Rao (1994) Chaperone-like activity and quaternary structure of alpha-crystallin. *J. Biol. Chem.* **269,** 27264-27268.
92. Rao, P. V., Q. L. Huang, J. Horwitz and J. S. Zigler (1995) Evidence that alpha-crystallin prevents non-specific protein aggregation in the intact eye lens. *Biochim. Biophys. Acta* **1245,** 439-447.
93. Lee, G. J., A. M. Roseman, H. R. Saibil and E. Vierling (1997) A small heat shock protein stably binds heat-denatured model substrates and can maintain a substrate in a folding-competent state. *EMBO J.* **16,** 659-671.
94. Brady, J. P., D. Garland, Y. Duglas-Tabor, W. G. Robison, A. Groome and E. F. Wawrousek (1997) Targeted disruption of the mouse alpha A-crystallin gene induces cataract and cytoplasmic inclusion bodies containing the small heat shock protein alpha B-crystallin. *Proc. Natl. Acad. Sci. U. S. A.* **94,** 884-889.
95. Boyle, D. L., L. Takemoto, J. P. Brady and E. F. Wawrousek (2003) Morphological characterization of the Alpha A- and Alpha B-crystallin double knockout mouse lens. *BMC Ophthalmol.* **3,** 3.

96. Das, K. P. and W. K. Surewicz (1995) Temperature-induced exposure of hydrophobic surfaces and its effect on the chaperone activity of alpha-crystallin. *FEBS Lett.* **369,** 321-325.
97. Bova, M. P., L. L. Ding, J. Horwitz and B. K. Fung (1997) Subunit exchange of alphaA-crystallin. *J. Biol. Chem.* **272,** 29511-29517.
98. Wang, K. and A. Spector (2000) alpha-crystallin prevents irreversible protein denaturation and acts cooperatively with other heat-shock proteins to renature the stabilized partially denatured protein in an ATP-dependent manner. *Eur. J. Biochem.* **267,** 4705-4712.
99. Bagnéris, C., O. A. Bateman, C. E. Naylor, N. Cronin, W. C. Boelens, N. H. Keep and C. Slingsby (2009) Crystal structures of alpha-crystallin domain dimers of alphaB-crystallin and Hsp20. *J. Mol. Biol.* **392,** 1242-1252.
100. Kappé, G., A. G. Purkiss, S. T. van Genesen, C. Slingsby and N. H. Lubsen (2010) Explosive Expansion of betagamma-Crystallin Genes in the Ancestral Vertebrate. *J. Mol. Evol.*
101. Hemmingsen, J. M., K. M. Gernert, J. S. Richardson and D. C. Richardson (1994) The tyrosine corner: a feature of most Greek key beta-barrel proteins. *Protein Sci.* **3,** 1927-1937.
102. Jaenicke, R. and C. Slingsby (2001) Lens crystallins and their microbial homologs: structure, stability, and function. *Crit. Rev. Biochem. Mol. Biol.* **36,** 435-499.
103. Bateman, O. A., R. Sarra, S. T. van Genesen, G. Kappé, N. H. Lubsen and C. Slingsby (2003) The stability of human acidic β-crystallin oligomers and hetero-oligomers. *Exp. Eye Res.* **77,** 409-422.
104. Takata, T., J. T. Oxford, B. Demeler and K. J. Lampi (2008) Deamidation destabilizes and triggers aggregation of a lens protein, βA3-crystallin. *Protein Sci.* **17,** 1565-1575.
105. Acosta-Sampson, L. and J. King (2010) Partially Folded Aggregation Intermediates of Human γD-, γC-, and γS-Crystallin Are Recognized and Bound by Human αB-Crystallin Chaperone. *J. Mol. Biol.* **401,** 134-152.
106. Robinson, N. E., K. J. Lampi, J. P. Speir, G. Kruppa, M. Easterling and A. B. Robinson (2006) Quantitative measurement of young human eye lens crystallins by direct injection Fourier transform ion cyclotron resonance mass spectrometry. *Mol. Vision* **12,** 704-711.
107. Kosinski-Collins, M. and J. King (2003) In vitro unfolding, refolding, and polymerization of human γD crystallin, a protein involved in cataract formation. *Protein Sci.* **12,** 480-490.
108. Kosinski-Collins, M. S., S. L. Flaugh and J. King (2004) Probing folding and fluorescence quenching in human gammaD crystallin Greek key domains using triple tryptophan mutant proteins. *Protein Sci.* **13,** 2223-2235.
109. Flaugh, S. L., M. S. Kosinski-Collins and J. King (2005) Interdomain side-chain interactions in human gammaD crystallin influencing folding and stability. *Protein Sci.* **14,** 2030-2043.
110. Flaugh, S. L., M. S. Kosinski-Collins and J. King (2005) Contributions of hydrophobic domain interface interactions to the folding and stability of human gammaD-crystallin. *Protein Sci.* **14,** 569-581.

111. Mills, I., S. Flaugh, M. Kosinski-Collins and J. King (2007) Folding and stability of the isolated Greek key domains of the long-lived human lens proteins γD-crystallin and γS-crystallin. *Protein Sci.* **16,** 2427-2444.
112. Basak, A., O. Bateman, C. Slingsby, A. Pande, N. Asherie, O. Ogun, G. B. Benedek and J. Pande (2003) High-resolution X-ray Crystal Structures of Human γD Crystallin (1.25Å) and the R58H Mutant (1.15Å) Associated with Aculeiform Cataract. *J. Mol. Biol.* **328,** 1137-1147.
113. Flaugh, S., I. Mills and J. King (2006) Glutamine deamidation destabilizes human γD-crystallin and lowers the kinetic barrier to unfolding. *J. Biol. Chem.* **281,** 30782.
114. Zhao, H., P. H. Brown, M. T. Magone and P. Schuck (2011) The Molecular Refractive Function of Lens γ-Crystallins. *J. Mol. Biol.* **411,** 680-699.
115. Kong, F. and J. King (2011) Contributions of aromatic pairs to the folding and stability of long-lived human γD-crystallin. *Protein Sci.* **20,** 513-528.
116. Liang, J. N. and B. Chakrabarti (1982) Spectroscopic investigations of bovine lens crystallins. 1. Circular dichroism and intrinsic fluorescence. *Biochemistry* **21,** 1847-1852.
117. Moreau, K. L. and J. King (2009) Hydrophobic Core Mutations Associated with Cataract Development in Mice Destabilize Human gammaD-Crystallin. *J. Biol. Chem.* **284,** 33285-33295.
118. Chen, J., S. L. Flaugh, P. R. Callis and J. King (2006) Mechanism of the highly efficient quenching of tryptophan fluorescence in human gammaD-crystallin. *Biochemistry* **45,** 11552-11563.
119. Chen, J., D. Toptygin, L. Brand and J. King (2008) Mechanism of the Efficient Tryptophan Fluorescence Quenching in Human γD-Crystallin Studied by Time-Resolved Fluorescence †. *Biochemistry* **47,** 10705-10721.
120. Chen, J., P. R. Callis and J. King (2009) Mechanism of the very efficient quenching of tryptophan fluorescence in human gamma D- and gamma S-crystallins: the gamma-crystallin fold may have evolved to protect tryptophan residues from ultraviolet photodamage. *Biochemistry* **48,** 3708-3716.
121. Lakowicz, J. R. (1999) Energy Transfer. In *Principles of Fluorescence Spectroscopy*. pp. 368-391. Kluwer Academic/Plenum Publishers.
122. Papanikolopoulou, K., I. Mills-Henry, S. Thol, Y. Wang, A. Gross, D. Kirschner, S. Decatur and J. King (2008) Formation of amyloid fibrils in vitro by human γD-crystallin and its isolated domains. *Mol. Vision* **14,** 81.
123. Wang, Y., S. Petty, A. Trojanowski, K. Knee, D. Goulet, I. Mukerji and J. King (2010) Formation of amyloid fibrils in vitro from partially unfolded intermediates of human gammaC-crystallin. *Invest. Ophthalmol. Visual Sci.* **51,** 672-678.
124. Meehan, S., T. P. J. Knowles, A. J. Baldwin, J. F. Smith, A. M. Squires, P. Clements, T. M. Treweek, H. Ecroyd, G. G. Tartaglia, M. Vendruscolo, C. E. MacPhee, C. M. Dobson and J. A. Carver (2007) Characterisation of Amyloid Fibril Formation by Small Heat-shock Chaperone Proteins Human αA-, αB- and R120G αB-Crystallins. *J. Mol. Biol.* **372,** 470-484.

125. Friedrich, M. and R. Truscott (2010) Large-Scale Binding of {alpha}-Crystallin to Cell Membranes of Aged Normal Human Lenses: A Phenomenon That Can Be Induced by Mild Thermal Stress. *Invest. Ophthalmol. Visual Sci.* **51,** 5145.
126. Wang, S. S.-S. and W.-S. Wen (2010) Examining the influence of ultraviolet C irradiation on recombinant human γD-crystallin. *Mol. Vision* **16,** 2777-2790.
127. Reddy, V. N. and F. J. Giblin (1984) Metabolism and function of glutathione in the lens. *Ciba Found. Symp.* **106,** 65-87.
128. Borkman, R. F., G. Knight and B. Obi (1996) The molecular chaperone alpha-crystallin inhibits UV-induced protein aggregation. *Exp. Eye Res.* **62,** 141-148.
129. Congdon, N., J. R. Vingerling, B. E. K. Klein, S. West, D. S. Friedman, J. Kempen, B. O'Colmain, S.-Y. Wu, H. R. Taylor and E. D. P. R. Group (2004) Prevalence of cataract and pseudophakia/aphakia among adults in the United States. *Arch. Ophthalmol. (Chicago, IL, U. S.)* **122,** 487-494.
130. Prevent Blindness America, N. E. I. (2008) Vision Problems in the U.S.**,** 1-42.
131. Frick, K., E. Gower and J. Kempen (2007) Economic impact of visual impairment and blindness in the United States. *Arch. Ophthalmol.*
132. Zhang, X., M. F. Cotch, A. Ryskulova, S. A. Primo, P. Nair, C. F. Chou, L. S. Geiss, L. E. Barker, A. F. Elliott, J. E. Crews and J. B. Saaddine (2012) Vision Health Disparities in the United States by Race/Ethnicity, Education, and Economic Status: Findings From Two Nationally Representative Surveys. *Am. J. Ophthalmol.* **154,** S53-S62.e1.
133. Abraham, A., N. Condon and E. W. Gower (2006) The New Epidemiology of Cataract. *Ophthalmol. Clinics N. America* **19,** 415-425.
134. Moreau, K. L. and J. A. King (2012) Protein misfolding and aggregation in cataract disease and prospects for prevention. *Trends Mol. Med.* **18,** 273-282.
135. Dillon, J. (1994) UV-B as a pro-aging and pro-cataract factor. *Doc. Ophthalmol.* **88,** 339-344.
136. Friedrich, M. G., J. Lam and R. J. W. Truscott (2012) Degradation of an old human protein. Age-dependent cleavage of S crystallin generates a peptide that binds to cell membranes. *J. Biol. Chem.*
137. Truscott, R. J. W. (2005) Age-related nuclear cataract—oxidation is the key. *Exp. Eye Res.* **80,** 709-725.
138. Palmquist, B. M., B. Philipson and P. O. Barr (1984) Nuclear cataract and myopia during hyperbaric oxygen therapy. *Br. J. Ophthalmol.* **68,** 113-117.
139. Wormstone, I. M. and M. A. Wride (2011) The ocular lens: a classic model for development, physiology and disease. *Philos. Trans. R. Soc., B* **366,** 1190-1192.
140. Michael, R. and A. J. Bron (2011) The ageing lens and cataract: a model of normal and pathological ageing. *Philos. Trans. R. Soc., B* **366,** 1278-1292.

141. West, S. K. (2005) Model of Risk of Cortical Cataract in the US Population with Exposure to Increased Ultraviolet Radiation due to Stratospheric Ozone Depletion. *Am. J. Epidemiol.* **162,** 1080-1088.
142. Harding, J. J. (2002) Viewing molecular mechanisms of ageing through a lens. *Ageing Res. Rev.* **1,** 465-479.
143. Hains, P. G. and R. J. W. Truscott (2010) Age-Dependent Deamidation of Lifelong Proteins in the Human Lens. *Invest. Ophthalmol. Visual Sci.* **51,** 3107-3114.
144. Wilmarth, P. A., S. Tanner, S. Dasari, S. R. Nagalla, M. A. Riviere, V. Bafna, P. A. Pevzner and L. L. David (2006) Age-related changes in human crystallins determined from comparative analysis of post-translational modifications in young and aged lens: does deamidation contribute to crystallin insolubility? *J. Proteome Res.* **5,** 2554-2566.
145. Mafia, K., R. Gupta, M. Kirk, L. Wilson, O. P. Srivastava and S. Barnes (2008) UV-A-induced structural and functional changes in human lens deamidated alphaB-crystallin. *Mol. Vision* **14,** 234-248.
146. Cheng, R., B. Lin, K. W. Lee and B. J. Ortwerth (2001) Similarity of the yellow chromophores isolated from human cataracts with those from ascorbic acid-modified calf lens proteins: evidence for ascorbic acid glycation during cataract formation. *Biochim. Biophys. Acta* **1537,** 14-26.
147. Grey, A. C. and K. L. Schey (2008) Distribution of bovine and rabbit lens alpha-crystallin products by MALDI imaging mass spectrometry. *Mol. Vision* **14,** 171-179.
148. Grey, A. C. and K. L. Schey (2009) Age-related changes in the spatial distribution of human lens alpha-crystallin products by MALDI imaging mass spectrometry. *Invest. Ophthalmol. Visual Sci.* **50,** 4319-4329.
149. Kamei, A., S. Iwata and J. Horwitz (1987) Characterization of water-insoluble proteins in human lens nuclei. *Jpn. J. Ophthalmol.* **31,** 433-439.
150. Costello, M., S. Johnsen, S. Metlapally, K. Gilliland, B. Ramamurthy, P. Krishna and D. Balasubramanian (2008) Ultrastructural analysis of damage to nuclear fiber cell membranes in advanced age-related cataracts from India. *Exp. Eye Res.* **87,** 147-158.
151. Costello, M. J., A. Burette, M. Weber, S. Metlapally, K. O. Gilliland, W. C. Fowler, A. Mohamed and S. Johnsen (2012) Electron tomography of fiber cell cytoplasm and dense cores of multilamellar bodies from human age-related nuclear cataracts. *Exp. Eye Res.* **101,** 72-81.
152. Fink, A. L. (1998) Protein aggregation: folding aggregates, inclusion bodies and amyloid. *Folding Des.* **3,** R9-R23.
153. Chiti, F. and C. M. Dobson (2006) Protein misfolding, functional amyloid, and human disease. *Annu. Rev. Biochem.* **75,** 333-366.
154. Furukawa, Y., K. Kaneko, K. Yamanaka and N. Nukina (2010) Mutation-dependent polymorphism of Cu,Zn-superoxide dismutase aggregates in the familial form of amyotrophic lateral sclerosis. *J. Biol. Chem.* **285,** 22221-22231.
155. Takahashi, T., K. Ohta and H. Mihara (2009) Rational design of amyloid beta peptide-binding proteins: Pseudo-Abeta beta-sheet surface

presented in green fluorescent protein binds tightly and preferentially to structured Abeta. *Proteins*.
156. Mitomi, Y., T. Nomura, M. Kurosawa, N. Nukina and Y. Furukawa (2012) Post-aggregation oxidation of mutant huntingtin controls the interactions between aggregates. *J. Biol. Chem.*
157. Zilka, N., E. Kontsekova and M. Novak (2008) Chaperone-like antibodies targeting misfolded tau protein: new vistas in the immunotherapy of neurodegenerative foldopathies. *J. Alzheimer's Dis.* **15,** 169-179.
158. Steinberg, M. H. (2008) Sickle Cell Anemia, the First Molecular Disease: Overview of Molecular Etiology, Pathophysiology, and Therapeutic Approaches. *Sci. World J.* **8,** 1295-1324.
159. Lomas, D. A. and R. W. Carrell (1993) A protein structural approach to the solution of biological problems: alpha 1-antitrypsin as a recent example. *Am. J. Physiol.* **265,** L211-L219.
160. Žerovnik, E., V. Stoka, A. Mirtič, G. Gunčar, J. Grdadolnik, R. A. Staniforth, D. Turk and V. Turk (2011) Mechanisms of amyloid fibril formation - focus on domain-swapping. *FEBS J.* **278,** 2263-2282.
161. Coppinger, J. A., D. M. Hutt, A. Razvi, A. V. Koulov, S. Pankow, J. R. Yates and W. E. Balch (2012) A chaperone trap contributes to the onset of cystic fibrosis. *PLoS One* **7,** e37682.
162. Pande, A., J. Pande, N. Asherie, A. Lomakin, O. Ogun, J. A. King, N. H. Lubsen, D. Walton and G. B. Benedek (2000) Molecular basis of a progressive juvenile-onset hereditary cataract. *Proc. Natl. Acad. Sci. U. S. A.* **97,** 1993-1998.
163. Pande, A., J. Pande, N. Asherie, A. Lomakin, O. Ogun, J. King and G. B. Benedek (2001) Crystal cataracts: human genetic cataract caused by protein crystallization. *Proc. Natl. Acad. Sci. U. S. A.* **98,** 6116-6120.
164. Pande, A., K. S. Ghosh, P. R. Banerjee and J. Pande (2010) Increase in Surface Hydrophobicity of the Cataract-Associated P23T Mutant of Human γD-Crystallin Is Responsible for Its Dramatically Lower, Retrograde Solubility. *Biochemistry***,** 100701114329098.
165. Vendra, V. P. R. and D. Balasubramanian (2010) Structural and aggregation behavior of the human γD-crystallin mutant E107A, associated with congenital nuclear cataract. *Mol. Vision* **16,** 2822-2828.
166. Banerjee, P. R., A. Pande, J. Patrosz, G. M. Thurston and J. Pande (2011) Cataract-associated mutant E107A of human gammaD-crystallin shows increased attraction to alpha-crystallin and enhanced light scattering. *Proc. Natl. Acad. Sci. U. S. A.* **108,** 574-579.
167. Moreau, K. L. and J. A. King (2012) Cataract-Causing Defect of a Mutant γ-Crystallin Proceeds through an Aggregation Pathway Which Bypasses Recognition by the α-Crystallin Chaperone. *PLoS One* **7,** e37256.
168. Taylor, H. R. (1999) Epidemiology of age-related cataract. *Eye (London, U. K.)* **13 (Pt 3b),** 445-448.
169. Trevithick, J. R. and K. P. Mitton (2000) Vitamins C and E in cataract risk reduction. *Int. Ophthalmol. Clinics* **40,** 59.

170. Minassian, D. C., V. Mehra and B. R. Jones (1984) Dehydrational crises from severe diarrhoea or heatstroke and risk of cataract. *Lancet* **1,** 751-753.
171. Brian, G. and H. Taylor (2001) Cataract blindness--challenges for the 21st century. *Bull. W. H. O.* **79,** 249-256.
172. Katoh, N., F. Jonasson, H. Sasaki, M. Kojima, M. Ono, N. Takahashi, K. Sasaki and R. E. S. Group (2001) Cortical lens opacification in Iceland. Risk factor analysis -- Reykjavik Eye Study. *Acta Ophthalmol. Scand.* **79,** 154-159.
173. Taylor, H. R. (1989) Ultraviolet radiation and the eye: an epidemiologic study. *Trans. Am. Ophthalmol. Soc.* **87,** 802-853.
174. Hayashi, L. C., N. Tamiya and E. Yano (1998) Correlation between UVB irradiation and the proportion of cataract--an epidemiological study based on a nationwide patient survey in Japan. *Ind. Health* **36,** 354-360.
175. Toh, T. a. Y., J. Morton, J. Coxon and M. J. Elder (2007) Medical treatment of cataract. *Clin. Exp. Ophthalmol.* **35,** 664-671.
176. Babizhayev, M. A., L. Burke, P. Micans and S. P. Richer (2009) N-Acetylcarnosine sustained drug delivery eye drops to control the signs of ageless vision: glare sensitivity, cataract amelioration and quality of vision currently available treatment for the challenging 50,000-patient population. *Clin. Interventions Aging* **4,** 31-50.
177. Shi, Q., H. Yan, M.-Y. Li and J. J. Harding (2009) Effect of a combination of carnosine and aspirin eye drops on streptozotocin -- induced diabetic cataract in rats. *Mol. Vision* **15,** 2129-2138.
178. Nahomi, R. B., B. Wang, C. T. Raghavan, O. Voss, A. Doseff, P. Santhoshkumar and R. H. Nagaraj (2013) Chaperone peptides of -crystallin inhibit epithelial cell apoptosis, protein insolubilization and opacification in experimental cataracts. *J. Biol. Chem.*
179. Giblin, F. J., L.-R. Lin, V. R. Leverenz and L. Dang (2011) A class I (Senofilcon A) soft contact lens prevents UVB-induced ocular effects, including cataract, in the rabbit in vivo. *Invest. Ophthalmol. Visual Sci.* **52,** 3667-3675.
180. Giblin, F. J., L.-R. Lin, M. F. Simpanya, V. R. Leverenz and C. E. Fick (2012) A Class I UV-blocking (senofilcon A) soft contact lens prevents UVA-induced yellow fluorescence and NADH loss in the rabbit lens nucleus in vivo. *Exp. Eye Res.* **102,** 17-27.
181. Hiramoto, K., H. Kobayashi, Y. Yamate, M. Ishii, T. Sato and M. Inoue (2013) UVB-induced epidermal pigmentation in mice eyes with no contact lens wear and non-UVB blocking and UVB blocking contact lens wear. *Contact Lens Anterior Eye* **36,** 28-31.
182. Andley, U. P., J. P. Malone and R. R. Townsend (2011) Inhibition of Lens Photodamage by UV-Absorbing Contact Lenses. *Invest. Ophthalmol. Visual Sci.* **52,** 8330-8341.
183. Wegener, A. R. (1994) In vivo studies on the effect of UV-radiation on the eye lens in animals. *Doc. Ophthalmol.* **88,** 221-232.

184. Ayala, M., R. Michael and P. Söderberg (2000) In vivo cataract after repeated exposure to ultraviolet radiation. *Exp. Eye Res.* **70,** 451-456.
185. Vrensen, G. F. (1994) UV-B and early cortical and nuclear changes in the human lens. *Doc. Ophthalmol.* **88,** 255-261.
186. Simpanya, M. F., R. R. Ansari, V. Leverenz and F. J. Giblin (2008) Measurement of lens protein aggregation in vivo using dynamic light scattering in a guinea pig/UVA model for nuclear cataract. *Photochem. Photobiol.* **84,** 1589-1595.
187. Michael, R., P. G. Söderberg and E. Chen (1996) Long-term development of lens opacities after exposure to ultraviolet radiation at 300 nm. *Ophthalmic Res.* **28,** 209-218.
188. Hains, P. G., M. F. Simpanya, F. Giblin and R. J. W. Truscott (2006) UV filters in the lens of the thirteen lined ground squirrel (Spermophilus tridecemlineatus). *Exp. Eye Res.* **82,** 730-737.
189. Zigman, S., T. Paxhia, T. McDaniel, M. F. Lou and N. T. Yu (1991) Effect of chronic near-ultraviolet radiation on the gray squirrel lens in vivo. *Invest. Ophthalmol. Visual Sci.* **32,** 1723-1732.
190. Goosey, J. D., J. S. Zigler and J. H. Kinoshita (1980) Cross-linking of lens crystallins in a photodynamic system: a process mediated by singlet oxygen. *Science (New York, NY)* **208,** 1278-1280.
191. Andley, U. P. and B. A. Clark (1989) Photoreactions of human lens monomeric crystallins. *Biochim. Biophys. Acta* **997,** 284-291.
192. Andley, U. P. and B. A. Clark (1989) Generation of oxidants in the near-UV photooxidation of human lens alpha-crystallin. *Invest. Ophthalmol. Visual Sci.* **30,** 706-713.
193. Andley, U. P., M. A. Sawardekar and J. L. Burris (1997) Action spectrum for photocross-linking of human lens proteins. *Photochem. Photobiol.* **65,** 556-559.
194. Andley, U. P. and B. A. Clark (1989) The effects of near-UV radiation on human lens beta-crystallins: protein structural changes and the production of O2- and H2O2. *Photochem. Photobiol.* **50,** 97-105.
195. Hibbard, L. B., N. J. Kirk and R. F. Borkman (1985) The in vitro photolysis of whole rat lenses using focused 290 nm laser radiation. *Exp. Eye Res.* **40,** 285-295.
196. Pirie, A. (1972) Fluorescence of N'-formylkynurenine and of protein exposed to sunlight. *Biochem. J.* **128,** 1365-1367.
197. Borkman, R. F., J. D. Tassin and S. Lerman (1981) The rates of photodestruction of tryptophan residues in human and bovine ocular lens proteins. *Exp. Eye Res.* **32,** 747-754.
198. Li, D., R. Borkman, R. Wang and J. Dillon (1990) Mechanisms of photochemically produced turbidity in lens protein solutions. *Exp. Eye Res.* **51,** 663-669.
199. Reszka, K. J., P. Bilski, C. F. Chignell and J. Dillon (1996) Free radical reactions photosensitized by the human lens component, kynurenine: an EPR and spin trapping investigation. *Free Radical Biol. Med.* **20,** 23-34.

200. Tsentalovich, Y. P., O. A. Snytnikova, P. S. Sherin and M. D. E. Forbes (2005) Photochemistry of kynurenine, a tryptophan metabolite: properties of the triplet state. *J. Phys. Chem. A* **109,** 3565-3568.
201. Xia, Z., Z. Yang, T. Huynh, J. A. King and R. Zhou (2013) UV-radiation Induced Disruption of Dry-Cavities in Human γD-crystallin Results in Decreased Stability and Faster Unfolding. *Sci. Reports* **3**.
202. Sasaki, H., Y. Sakamoto, C. Schnider, N. Fujita, N. Hatsusaka, D. H. Sliney and K. Sasaki (2011) UV-B exposure to the eye depending on solar altitude. *Eye Contact Lens* **37,** 191-195.
203. Sliney, D. H. (1994) UV radiation ocular exposure dosimetry. *Doc. Ophthalmol.* **88,** 243-254.
204. Sliney, D. H. (1995) UV radiation ocular exposure dosimetry. *J. Photochem. Photobiol. B* **31,** 69-77.
205. Schmalwieser, A. W., A. Cabaj, G. Schauberger, H. Rohn, B. Maier and H. Maier (2010) Facial Solar UV Exposure of Austrian Farmers During Occupation. *Photochem. Photobiol*.
206. Christiaens, F. J., A. Chardon, A. Fourtanier and J. E. Frederick (2005) Standard ultraviolet daylight for nonextreme exposure conditions. *Photochem. Photobiol.* **81,** 874-878.
207. Stefani, M. and C. M. Dobson (2003) Protein aggregation and aggregate toxicity: new insights into protein folding, misfolding diseases and biological evolution. *J. Mol. Med.* **81,** 678-699.
208. Lagerwerf, S., M. G. Vrouwe, R. M. Overmeer, M. I. Fousteri and L. H. F. Mullenders (2011) DNA damage response and transcription. *DNA Repair* **10,** 743-750.
209. Friedberg, E. C. (2001) How nucleotide excision repair protects against cancer. *Nat. Rev. Cancer* **1,** 22-33.
210. Yang, W. (2011) Surviving the Sun: Repair and bypass of DNA UV lesions. *Protein Sci.* **20,** 1781-1789.
211. Setlow, R. B. and W. L. Carrier (1966) Pyrimidine dimers in ultraviolet-irradiated DNA's. *J. Mol. Biol.* **17,** 237-254.
212. Cao, C. and Y. Wan (2009) Parameters of protection against ultraviolet radiation-induced skin cell damage. *J. Cell. Physiol.* **220,** 277-284.
213. Evans, P., C. Slingsby and B. A. Wallace (2008) Association of partially folded lens βB2-crystallins with the α-crystallin molecular chaperone. *Biochem. J.* **409,** 691.
214. Wistow, G., C. Slingsby, T. Blundell, H. Driessen, W. De Jong and H. Bloemendal (1981) Eye-lens proteins: the three-dimensional structure of beta-crystallin predicted from monomeric gamma-crystallin. *FEBS Lett.* **133,** 9-16.
215. Ji, F., J. Jung, L. M. I. Koharudin and A. M. Gronenborn (2012) The Human W42R D-Crystallin Mutant Structure Provides a Link between Congenital and Age-related Cataracts. *J. Biol. Chem.*
216. Andley, U. P. and S. F. Chapman (1986) Conformational changes of bovine lens crystallins in a photodynamic system. *Photochem. Photobiol.* **44,** 67-74.

217. Mandal, K., S. K. Bose and B. Chakrabarti (1986) Sensitizer-induced conformational changes in lens crystallin--I. Photodynamic action of methylene blue and N-formylkynurenine on bovine alpha-crystallin. *Photochem. Photobiol.* **43,** 515-523.
218. Mandal, K., M. Kono, S. K. Bose, J. Thomson and B. Chakrabarti (1988) Structure and stability of gamma-crystallins--IV. Aggregation and structural destabilization in photosensitized reactions. *Photochem. Photobiol.* **47,** 583-591.
219. Estey, T., Y. Chen, J. F. Carpenter and V. Vasiliou (2010) Structural and Functional Modifications of Corneal Crystallin ALDH3A1 by UVB Light. *PLoS One* **5,** e15218.
220. Xu, J., J. Chen, D. Toptygin, O. Tcherkasskaya, P. Callis, J. King, L. Brand and J. R. Knutson (2009) Femtosecond fluorescence spectra of tryptophan in human gamma-crystallin mutants: site-dependent ultrafast quenching. *J. Am. Chem. Soc.* **131,** 16751-16757.
221. Hofrichter, J., P. D. Ross and W. A. Eaton (1974) Kinetics and mechanism of deoxyhemoglobin S gelation: a new approach to understanding sickle cell disease. *Proc. Natl. Acad. Sci. U. S. A.* **71,** 4864-4868.
222. Grossweiner, L. I. (1984) Photochemistry of proteins: a review. *Curr. Eye Res.* **3,** 137-144.
223. Gasteiger, E., C. Hoogland, A. Gattiker, S. Duvaud, M. R. Wilkins, R. D. Appel and A. Bairoch (2005) Protein Identification and Analysis Tools on the ExPASy Server. In *The Proteomics Protocols Handbook*. (Edited by J. M. Walker), pp. 571-607. Humana Press.
224. Lucas, B., M. Barat, J. Fayeton and C. Jouvet (2009) Mechanisms of UV Photodissociation of Small Protonated Peptides (dagger). *Eur. Phys. J. D*.
225. Noell, W. K., V. S. Walker, B. S. Kang and S. Berman (1966) Retinal damage by light in rats. *Invest. Ophthalmol.* **5,** 450-473.
226. Borkman, R. F., L. B. Hibbard and J. Dillon (1986) The photolysis of tryptophan with 337.1 nm laser radiation. *Photochem. Photobiol.* **43,** 13-19.
227. Hains, P. G. and R. J. W. Truscott (2007) Post-Translational Modifications in the Nuclear Region of Young, Aged, and Cataract Human Lenses. *J. Proteome Res.* **6,** 3935-3943.
228. Chelnokov, E., L. Soustov, N. Sapogova, M. Ostrovsky and N. Bityurin (2008) Nonreciprocal XeCl laser-induced aggregation of beta-crystallins in water solution. *Opt. Express* **16,** 18798-18803.
229. Berthoud, V. M. and E. C. Beyer (2009) Oxidative Stress, Lens Gap Junctions, and Cataracts. *Antioxid. Redox Signaling* **11,** 339-353.
230. Hartl, F. U., A. Bracher and M. Hayer-Hartl (2011) Molecular chaperones in protein folding and proteostasis. *Nature* **475,** 324-332.
231. Schafheimer, N. and J. King (2013) Tryptophan Cluster Protects Human γD-Crystallin from Ultraviolet Radiation-Induced Photo-Aggregation In vitro. *Photochem. Photobiol*.
232. Kettenhofen, N. J. and M. J. Wood (2010) Formation, reactivity, and detection of protein sulfenic acids. *Chem. Res. Toxicol.* **23,** 1633-1646.

233. McCall, J. D. and K. S. Anseth (2012) Thiol–Ene Photopolymerizations Provide a Facile Method To Encapsulate Proteins and Maintain Their Bioactivity. *Biomacromolecules* **13,** 2410-2417.
234. Shen, H., J. Spikes, P. Kopeeková and J. Kopeek (1996) Photodynamic crosslinking of proteins. I. Model studies using histidine-and lysine-containing N-(2-hydroxypropyl) methacrylamide copolymers. *J. Photochem. Photobiol. B* **34,** 203-210.
235. Lee, J. S., J. H. Liao, S. H. Wu and S. H. Chiou (1997) alpha-Crystallin acting as a molecular chaperonin against photodamage by UV irradiation. *J. Protein Chem.* **16,** 283-289.
236. Ha, J.-w., A. B. Schwahn and K. M. Downard (2010) Ability of N-acetylcarnosine to protect lens crystallins from oxidation and oxidative damage by radical probe mass spectrometry (RP-MS). *Rapid Commun. Mass Spectrom.* **24,** 2900-2908.
237. Hightower, K. R. (1994) A review of the evidence that ultraviolet irradiation is a risk factor in cataractogenesis. *Doc. Ophthalmol.* **88,** 205-220.
238. Hockwin, O., M. Kojima, Y. Sakamoto, A. Wegener, Y. Shui and K. Sasaki (1999) UV damage to the eye lens: further results from animal model studies: a review. *J. Epidemiology, Jpn.* **9,** S39.
239. Hains, P. G. and R. J. W. Truscott (2008) Proteomic analysis of the oxidation of cysteine residues in human age-related nuclear cataract lenses. *Biochim. Biophys. Acta, Proteins Proteomics* **1784,** 1959-1964.
240. Dalsgaard, T. K., M. Triquigneaux, L. Deterding, F. Summers, K. Ranguelova, G. Mortensen and R. P. Mason (2013) Site-Specific Detection of Radicals on α-Lactalbumin after a Riboflavin-Sensitized Reaction, Detected by Immuno-spin Trapping, ESR, and MS. *J. Agric. Food Chem.* **61,** 418-426.
241. Gomes, A., E. Fernandes and J. L. F. C. Lima (2005) Fluorescence probes used for detection of reactive oxygen species. *J. Biochem. Biophys. Methods* **65,** 45-80.
242. Wardman, P. (2007) Fluorescent and luminescent probes for measurement of oxidative and nitrosative species in cells and tissues: progress, pitfalls, and prospects. *Free Radical Biol. Med.* **43,** 995-1022.
243. Ehrenshaft, M., M. G. Bonini, L. Feng, C. F. Chignell and R. P. Mason (2010) Partial Colocalization of Oxidized, N-formylkynurenine-containing Proteins in Mitochondria and Golgi of Keratinocytes. *Photochem. Photobiol.*
244. Zamadar, M., D. Aebisher and A. Greer (2009) Singlet Oxygen Delivery Through the Porous Cap of a Hollow-Core Fiber Optic Device. *J. Phys. Chem. B*.
245. Das, P., J. A. King and R. Zhou (2011) Aggregation of γ-crystallins associated with human cataracts via domain swapping at the C-terminal β-strands. *Proc. Natl. Acad. Sci. U. S. A.* **108,** 10514-10519.
246. Berthomieu, C. and R. Hienerwadel (2009) Fourier transform infrared (FTIR) spectroscopy. *Photosynth. Res.* **101,** 157-170.

247. Fatima, U., S. Sharma and P. Guptasarma (2010) Structures of Differently Aggregated and Precipitated forms of gammaB Crystallin : An FTIR Spectroscopic and EM Study. *Protein Pept. Lett.* **17,** 1155-1162.
248. Leitner, A., T. Walzthoeni, A. Kahraman, F. Herzog, O. Rinner, M. Beck and R. Aebersold (2010) Probing native protein structures by chemical cross-linking, mass spectrometry, and bioinformatics. *Mol. Cell. Proteomics* **9,** 1634-1649.
249. Rappsilber, J. (2011) The beginning of a beautiful friendship: Cross-linking/mass spectrometry and modelling of proteins and multi-protein complexes. *J. Struct. Biol.* **173,** 530-540.
250. Sinz, A. (2006) Chemical cross-linking and mass spectrometry to map three-dimensional protein structures and protein–protein interactions. *Mass Spectrom. Rev.* **25,** 663-682.
251. Fischer, L., Z. A. Chen and J. Rappsilber (2013) Quantitative cross-linking/mass spectrometry using isotope-labelled cross-linkers. *J. Proteomics***,** 1-9.

CHAPTER 6:

APPENDICES

Appendix A: Fluorimeter Photo-Bleaching Studies

1. Background

HγD-Crys contains two highly conserved tryptophan pairs, one pair in each domain, along with 14 tyrosine residues. Tryptophan and tyrosine residues have distinct absorption and fluorescence spectra. Previous studies used the fluorescence spectrum of HγD-Crys to monitor its folded state (107, 109, 115). Other studies examining the response of mixtures of lens proteins to UVR within the lens or *in vitro* saw a decrease in tryptophan fluorescence over time, with photo-bleaching or photo-product fluorescence developing over long exposures (194, 195, 198). Data from chapter 1 monitoring the absorption spectrum of HγD-Crys suggested that under exposure to 2 mW/cm^2 of a spectrum of UVA/UVB *in vitro* the protein's aromatic residues were largely unmodified after 36 minutes, at which point significant photo-aggregation had occurred. It appeared that damage to the aromatics played no significant role in the *in vitro* photo-aggregation under study here, but previous work studying UVR-induced damage to lens proteins suggested a central role for photo-bleaching type damage.

2. Purpose

To determine whether photo-bleaching of aromatic residue fluorescence occurs when HγD-Crys is exposed to UVR *in vitro*.

3. Methods

To avoid the interference of light scattering aggregation and for ease of sample reading, we chose to use as a radiation source the beam of a Hitachi F-4500 fluorescence spectrometer. I exposed WT HγD-Crys, W130-only HγD-Crys,

and NoTrp HγD-Crys to long periods of exposure at 302 nm (the center of the range delivered by the UVA/UVB bulb used in the photo-aggregation experiments). 3 ml samples were prepared at 10 μg/ml in 10 mM sodium phosphate (pH 7), 1 mM EDTA. Samples were irradiated in a capped quartz cuvette (Starna) while being kept at 37°C with constant stirring. The fluorimeter was set to expose the sample for 21 hours at 302 nm (slits at 10 nm) halting every hour to read the fluorescence emission spectrum at ex. 295 nm em. 310-400 nm (for WT and W130-only HγD-Crys), and ex. 274 nm em. 290-380 nm (NoTrp HγD-Crys) before resuming exposure at 302 nm.

4. Results and Discussion

WT HγD-Crys' tryptophan fluorescence spectra intensity increased to the 3 hour exposure point while red-shifting, then decreased steadily for the remaining 18 hours (Fig. A.1a). The steady decrease is likely photo-bleaching, demonstrating that with steady, long exposure at 302 nm, a drop in tryptophan fluorescence was observed with recombinant HγD-Crys *in vitro*, corroborating previous studies that observed similar loss in irradiated lens protein. The expanded UVA/UVB range utilized in the photo-aggregation experiments may cause a different set of photochemical reactions to occur than isolated 302 nm light, such that other reactions leading to aggregation dominate under those conditions while covalent tryptophan damage is out-competed. It also seems likely that the shorter timescale and more intense exposure of the UVA/UVB lamp allows observation of only quicker photo-damage reactions, and that longer,

less intense exposure allows observation of eventual damage to the aromatic residues.

The early increase in fluorescence could represent a conformational change induced by photodamage. Partial unfolding of a fraction of the HγD-Crys sample would relieve the native state quenching the tryptophan pairs are subject to, possibly compensating for loss of fluorescence due to tryptophan damage. Photoproducts formed by damaging the tryptophans could be absorbing and fluorescing, red-shifting the peak of the observed spectra accordingly.

W130-only HγD's lone tryptophan's fluorescence drops steadily throughout the 21 hour exposure, indicating photo-bleaching similar to WT. The lack of an initial rise in fluorescence intensity is consistent with an unfolding explanation of WT's initial rise; W130-only would experience no relief of quenching upon conformational change, as only a single non-quenched tryptophan was present. W130-only HγD-Crys also saw a red-shift in its fluorescence spectrum; WT's red-shift explanation likely suits the triple mutant too.

NoTrp HγD-Crys was used to monitor tyrosine fluorescence, as the presence of tryptophan, a stronger fluorophore, would otherwise obscure it. NoTrp's tyrosine fluorescence drops steadily over the course of 21 hours of 302 nm exposure, suggesting tyrosines are photo-bleached as well. The lack of a red-shift at later spectra suggests the products being formed do not absorb and fluoresce in a similar range as WT.

Together, these results indicate HγD-Crys' tryptophans and tyrosines are capable of being photo-bleached, consistent with previous studies on UVR

exposure of lens proteins. It is likely the short, intense UVA/UVB exposure brings a different set of photochemical reactions to prominence than the longer, less intense 302 nm exposure, which outcompete aromatic damage and cause photo-aggregation.

a

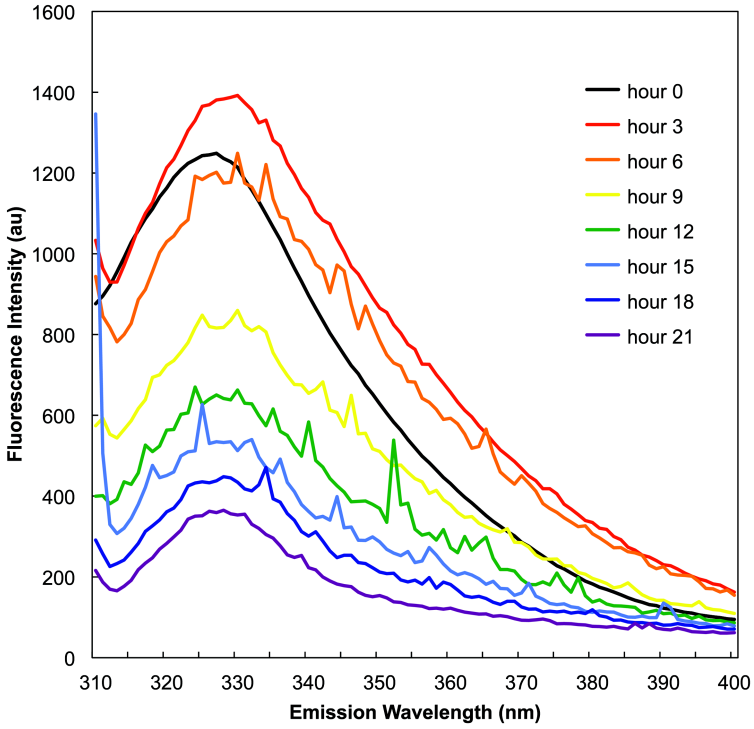
Fluorescence Intensity (au)
Emission Wavelength (nm)
hour 0
hour 3
hour 6
hour 9
hour 12
hour 15
hour 18
hour 21

b

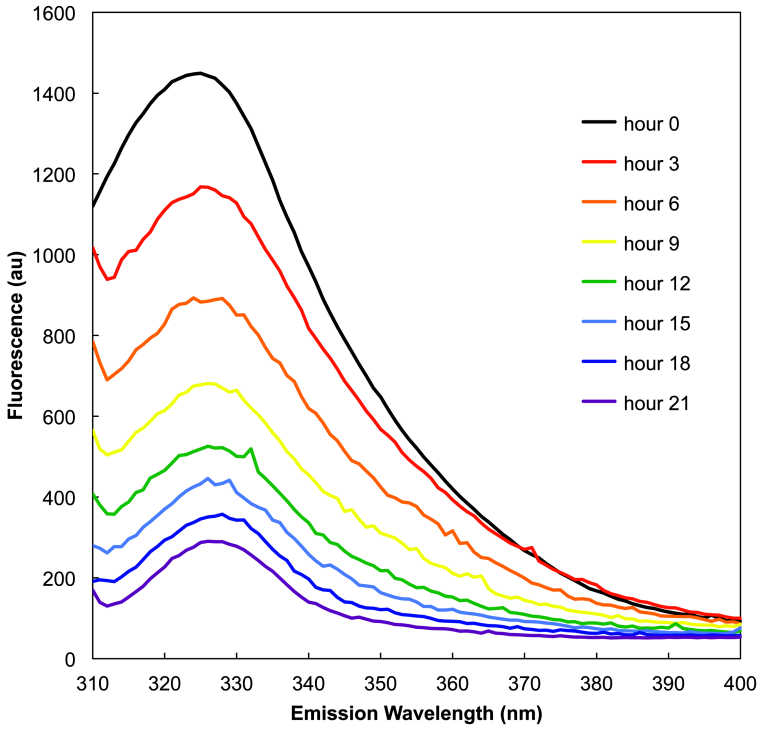
Fluorescence (au)
Emission Wavelength (nm)
hour 0
hour 3
hour 6
hour 9
hour 12
hour 15
hour 18
hour 21

c

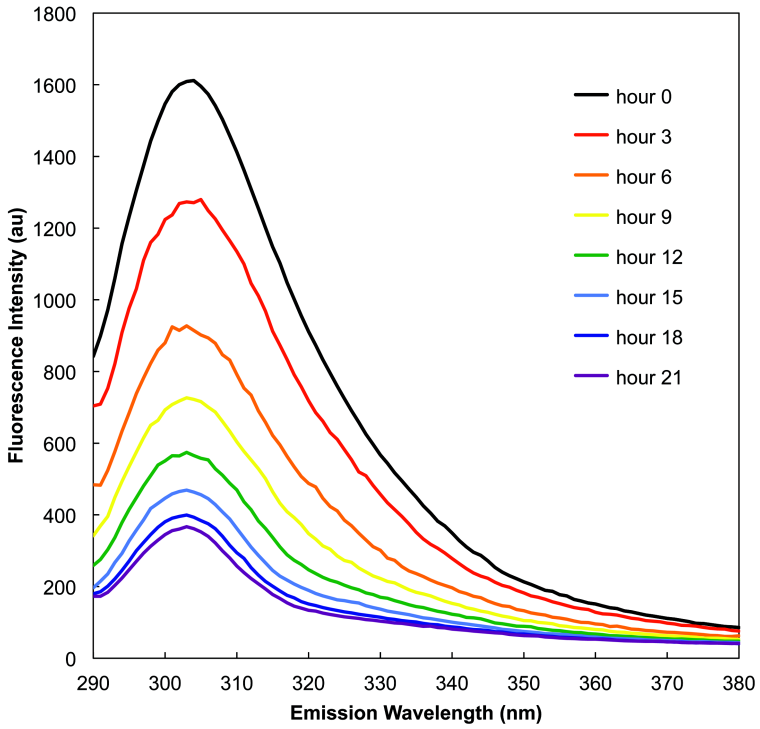

Figure 6A.1 Photo-bleaching of Fluorescence Spectra of WT, W130-only, and NoTrp HγD-Crys Over Exposure to 302 nm Light. Fluorescence spectra of HγD-Crys constructs over 302 nm fluorimeter irradiation time. (a) WT HγD-Crys tryptophan fluorescence, (b) W130-only HγD-Crys tryptophan fluorescence, (c) NoTrp HγD-Crys tyrosine fluorescence. Hour 0 (black), 3 (red), 6 (orange), 9 (yellow), 12 (green), light blue (15), dark blue (18), 21 (purple).

Appendix B: Photo-aggregation Equipment Setup

Purpose: To clarify the details of the lamp and sample arrangement, photographs of the UVR exposure cabinet are included here.

Discussion: The UV handlamp was arranged vertically, with its base flush with the side of the cabinet, exposing the cabinet wall with radiation (Fig 6B.1). It was aligned with the tape on the cabinet floor. The sample cuvette sat atop a metal block (a pipette canister lid), with a tape marked position. The goal of these markings was to be as consistent as possible in sample positioning between experiments. Thus each day the cuvette always sat at the same height and depth in relation to the cabinet, with its broad side facing the lamp and its quartz material designation number facing out of the cabinet. Before each experiment, a radiometer sensor was placed at the cuvette's position, and with it the block was moved to a distance yielding a 2 mW/cm^2 exposure, as it was found that the lamp's intensity varied slightly over a given bulb's lifetime (data not shown). The Cary UV/Vis spectrometer used to read turbidity was positioned on the benchtop directly above the cabinet for ease of access.

While the lamp was on, I wore UV blocking lab goggles when opening the cabinet and accessing the sample.

a

b

Figure 6B.1 Photo-aggregation sample cabinet (a) from outside, and (b) zoomed in to view sample placement.

Appendix C: Oxygen-dependent Development of Dimeric Gel-Visible Photo-Products and HγD-Crys Monomer Depletion

Purpose: The development of light-scattering photoaggregation was shown to be entirely dependent on the presence of oxygen. Given the distinction between the light-scattering photoaggregation and the initial dimer formation seen in Chapter 3, in terms of recognition by HαB-Crys and the effects of the Y16A and C18S mutations, I wanted to determine whether dimer formation was also oxygen dependent.

Results and Discussion: Photoaggregation samples of WT HγD-Crys were prepared as in Chapter 2, in an anaerobic chamber before being sealed and removed, and then exposed to UVR. Samples were extracted over exposure time and analyzed via SDS-PAGE and band density quantification (Fig. C.1). Over an hour of exposure in the absence of oxygen, no dimer band appeared and the monomeric HγD-Crys band did not appreciably diminish. At 60 min. exposure time, samples were unsealed and exposed to oxygen. The dimer band appeared and the monomer band began to diminish only after oxygen was introduced to the sample. This demonstrates that, similar to the light-scattering photoaggregation, the initial dimer formation and depletion of monomeric HγD-Crys are entirely dependent on oxygen. The mechanisms behind these reactions likely depend on a ROS.

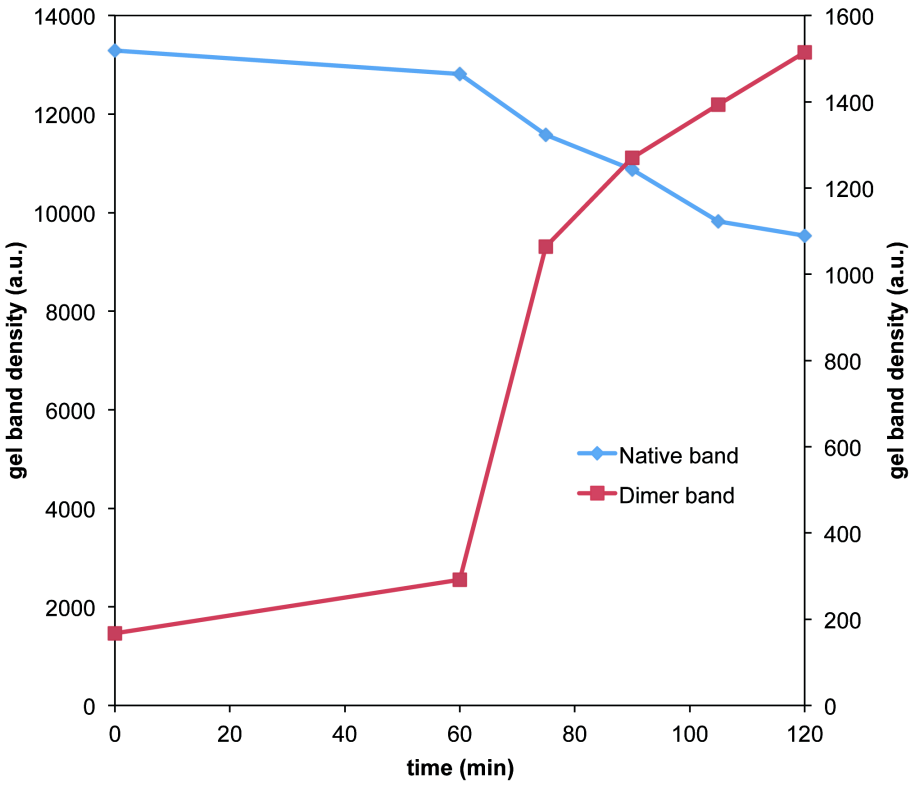

Figure 6C.1. Oxygen Dependent Development of Gel-Visible Dimer and Depletion of Monomer Band. Samples taken over UVR exposure time were analyzed via SDS-PAGE, visualized with Krypton staining, and scanned and quantified. Native band quantification shown in blue (left axis), dimer band quantification shown in red (right axis).

If it were up to me, I'd have failed you